MOLECULAR LANTHANIDE AND ACTINIDE COMPOUNDS WITH CHALCOGENOLATE LIGANDS

By

WEN WU

A dissertation submitted to the

School of Graduate Studies

Rutgers, The State University of New Jersey

In partial fulfillment of the requirements

For the degree of

Doctor of Philosophy

Graduate Program in Chemistry and Chemical Biology

Written under the direction of

John G. Brennan

And approved by

_____

_____

_____

_____

New Brunswick, New Jersey

May 2019

ABSTRACT OF THE DISSERTATION

Molecular Lanthanide and Actinide Compounds with Chalcogenolate Ligands

by WEN WU

Dissertation Director:

John G. Brennan

A series of novel molecular lanthanide and actinide chalcogenolate compounds have been prepared with different neutral donor ligands.

Three lanthanide fluorinated selenolate monomers $(DME)_2Ln(SeC_6F_5)_3$ (Ln = Nd, Er, Tm, DME = 1,2-Dimethoxyethane) were synthesized in high yields by reductive cleavage of the Se-Se bond in $(SeC_6F_5)_2$ with elemental Ln in DME. Their structural and optical properties are discussed. Emission measurements indicate that these compounds are bright NIR sources.

A number of dimeric thorium disulfide and diselenide compounds have been prepared with sterically undemanding ancillary chalcogenolate ligands. Five complexes, $(py)_6Th_2I_4(S_2)_2$, $(py)_6Th_2Br_2(SC_6F_5)_2(S_2)_2$, $(py)_6Th_2I_4(Se_2)_2$, $(py)_6Th_2I_2(SC_6F_5)_2(Se_2)_2$, and $(py)_6Th_2Br_2(SC_6F_5)_2(Se_2)_2$ (py = pyridine) were isolated in high yields by first reducing mixtures of metal Th, chalcogenolate ligands and halide sources (I_2 or PhSeBr)

in py, followed by in-situ ligand based redox reactions with elemental sulfur or selenium. These are the first examples of thorium compounds with bridging dichalcogenide ligands. Attempts to prepare chloride derivatives gave mixtures of $(py)_4ThCl_4$ and either $(py)_6Th_2Cl_2(SC_6F_5)_2(S_2)_2$ or $(py)_8Th_4Se_4(SePh)_4(SC_6F_5)_4$. A computational analysis of experimental ^{77}Se NMR chemical shifts reveals that the dimeric structures with two bridging dichalcogenides are maintained in solution. Thermolysis of $(py)_6Th_2I_4(Se_2)_2$ leads to the formation of solid-state $ThSe_2$ and I_2.

The identities of chalcogenolate ligands and neutral donor ligands have been found to influence the structures of thorium compounds. Three Th monomers, $(bipy)_2Th(SC_6F_5)_4$, $(Hpz)_4(pz)Th(SC_6F_5)_3$, $(Hdmpz)_2(dmpz)_2Th(SC_6F_5)_2$ and three Th dimers, $(pzn)_4Th_2(SC_6F_5)_8$, $(Hpz)_4(pz)_2Th_2(SePh)_6$, $(Hdmpz)_4(dmpz)_2Th_2(SC_6F_5)_6$ (bipy=2,2'-bipyridine, pzn = pyrazine; Hpz = pyrazole, Hdmpz= 3,5-dimethylpyrazole) have been prepared and characterized. Reaction of Th, $(SeC_6F_5)_2$ and Hpz in toluene also results in a thorium cluster $(Hpz)_8Th_4Se_4(SeC_6F_5)_8$ with Th_4Se_4 cubane core.

Several thorium and uranium oxo- and fluoro- compounds were also synthesized. Oxo compounds $(py)_6Th_2O(Se_2)I_4$, $(py)_6U_2O(Se_2)I_4$, and $(py)_{10}Th_6O_3(Se_2)_8(SC_6F_5)_2$ were prepared by adding elemental Se and SeO_2 into the mixture of metal Th or U, chalcogenolate ligands and halide sources in py. Two fluoride complexes have also been prepared. Coming from the reactions of metal Th or U, $(SC_6F_5)_2$ and I_2 in py, $(py)_4ThI_3F$ contains fluoride from the original $(SC_6F_5)_2$; while the uranium derivative, $(py)_3UI_3(SC_6F_5)$ follows stoichiometry of the starting materials.

Acknowledgements

First of all, I would like to express my deepest gratitude to my advisor, Professor John Brennan for his continuous guidance and support during the past five years. His knowledge, experience, professionalism and scientific rigor benefits me a lot on my research, and I appreciate his patience and the great amount of time he has spent on me to make me better.

I would like to thank my committee members, Professor Alan Goldman, Professor Tewodros Asefa and Professor Richard Riman for their helpful suggestions.

Special thanks to Dr. Thomas Emge for his help in collecting and processing the X-ray diffraction data and sharing a lot of crystallographic knowledge with me.

I am grateful to Dr. Anna Kornienko for teaching me experimental skills when I first joined the group and her continuous guidance and assistance in the lab. Thank my labmates, Dr. Marissa Ringgold, Matthew Stuber, and Garret Gotthelf for their help and insightful discussion.

Many thanks to our collaborators, Dr. Ajith Kumar, Dr. Peter Hrobárik, Dr. Dechao Yu, Dr. Nathan Rudd and Bo Li for their help in characterization of the compounds.

I would also like to thank my friends, Dr. Ruofan Yan, Dr. Yingfu Lin, Dr. Yuanyuan Wang, Xue Yang, Yu Liu, Zhengbo Zhu, Yao Cao, Qi Zhang, Mingjie Dong, Qiongyi Shang and Wenjia Gu for the companionship in these years.

Finally, I deeply thank my parents for their endless support, encouragement and love.

Dedication

To my family

Table of Contents

List of Tables

List of Illustrations

List of Abbreviations

Ln	lanthanide
An	actinide
py	pyridine
DME	1,2-dimethoxyethane
THF	tetrahydrofuran
tol	toluene
bipy	2,2'-bipyridine
pzn	pyrazine
Hpz	pyrazole
Hdmpz	3,5-dimethylpyrazole
Ph	C_6H_5
E	O, S, Se, or Te
NMR	nuclear magnetic resonance spectroscopy
PXRD	Powder X-ray Diffraction
ORTEP	Oak Ridge Thermal Ellipsoid Plot

Part of Chapter 1 of this thesis has been published as:

Wu, W.; Zhang, X.; Kornienko, A. Y.; Kumar, G. A.; Yu, D.; Emge, T. J.; Riman, R.E.; Brennan, J. G. Efficient NIR Emission from Nd, Er, and Tm Complexes with Fluorinated Selenolate Ligands. *Inorg. Chem.* **2018**, *57*, 1912-1918.

Part of Chapter 2 of this thesis has been published as:

Wu, W.; Rehe, D.; Hrobárik, P.; Kornienko, A. Y.; Emge, T. J.; Brennan, J. G. Molecular Thorium Compounds with Dichalcogenide Ligands – Synthesis, Structure, ^{77}Se NMR Study and Thermolysis. *Inorg. Chem.* **2018**, *57*, 14821-14833.

Part of Chapter 3 of this thesis has been published as:

Ringgold, M.; **Wu, W.**; Stuber, M.; Kornienko, A. Y.; Emge, T. J.; Brennan, J. G. Monomeric Thorium Chalcogenolates with Bipyridine and Terpyridine Ligands. *Dalton Trans.* **2018**, *47*, 14652-14661.

Introduction

The f-block elements, including lanthanides (Ln) and actinides (An), are presented at the bottom of the periodic table and are also called inner transition elements. Their electronic and chemical characteristics, such as the involvement of f-electrons, large ionic radii, flexible coordination geometries, have resulted in many materials with unique electronic, luminescent, and magnetic properties.[1]

Lanthanides:

In the lanthanide series, the 4f orbitals are gradually filled (Table I.1). Figure I.1 shows the radial distribution functions of the atomic orbitals. The 4f orbitals are radially contracted and well shielded by filled $5s^2$ and $5p^6$ orbitals. As the 5s and 5p are higher in energy and the orbitals are more spatially extended, the 4f electrons are highly localized, and therefore do not participate significantly in bonding. As a result, the spectroscopic and magnetic properties of the lanthanide ions are essentially unaffected by environment.

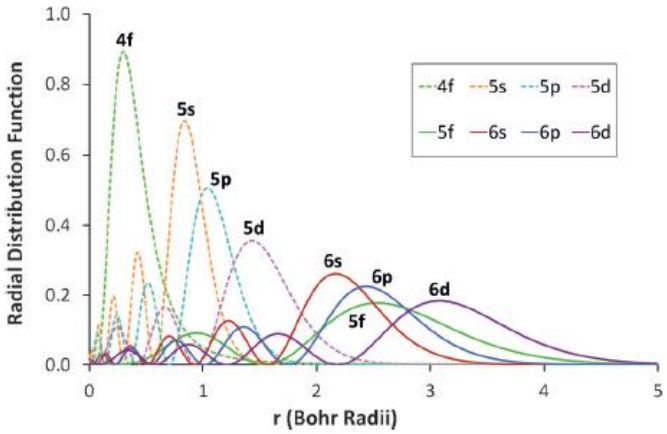

Figure I.1. Illustrative radial distribution functions for 4f, 5s, 5p, 5d, 5f, 6s, 6p, and 6d atomic orbitals.[2]

Table I.1. Electron configurations of lanthanide elements

Element	Electron Configuration
Ln	$[Xe]5d^16s^2$
Ce	$[Xe]4f^15d^16s^2$
Pr	$[Xe]4f^36s^2$
Nd	$[Xe]4f^46s^2$
Pm	$[Xe]4f^56s^2$
Sm	$[Xe]4f^66s^2$
Eu	$[Xe]4f^76s^2$
Gd	$[Xe]4f^75d^16s^2$
Tb	$[Xe]4f^96s^2$
Dy	$[Xe]4f^{10}6s^2$
Ho	$[Xe]4f^{11}6s^2$
Er	$[Xe]4f^{12}6s^2$
Tm	$[Xe]4f^{13}6s^2$
Yb	$[Xe]4f^{14}6s^2$
Lu	$[Xe]4f^{14}5d^16s^2$

The most stable oxidation state for all lanthanide elements is the +3 state. According to the Hard-Soft-Acid-Base (HSAB) theory, Ln^{3+} ions are hard Lewis acids, and therefore favors hard Lewis bases with electronegative donor atoms, including nitrogen, oxygen, or halide.[3] As the coordination environment in lanthanide complexes mainly depends on the identities of the ligands, the coordination number has a wider variety and there is no characteristic coordination number as is typically observed for transition metals. With sterically undemanding ligands, such as H_2O or THF, typical coordination numbers range from 7 to 9.[4] While with bulky ligands such as $-N(SiMe_3)_2$, [5] the repulsions between the bulky substituent groups determines how many ligands enter the coordination sphere. The use of small bidentate ligands such as nitrate or 2,2-bipyridine can also lead to coordination numbers up to 12, i.e. in $La(NO_3)_3$(18-crown-6).[6]

Tris(cyclopentadienyl) lanthanide complexes, $(C_5H_5)_3Ln$, were the first well-characterized organometallic complexes of the lanthanide metals.[7] The C_5H_5 (Cp) ligand are used to stabilize and solubilize Ln^{3+} ions without the presence of oxides, nitrides or halides. C_5Me_5 (Cp*) ligand was introduced into lanthanide chemistry later in the 1980s.[8] This ligand has all the favorable aspects of the C_5H_5 group plus a larger size and enhanced solubilizing capacity. These ligand systems demonstrated that the lanthanides could be useful in complexing, activating, and transforming many types of unsaturated substrates which previously had been thought to be reactive only with transition metals.[9]

Lanthanide-chalcogen chemistry has been investigated recently. It is a challenge to synthesize lanthanide chalcogenolates due to the nature of the bonding between these "hard" lanthanide metal ions and the "soft" chalcogens (S, Se, Te). First several compounds with lanthanide–chalcogen bonds were synthesized with ancillary Cp or Cp* ligands,[10] because at that time it was believed that theses bulky ligands were necessary to stabilize the structures. But as the steric demands of the ancillary ligands made it impossible to extract bonding information between lanthanide and chalcogen, molecular $Ln(ER)_3$ ($R=C_6H_5$ or C_6F_5) compounds in Lewis base solvents, such as py,[11] THF,[11a,12] and DME,[11a,13] have been investigated. For example, Figure I.2 shows the structure of $(THF)_3Yb(SC_6F_5)_3$.[12b] The bond distances between Yb and S are 2.678(2) Å for Yb-S(1), 2.680(2) Å for Yb-S(3), 2.642(2) Å for Yb-S(2), respectively. There appears to be a structural trans-influence, with the Yb-S bond trans to SC_6F_5 being

significantly longer than the Yb-S bond trans to the neutral THF donor. This trans influence found in octahedral Ln coordination complexes results from covalent interactions between ligand-based p orbitals and the Ln 5d orbitals.

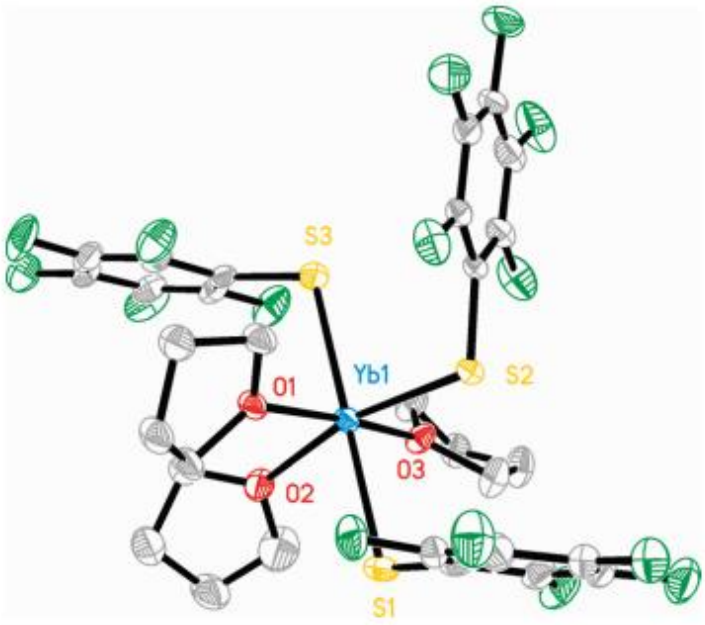

Figure I.2. ORTEP diagram of $(THF)_3Yb(SC_6F_5)_3$ [12b].

In addition to the significance of fundamental research, lanthanide elements also arouse interest because of their unique properties for practical applications. The most important aspect is luminescence.

Luminescent Ln^{3+} ions can realize emissions from visible to near-infrared (NIR) regions of the electromagnetic spectrum, and many reviews have summarized the achievements on understanding of the emission process and designing novel functional materials with optimized optical properties.[14] Currently, the three most promising candidates for efficient NIR emission are Nd^{3+}, Er^{3+} and Tm^{3+}.[15] However, the f–f transitions of Ln^{3+} ions are forbidden, and this leads to weak intensities because of low absorption coefficients. To increase the intensity of Ln emissions, one of the feasible

approaches is to design the complexes with certain ligands, that can stimulate the emission of Ln^{3+} ions as sensitizers, or prevent non-radiative relaxation processes.

Several lanthanide complexes with OC_6F_5 [16] or SC_6F_5 [13,17] ligands have been previously studied. The fluorination of the aromatic ligands leads to improved NIR emissions by reducing the number of C-H functional groups which vibrationally quench the emissions and shorten excited-state lifetime. In these compounds, Ln^{3+} ions bound to more electronegative chalcogen elements (E; E= O, S). The Ln-E bonds have low phonon energy and increase the separation between the Ln^{3+} ions and the aryl group, which improves the excited-state Ln lifetimes and quantum efficiencies, resulting in highly NIR emissive molecules.

Lanthanide ions with per-fluorobenzeneselenolate (SeC_6F_5) should also be candidates of bright NIR emission sources, because the lower-energy of Ln-Se vibrations and the longer Ln-Se bonds should both further decouple the ligand vibrational modes from the metal excited states. These two effects, combined with ring fluorination, should lengthen excited-state Ln lifetimes and increase quantum efficiencies.

Actinides:

Actinide chemistry has attracted increasing attention during the past few decades. Table I.2 summarizes the electron configurations of actinide elements. Unlike lanthanide elements in which the 4f orbitals are well shielded by filled 5s and 5p orbitals, the 5f orbitals of actinide elements are not shielded by the filled 6s and 6p subshells

(Figure I.1).

Table I.2. Electron configurations of actinide elements

Element	Electron Configuration
Ac	[Rn]$6d^1 7s^2$
Th	[Rn]$6d^2 7s^2$
Pa	[Rn]$5f^2 6d^1 7s^2$
U	[Rn]$5f^3 6d^1 7s^2$
Np	[Rn]$5f^4 6d^1 7s^2$
Pu	[Rn]$5f^6 7s^2$
Am	[Rn]$5f^7 7s^2$
Cm	[Rn]$5f^7 6d^1 7s^2$
Bk	[Rn]$5f^9 7s^2$
Cf	[Rn]$5f^{10} 7s^2$
Es	[Rn]$5f^{11} 7s^2$
Fm	[Rn]$5f^{12} 7s^2$
Md	[Rn]$5f^{13} 7s^2$
No	[Rn]$5f^{14} 7s^2$
Lr	[Rn]$5f^{14} 6d^1 7s^2$

In addition, relativistic effects become non-negligible in actinide elements. As the velocity of the electrons increases towards the speed of light, their mass also increases, which leads to a contraction of the s and p orbitals, and an expansion of 5f orbitals of actinide elements. This results in 5f electrons being less tightly bound.

The partial shielding of 5f orbitals by filled 6s and 6p orbitals, small energy difference between the 5f and 6d orbitals, and complications associated with relativistic effects, all lead to materials with fascinating chemical and physical properties, which are important in a variety of fields, such as radioactive-waste treatment,[18] actinide separation,[19] and catalytic reactions.[20]

The majority of the studies are based on thorium and uranium, due to the

accessibility of raw materials and the long half-life time of the relatively weakly α-emitting isotope ^{232}Th and ^{238}U.

The covalency in actinide complexes remains controversial.[21] While the metal–ligand bonds of 5f elements are considered primarily electrostatic, the covalent contributions have been noted in several compounds with a wide range of ligand types.[22] This includes uranocene, $U(C_8H_8)_2$, and the structure and stability of this molecule was predicted by Streitweiser[23] before it was synthesized, based on an analysis of the symmetry properties of the actinide 5f orbitals and the orbitals of the cyclooctatetraenide (COT) anion. Covalent contributions to uranocene stability were confirmed later in a synchrotron photoelectron spectroscopy study that demonstrated significant overlap between the uranium 5f and COT orbitals.[22a] Another example is the research on actinide carbonyl complexes, such as $(Me_3SiC_5H_4)_3U(CO)$[22d] and $(C_5Me_4H)U(CO)$.[22e] The decreased vibration frequency of carbonyl stretching absorption ν_{CO} indicates a strong U-CO backbonding interaction, presumably between the U 5f π and the CO π* orbitals. Therefore, it is important to have a series of actinide molecules that can be used to probe actinide-ligand bonding and help to understand the extent of covalency in these bonds.

Coordination chemistry of the actinides has traditionally been based on hard donor ligands, which contain nitrogen or oxygen atoms.[24] The research of the actinide complexes with softer donors (E, E = S, Se, Te) is relatively unexplored. In recent years, a growing number of new actinide chalcogenolate complexes has been published and

most of the research focused on uranium species.[25] Thorium chemistry is relatively unexplored, as only a few molecular thorium compounds containing Th-E bonds have been reported.[26] Although there are some examples of molecular actinide chalcogenolates, many of them contain sterically bulky anions, such as Cp* and $N(SiMe_3)_2$. It would be valuable to synthesize actinide chalcogenolate complexes in which the chalcogenolate is the only coordinated anion, as it may help to better understand how the bonding between actinide and chalcogen may impact the structure, stability or physical properties of these materials without significant steric restrictions. In addition, these molecules could be possible frameworks to build large clusters.

Self-assembling clusters can be useful models to understand the relationship between the structure and the properties of materials. When compared to that of transition metals or lanthanides, actinide cluster chemistry is relatively less developed. The most explored system is that of actinyl peroxides, which have yielded many unique topologies, including fullerene-type U_{60},[27] and the largest cluster $U_{120}Ox_{90}$, where U and Ox represent uranyl and oxalate, respectively.[28] There also exists some examples of actinide clusters with oxide or hydroxide bridges,[29] and many of them were built from uranyl ions in aqueous solution. However, the clusters of An and chalcogen based anions (E^{2-}, EE^{2-}, ER; E = S, Se, Te) in nonaqueous solution are rarely reported. By conducting studies in nonaqueous solution, it is possible to remove the complicating factors of solvent exchange and hydrolysis, and to provide more direct comparisons of chemical reactivity and structural chemistry based on the identities of metal, oxidation

states, and ligand types. One notable example is the uranium cluster $(py)_8U_4Se_4(SePh)_8$,[30] which has a U_4Se_4 distorted cubane core, and is comparable to the lanthanide counterpart $(py)_8Yb_4Se_4(SePh)_4$ (Figure I.3).[31] The lanthanide cluster does not contain any bridging $SePh^-$ anions because of the +3 charge on ytterbium compared to +4 for uranium.

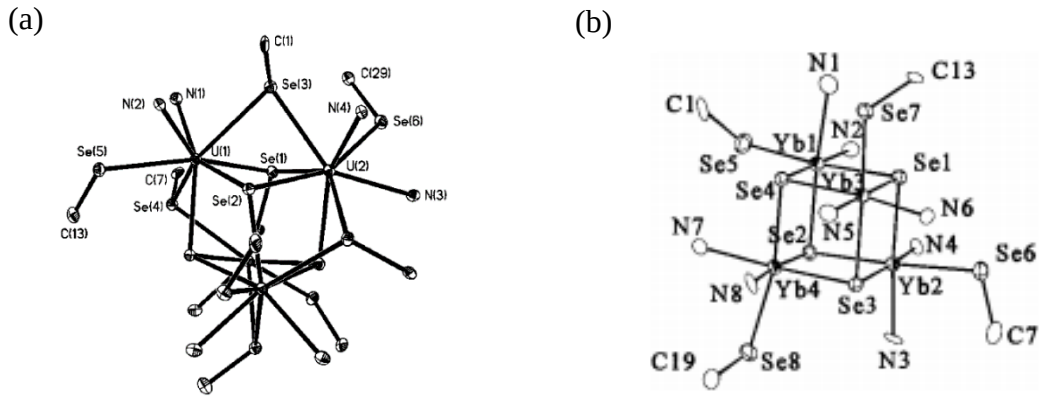

Figure I.3. Structures of (a) $(py)_8U_4Se_4(SePh)_8$ and (b) $(py)_8Yb_4Se_4(SePh)_4$.

This research indicates that the oxidation of uranium metal by chalcogenolate ligands is a useful synthetic approach for isolating uranium chalcogenolate compounds without the need for stabilizing ancillary ligands. This approach should also work on thorium to target new molecular and cluster compounds.

In this thesis, Chapter 1 discusses the synthesis, characterization, and NIR emission properties of three molecular lanthanide fluorinated selenolate complexes $(DME)_2Ln(SeC_6F_5)_3$ (DME=1,2-Dimethoxyethane; Ln= Nd, Er, Tm). These complexes are isostructural, and all have relatively short Ln-F dative interactions. Emission measurements indicate that these compounds are bright NIR sources.

Chapter 2 describes the synthesis and characterization of a series of dimeric

thorium compounds with E_2^{2-} (E = S, Se) bridging ligands. ^{77}Se NMR and DFT calculations are used to show that the well-defined solid-state structures are maintained in solution, and an investigation into the thermal decomposition reactions of the halogenated materials shows that $ThSe_2$, rather than ternary solid-state compounds, is produced.

Chapter 3 outlines the synthesis and structures of thorium chalcogenolate compounds with different neutral donor ligands, such as 2,2'-bipyridine, pyrazine, pyrazole and 3,5-dimethylpyrazole. The different identities of the chalcogenolate ligands and neutral donor ligands lead to various structures with significant different coordination geometries.

Chapter 4 focuses on actinide oxychalcogenides and halides. Three actinide oxychalcogenides have been isolated and characterized and these are the first examples of actinide compounds containing both oxo and dichalcogenido bridges. Two actinide halides have also been synthesized and shown the influence of the metal identity on the final structures.

Reference

(1) (a) Dorenbos, P. Determining binding energies of valence-band electrons in insulators and semiconductors via lanthanide spectroscopy. *Physical Review B* **2013**, *87*, 035118.(b) Marks, T. J. Introduction to the "Recent Advances in f-Element Organometallic Chemistry" Special Issue of Organometallics. *Organometallics* **2013**, *32*, 1133-1136.(c) Liddle, S. T.; van Slageren, J. Improving f-element single molecule magnets. *Chem. Soc. Rev.* **2015**, *44*, 6655-6669.(d) Berthet, J.-C.; Thuéry, P.; Ephritikhine, M. Advances in f-element cyanide chemistry. *Dalton Trans.* **2015**, *44*, 7727-7742.(e) Xu, L.-J.; Xu, G.-T.; Chen, Z.-N. Recent advances in lanthanide luminescence with metal-organic chromophores as sensitizers. *Coord. Chem. Rev.* **2014**, *273*, 47-62.

(2) Liddle, S. T. The renaissance of non-aqueous uranium chemistry. *Angew. Chem. Int. Ed.* **2015**, *54*, 8604-8641.

(3) Nief, F. Complexes containing bonds between group 3, lanthanide or actinide metals and non-first-row main group elements (excluding halogens). *Coord. Chem. Rev.* **1998**, *178-180*, 13-81.

(4) Cotton, S. A.; Harrowfield, J. M. Lanthanides: Coordination Chemistry. *Encyclopedia of Inorganic and Bioinorganic Chemistry* **2011**.

(5) Bradley, D. C.; Ghotra, J. S.; Hart, F. A. Low co-ordination numbers in lanthanide and actinide compounds. Part I. The preparation and characterization of tris{bis(trimethylsilyl)-amido}lanthanides. *J. Chem. Soc. Dalton Trans.* **1973**, 1021-1023.

(6) Backer-Dirks, J. D. J.; Cooke, J. E.; Galas, A. M. R.; Ghotra, J. S.; Gray, C. J.; Hart, F. A.; Hursthouse, M. B. Complexes of lanthanide ions with the crown ether 1, 4, 7, 10, 13, 16-hexaoxacyclo-octadecane. *J. Chem. Soc. Dalton Trans.* **1980**, 2191-2198.

(7) Birmingham, J. M.; Wilkinson, G. The Cyclopentadienides of Scandium, Yttrium and Some Rare Earth Elements. *J. Am. Chem. Soc.* **1956**, *78*, 42-44.

(8) (a) Evans, W. J.; Hughes, L. A.; Hanusa, T. P. Synthesis and crystallographic characterization of an unsolvated, monomeric samarium bis(pentamethylcyclopentadienyl) organolanthanide complex, $(C_5Me_5)_2Sm$. *J. Am. Chem. Soc.* **1984**, *106*, 4270-4272.(b) Evans, W. J.; Hughes, L. A.; Hanusa, T. P. Synthesis and x-ray crystal structure of bis(pentamethylcyclopentadienyl) complexes of samarium and europium: $(C_5Me_5)_2Sm$ and $(C_5Me_5)_2Eu$. *Organometallics* **1986**, *5*, 1285-1291.

(9) Evans, W. J.; Davis, B. L. Chemistry of Tris(pentamethylcyclopentadienyl) f-

Element Complexes, $(C_5Me_5)_3M$. *Chem. Rev.* **2002**, *102*, 2119-2136.

(10) (a) Berg, D. J.; Andersen, R. A.; Zalkin, A. Electron-transfer chemistry of $(Me_5C_5)_2Yb$: cleavage of diorganoperoxide and related chalcogenides to give $(Me_5C_5)_2Yb(ER)(L)$(E= O, S, Se, or Te; L= a Lewis base). Crystal structure of $(Me_5C_5)_2Yb$ (TePh)(NH_3). *Organometallics* **1988**, *7*, 1858-1863.(b) Recknagel, A.; Noltemeyer, M.; Stalke, D.; Pieper, U.; Schmidt, H.-G.; Edelmann, F. T. Monomere Organosamarium (III) Chalkogenolate durch reduktive Spaltung von E–E-Bindungen (E= S, Se, Te). *J. Organomet. Chem.* **1991**, *411*, 347-356.(c) Tilley, T. D.; Andersen, R. A.; Zalkin, A.; Templeton, D. H. Bis (pentamethylcyclopentadienyl) carboxylato and-dithiocarbamato derivatives of neodymium (III) and ytterbium (III). Crystal structure of bis (pentamethylcyclopentadienyl)(diethyldithiocarbamato) ytterbium (III). *Inorg. Chem.* **1982**, *21*, 2644-2647.

(11) (a) Melman, J. H.; Rohde, C.; Emge, T. J.; Brennan, J. G. Trivalent Lanthanide Compounds with Fluorinated Thiolate Ligands: Ln−F Dative Interactions Vary with Ln and Solvent. *Inorg. Chem.* **2002**, *41*, 28-33.(b) Lee, J.; Brewer, M.; Berardini, M.; Brennan, J. G. Trivalent Lanthanide Chalcogenolates: Synthesis, Structure, and Thermolysis Chemistry. *Inorg. Chem.* **1995**, *34*, 3215-3219.

(12) (a) Lee, J.; Freedman, D.; Melman, J. H.; Brewer, M.; Sun, L.; Emge, T. J.; Long, F. H.; Brennan, J. G. Trivalent Lanthanide Chalcogenolates: $Ln(SePh)_3$, $Ln_2(EPh)_6$, $Ln_4(SPh)_{12}$, and $[Ln(EPh)_3]n$ (E = S, Se). How Metal, Chalcogen, and Solvent Influence Structure. *Inorg. Chem.* **1998**, *37*, 2512-2519.(b) Krogh-Jespersen, K.; Romanelli, M. D.; Melman, J. H.; Emge, T. J.; Brennan, J. G. Covalent Bonding and the Trans Influence in Lanthanide Compounds. *Inorg. Chem.* **2010**, *49*, 552-560.

(13) Banerjee, S.; Kumar, G. A.; Emge, T. J.; Riman, R. E.; Brennan, J. G. Thiolate-Bound Thulium Compounds: Synthesis, Structure, and NIR Emission. *Chem. Mater.* **2008**, *20*, 4367-4373.

(14) (a) Eliseeva, S. V.; Bünzli, J.-C. G. Lanthanide luminescence for functional materials and bio-sciences. *Chem. Soc. Rev.* **2010**, *39*, 189-227.(b) Binnemans, K. Lanthanide-based luminescent hybrid materials. *Chem. Rev.* **2009**, *109*, 4283-4374.(c) Bünzli, J.-C. G. Lanthanide luminescence for biomedical analyses and imaging. *Chem. Rev.* **2010**, *110*, 2729-2755.(d) Rocha, J.; Carlos, L. D.; Paz, F. A. A.; Ananias, D. Luminescent multifunctional lanthanides-based metal–organic frameworks. *Chem. Soc. Rev.* **2011**, *40*, 926-940.(e) Buenzli, J.-C. G. On the design of highly luminescent lanthanide complexes. *Coord. Chem. Rev.* **2015**, *293*, 19-47.(f) Long, J.; Guari, Y.; Ferreira, R. A. S.; Carlos, L. D.; Larionova, J. Recent advances in luminescent lanthanide based Single-Molecule Magnets. *Coord. Chem. Rev.* **2018**, *363*, 57-70.

(15) Kumar, G. A.; Riman, R. E.; Brennan, J. G. NIR emission from molecules and clusters with lanthanide–chalcogen bonds. *Coord. Chem. Rev.* **2014**, *273*, 111-124.

(16) Norton, K.; Kumar, G. A.; Dilks, J. L.; Emge, T. J.; Riman, R. E.; Brik, M. G.; Brennan, J. G. Lanthanide compounds with fluorinated aryloxide Ligands: Near-infrared emission from Nd, Tm, and Er. *Inorg. Chem.* **2009**, *48*, 3573-3580.

(17) (a) Kumar, G. A.; Riman, R. E.; Diaz Torres, L. A.; Barbosa Garcia, O.; Banerjee, S.; Kornienko, A.; Brennan, J. G. Chalcogenide-bound erbium complexes: Paradigm molecules for infrared fluorescence emission. *Chem. Mater.* **2005**, *17*, 5130-5135.(b) Banerjee, S.; Huebner, L.; Romanelli, M. D.; Kumar, G. A.; Riman, R. E.; Emge, T. J.; Brennan, J. G. Oxoselenido clusters of the lanthanides: Rational introduction of oxo ligands and near-IR emission from Nd (III). *J. Am. Chem. Soc.* **2005**, *127*, 15900-15906.

(18) (a) Dam, H. H.; Reinhoudt, D. N.; Verboom, W. Multicoordinate ligands for actinide/lanthanide separations. *Chem. Soc. Rev.* **2007**, *36*, 367-377.(b) Bots, P.; Morris, K.; Hibberd, R.; Law, G. T.; Mosselmans, J. F. W.; Brown, A. P.; Doutch, J.; Smith, A. J.; Shaw, S. Formation of stable uranium (VI) colloidal nanoparticles in conditions relevant to radioactive waste disposal. *Langmuir* **2014**, *30*, 14396-14405.

(19) (a) Lewis, F. W.; Harwood, L. M.; Hudson, M. J.; Drew, M. G. B.; Desreux, J. F.; Vidick, G.; Bouslimani, N.; Modolo, G.; Wilden, A.; Sypula, M.; Vu, T.-H.; Simonin, J.-P. Highly Efficient Separation of Actinides from Lanthanides by a Phenanthroline-Derived Bis-triazine Ligand. *J. Am. Chem. Soc.* **2011**, *133*, 13093-13102.(b) Hudson, M. J.; Harwood, L. M.; Laventine, D. M.; Lewis, F. W. Use of Soft Heterocyclic N-Donor Ligands To Separate Actinides and Lanthanides. *Inorg. Chem.* **2013**, *52*, 3414-3428.

(20) (a) Batrice, R. J.; Kefalidis, C. E.; Maron, L.; Eisen, M. S. Actinide-Catalyzed Intermolecular Addition of Alcohols to Carbodiimides. *J. Am. Chem. Soc.* **2016**, *138*, 2114-2117.(b) Karmel, I. S. R.; Fridman, N.; Tamm, M.; Eisen, M. S. Mono(imidazolin-2-iminato) Actinide Complexes: Synthesis and Application in the Catalytic Dimerization of Aldehydes. *J. Am. Chem. Soc.* **2014**, *136*, 17180-17192.

(21) (a) Neidig, M. L.; Clark, D. L.; Martin, R. L. Covalency in f-element complexes. *Coord. Chem. Rev.* **2013**, *257*, 394-406.(b) Jones, M. B.; Gaunt, A. J. Recent Developments in Synthesis and Structural Chemistry of Nonaqueous Actinide Complexes. *Chem. Rev.* **2013**, *113*, 1137-1198.

(22) (a) Brennan, J. G.; Green, J. C.; Redfern, C. M. Covalency in bis ([8] annulene) uranium from photoelectron spectroscopy with variable photon energy. *J. Am. Chem. Soc.* **1989**, *111*, 2373-2377.(b) Choppin, G. R. Covalency in f-element bonds. *J. Alloys Compd.* **2002**, *344*, 55-59.(c) Smiles, D. E.; Wu, G.; Hrobárik, P.; Hayton, T. W. Use of ^{77}Se and ^{125}Te NMR Spectroscopy to Probe Covalency of the Actinide-Chalcogen Bonding in $[Th(E_n)\{N(SiMe_3)_2\}_3]^-$ (E = Se, Te; n = 1, 2) and Their Oxo-Uranium(VI) Congeners. *J. Am. Chem. Soc.* **2016**, *138*, 814-825.(d) Brennan, J. G.; Andersen, R. A.; Robbins, J. L. Preparation of the first molecular carbon monoxide complex of uranium, $(Me_3SiC_5H_4)_3UCO$. *J. Am. Chem. Soc.* **1986**, *108*, 335-336.(e) Parry, J.; Carmona, E.; Coles, S.; Hursthouse, M. Synthesis and single crystal X-ray diffraction study on the first isolable carbonyl complex of an actinide,$(C_5Me_4H)_3U(CO)$. *J. Am. Chem. Soc.* **1995**, *117*, 2649-2650.

(23) Streitwieser, A., Jr.; Mueller-Westerhoff, U. Bis(cyclooctatetraenyl)uranium (uranocene). A new class of sandwich complexes that utilize atomic f orbitals. *J. Amer. Chem. Soc.* **1968**, *90*, 7364.

(24) (a) Mishra, S. Anhydrous scandium, yttrium, lanthanide and actinide halide complexes with neutral oxygen and nitrogen donor ligands. *Coord. Chem. Rev.* **2008**, *252*, 1996-2025.(b) Camp, C.; Pécaut, J.; Mazzanti, M. Tuning Uranium–Nitrogen Multiple Bond Formation with Ancillary Siloxide Ligands. *J. Am. Chem. Soc.* **2013**, *135*, 12101-12111.(c) Fortier, S.; Kaltsoyannis, N.; Wu, G.; Hayton, T. W. Probing the Reactivity and Electronic Structure of a Uranium(V) Terminal Oxo Complex. *J. Am. Chem. Soc.* **2011**, *133*, 14224-14227.(d) Thuéry, P. The first crystal structure of an actinide complex of the macrocyclic ligand DOTA: a two-dimensional uranyl–organic framework. *CrystEngComm* **2008**, *10*, 808-810.

(25) (a) Montalvo, E.; Miller, K. A.; Ziller, J. W.; Evans, W. J. Reactivity of Tuck-in and Tuck-over Uranium Metallocene Complexes. *Organometallics* **2010**, *29*, 4159-4170.(b) Siladke, N. A.; Ziller, J. W.; Evans, W. J. Insertion, Isomerization, and Cascade Reactivity of the Tethered Silylalkyl Uranium Metallocene $(\eta^5\text{-}C_5Me_4SiMe_2CH_2\text{-}\kappa C)_2U$. *J. Am. Chem. Soc.* **2011**, *133*, 3507-3516.(c) Tourneux, J.-C.; Berthet, J.-C.; Cantat, T.; Thuéry, P.; Mézailles, N.; Ephritikhine, M. Exploring the Uranyl Organometallic Chemistry: From Single to Double Uranium−Carbon Bonds. *J. Am. Chem. Soc.* **2011**, *133*, 6162-6165.(d) Zhang, L.; Hou, G.; Zi, G.; Ding, W.; Walter, M. D. Preparation of a uranium metallacyclocumulene and its reactivity towards unsaturated organic molecules. *Dalton Trans.* **2017**, *46*, 3716-3728.(e) Matson, E. M.; Goshert, M. D.; Kiernicki, J. J.; Newell, B. S.; Fanwick, P. E.; Shores, M. P.; Walensky, J. R.; Bart, S. C. Synthesis of terminal uranium (IV) disulfido and diselenido compounds by activation of elemental sulfur and selenium. *Chem. Eur. J.* **2013**,

19, 16176-16180.(f) Graves, C. R.; Scott, B. L.; Morris, D. E.; Kiplinger, J. L. Selenate and tellurate complexes of pentavalent uranium. *Chem. Commun.* **2009**, 776-778.(g) Camp, C.; Antunes, M. A.; García, G.; Ciofini, I.; Santos, I. C.; Pécaut, J.; Almeida, M.; Marçalo, J.; Mazzanti, M. Two-electron versus one-electron reduction of chalcogens by uranium(iii): synthesis of a terminal U(v) persulfide complex. *Chem. Sci.* **2014**, *5*, 841-846.(h) Cantat, T.; Arliguie, T.; Noël, A.; Thuéry, P.; Ephritikhine, M.; Floch, P. L.; Mézailles, N. The U═C Double Bond: Synthesis and Study of Uranium Nucleophilic Carbene Complexes. *J. Am. Chem. Soc.* **2009**, *131*, 963-972.(i) Evans, W. J.; Walensky, J. R.; Ziller, J. W. Reaction Chemistry of the U^{3+} Metallocene Amidinate $(C_5Me_5)_2[^iPrNC(Me)N^iPr]U$ Including the Isolation of a Uranium Complex of a Monodentate Acetate. *Inorg. Chem.* **2010**, *49*, 1743-1749.(j) Gardner, B. M.; King, D. M.; Tuna, F.; Wooles, A. J.; Chilton, N. F.; Liddle, S. T. Assessing crystal field and magnetic interactions in diuranium-μ-chalcogenide triamidoamine complexes with U^{IV}–E–U^{IV} cores (E = S, Se, Te): implications for determining the presence or absence of actinide–actinide magnetic exchange. *Chem. Sci.* **2017**, *8*, 6207-6217.(k) Spencer, L. P.; Yang, P.; Scott, B. L.; Batista, E. R.; Boncella, J. M. Oxidative Addition to U(V)−U(V) Dimers: Facile Routes to Uranium(VI) Bis(imido) Complexes. *Inorg. Chem.* **2009**, *48*, 11615-11623.(l) Arnold, P. L.; Stevens, C. J.; Bell, N. L.; Lord, R. M.; Goldberg, J. M.; Nichol, G. S.; Love, J. B. Multi-electron reduction of sulfur and carbon disulfide using binuclear uranium(iii) borohydride complexes. *Chem. Sci.* **2017**, *8*, 3609-3617.(m) Tourneux, J.-C.; Berthet, J.-C.; Thuéry, P.; Mézailles, N.; Le Floch, P.; Ephritikhine, M. Easy access to uranium nucleophilic carbene complexes. *Dalton Trans.* **2010**, *39*, 2494-2496.(n) Duhović, S.; Monreal, M. J.; Diaconescu, P. L. Reactions of Aromatic Heterocycles with Uranium Alkyl Complexes. *Inorg. Chem.* **2010**, *49*, 7165-7169.(o) Kiernicki, J. J.; Staun, S. L.; Zeller, M.; Bart, S. C. A Uranium(IV) Triamide Species with Brønsted Basic Ligand Character: Metal–Ligand Cooperativity in the f Block. *Organometallics* **2017**, *36*, 665-672.(p) Vidjayacoumar, B.; Ilango, S.; Ray, M. J.; Chu, T.; Kolpin, K. B.; Andreychuk, N. R.; Cruz, C. A.; Emslie, D. J. H.; Jenkins, H. A.; Britten, J. F. Rigid NON- and NSN-ligand complexes of tetravalent and trivalent uranium: comparison of U–OAr2 and U–SAr2 bonding. *Dalton Trans.* **2012**, *41*, 8175-8189.(q) Tourneux, J.-C.; Berthet, J.-C.; Cantat, T.; Thuéry, P.; Mézailles, N.; Le Floch, P.; Ephritikhine, M. Uranium(IV) Nucleophilic Carbene Complexes. *Organometallics* **2011**, *30*, 2957-2971.(r) Lam, O. P.; Franke, S. M.; Heinemann, F. W.; Meyer, K. Reactivity of U–E–U (E = S, Se) Toward CO_2, CS_2, and COS: New Mixed-Carbonate Complexes of the Types U–CO_2E–U (E = S, Se), U–CS_2E–U (E = O, Se), and U–COSSe–U. *J. Am. Chem. Soc.* **2012**, *134*, 16877-16881.(s) Franke, S. M.; Heinemann, F. W.; Meyer, K. Reactivity of uranium(iv) bridged chalcogenido complexes U^{IV}–E–U^{IV} (E = S, Se) with elemental sulfur and selenium: synthesis of

polychalcogenido-bridged uranium complexes. *Chem. Sci.* **2014**, *5*, 942-950.(t) Matson, E. M.; Breshears, A. T.; Kiernicki, J. J.; Newell, B. S.; Fanwick, P. E.; Shores, M. P.; Walensky, J. R.; Bart, S. C. Trivalent Uranium Phenylchalcogenide Complexes: Exploring the Bonding and Reactivity with CS_2 in the Tp*$_2$UEPh Series (E = O, S, Se, Te). *Inorg. Chem.* **2014**, *53*, 12977-12985.(u) Spencer, L. P.; Yang, P.; Scott, B. L.; Batista, E. R.; Boncella, J. M. Uranium(VI) Bis(imido) Chalcogenate Complexes: Synthesis and Density Functional Theory Analysis. *Inorg. Chem.* **2009**, *48*, 2693-2700.(v) Jones, M. B.; Gaunt, A. J.; Gordon, J. C.; Kaltsoyannis, N.; Neu, M. P.; Scott, B. L. Uncovering f-element bonding differences and electronic structure in a series of 1 : 3 and 1 : 4 complexes with a diselenophosphinate ligand. *Chem. Sci.* **2013**, *4*, 1189-1203.(w) Cleaves, P. A.; Kefalidis, C. E.; Gardner, B. M.; Tuna, F.; McInnes, E. J. L.; Lewis, W.; Maron, L.; Liddle, S. T. Terminal Uranium (V/VI) Nitride Activation of Carbon Dioxide and Carbon Disulfide: Factors Governing Diverse and Well‐Defined Cleavage and Redox Reactions. *Chem. Eur. J.* **2017**, *23*, 2950-2959.(x) Behrle, A. C.; Kerridge, A.; Walensky, J. R. Dithio- and Diselenophosphinate Thorium(IV) and Uranium(IV) Complexes: Molecular and Electronic Structures, Spectroscopy, and Transmetalation Reactivity. *Inorg. Chem.* **2015**, *54*, 11625-11636.(y) Kiernicki, J. J.; Fanwick, P. E.; Bart, S. C. Utility of a redox-active pyridine(diimine) chelate in facilitating two electron oxidative addition chemistry at uranium. *Chem. Commun.* **2014**, *50*, 8189-8192.(z) Maria, L.; Santos, I. C.; Santos, I. Uranium(iii) complexes supported by hydrobis(mercaptoimidazolyl)borates: synthesis and oxidation chemistry. *Dalton Trans.* **2018**, *47*, 10601-10612.

(26) (a) Wu, W.; Rehe, D.; Hrobárik, P.; Kornienko, A. Y.; Emge, T. J.; Brennan, J. G. Molecular Thorium Compounds with Dichalcogenide Ligands: Synthesis, Structure, 77Se NMR Study, and Thermolysis. *Inorg. Chem.* **2018**, *57*, 14821-14833.(b) Stuber, M. A.; Kornienko, A. Y.; Emge, T. J.; Brennan, J. G. Tetrametallic Thorium Compounds with Th_4E_4 (E = S, Se) Cubane Cores. *Inorg. Chem.* **2017**, *56*, 10247-10256.(c) Ren, W.; Song, H.; Zi, G.; Walter, M. D. A bipyridyl thorium metallocene: synthesis, structure and reactivity. *Dalton Trans.* **2012**, *41*, 5965-5973.(d) Settineri, N. S.; Garner, M. E.; Arnold, J. A Thorium Chalcogenolate Series Generated by Atom Insertion into Thorium–Carbon Bonds. *J. Am. Chem. Soc.* **2017**, *139*, 6261-6269.(e) Ren, W.; Zi, G.; Fang, D.-C.; Walter, M. D. Thorium Oxo and Sulfido Metallocenes: Synthesis, Structure, Reactivity, and Computational Studies. *J. Am. Chem. Soc.* **2011**, *133*, 13183-13196.(f) Smiles, D. E.; Wu, G.; Kaltsoyannis, N.; Hayton, T. W. Thorium–ligand multiple bonds via reductive deprotection of a trityl group. *Chem. Sci.* **2015**, *6*, 3891-3899.(g) Zhou, E.; Ren, W.; Hou, G.; Zi, G.; Fang, D.-C.; Walter, M. D. Small Molecule Activation Mediated by a Thorium Terminal Imido Metallocene. *Organometallics* **2015**, *34*, 3637-3647.(h) Rehe, D.; Kornienko, A. Y.; Emge, T. J.; Brennan, J. G. Thorium Compounds with Bonds to Sulfur

or Selenium: Synthesis, Structure, and Thermolysis. *Inorg. Chem.* **2016**, *55*, 6961-6967.(i) Yang, P.; Zhou, E.; Fang, B.; Hou, G.; Zi, G.; Walter, M. D. Preparation of $(\eta^5\text{-}C_5Me_5)_2Th(bipy)$ and Its Reactivity toward Small Molecules. *Organometallics* **2016**, *35*, 2129-2139.(j) Ringgold, M.; Rehe, D.; Hrobárik, P.; Kornienko, A. Y.; Emge, T. J.; Brennan, J. G. Thorium Cubanes–Synthesis, Solid-State and Solution Structures, Thermolysis, and Chalcogen Exchange Reactions. *Inorg. Chem.* **2018**, *57*, 7129-7141.

(27) Sigmon, G. E.; Unruh, D. K.; Ling, J.; Weaver, B.; Ward, M.; Pressprich, L.; Simonetti, A.; Burns, P. C. Symmetry versus Minimal Pentagonal Adjacencies in Uranium‐Based Polyoxometalate Fullerene Topologies. *Angew. Chem. Int. Ed.* **2009**, *48*, 2737-2740.

(28) Ling, J.; Qiu, J.; Burns, P. C. Uranyl Peroxide Oxalate Cage and Core–Shell Clusters Containing 50 and 120 Uranyl Ions. *Inorg. Chem.* **2012**, *51*, 2403-2408.

(29) Qiu, J.; Burns, P. C. Clusters of actinides with oxide, peroxide, or hydroxide bridges. *Chem. Rev.* **2012**, *113*, 1097-1120.

(30) Gaunt, A. J.; Scott, B. L.; Neu, M. P. U (IV) chalcogenolates synthesized via oxidation of uranium metal by dichalcogenides. *Inorg. Chem.* **2006**, *45*, 7401-7407.

(31) Freedman, D.; Melman, J. H.; Emge, T. J.; Brennan, J. G. Cubane clusters containing lanthanide ions:$(py)_8Yb_4Se_4(SePh)_4$ and $(py)_{10}Yb_6S_6(SPh)_6$. *Inorg. Chem.* **1998**, *37*, 4162-4163.

Chapter 1. Lanthanide Complexes with Fluorinated Selenolate Ligands

1.1 Introduction

Luminescent lanthanide (Ln) ions have a remarkable range of potential applications,[1] from biomedicine[2] to telecommunications.[3] Depending on the coordination environment and stimulation source, trivalent Ln ions exhibit emissions from the visible to near-infrared (NIR) regions of the electromagnetic spectrum. There is considerable effort focused on optimization of the NIR emission process to design functional materials with superior optical properties.[4] Currently, the three most promising candidates for efficient NIR emission are Nd, Er, and Tm.[4e,5]

Problems common to most molecular Ln NIR emission sources are weak intensity due to the spin-forbidden nature of f–f transitions of Ln^{3+} ions, and vibrational quenching of the excited state. Numerous approaches to enhanced emission efficiency have been advanced, including the incorporation of antennae ligands[6] that capture energy to increase excited state populations, and the design of ligands with minimal C-H bonds,[7] since high-energy C-H vibrations are primarily responsible for vibrational quenching of lanthanide excited states. This latter approach includes the replacement of H by D[7a-c] in organometallic ligands, as well as the replacement of H with F.[7d-f] An alternative approach to reduce vibrational quenching involves designing Ln coordination complexes[8] or clusters[9] where the anions bind to Ln through heavier 3rd

or 4th row atoms (i.e. S, Se). Studies of Ln complexes with OC_6F_5[8e,10] and SC_6F_5[8b-d,9a] ligands have clearly demonstrated that the thiolates have superior emission properties, for two reasons: first, the Ln-S bond has a lower phonon energy that does not favor vibrational quenching and second, Ln-S bonds are longer than Ln-O bonds, effectively increasing the distance between the Ln^{3+} ions and the aryl group and decoupling the ligand vibrational modes from the metal excited states. These two effects, combined with ring fluorination, lengthen excited-state Ln lifetimes to increase quantum efficiencies, resulting in highly NIR emissive materials.

Lanthanide ions with per-fluorobenzeneselenolate (SeC_6F_5) ligands are potentially more emissive than their thiolate analogs, because the lower-energy of Ln-Se vibrations and longer Ln-Se bonds both further decouple Ln* from ligand vibrational processes. In this chapter, the synthesis, characterization, and NIR emission properties of three molecular lanthanide fluorinated selenolate complexes $(DME)_2Ln(SeC_6F_5)_3$ (DME=1,2-Dimethoxyethane; Ln= Nd **(1)**, Er (**2**), Tm (**3**)) are described.

1.2 Synthesis and Structure

Monometallic lanthanide complexes with fluorinated selenolate ligands $(DME)_2Ln(SeC_6F_5)_3$ (Ln = Nd, Er, Tm) have been successfully prepared by the redox reaction of Ln metals with $C_6F_5SeSeC_6F_5$ in DME as the donor solvent, with trace mercury added to catalyze the reaction (Scheme 1.1).

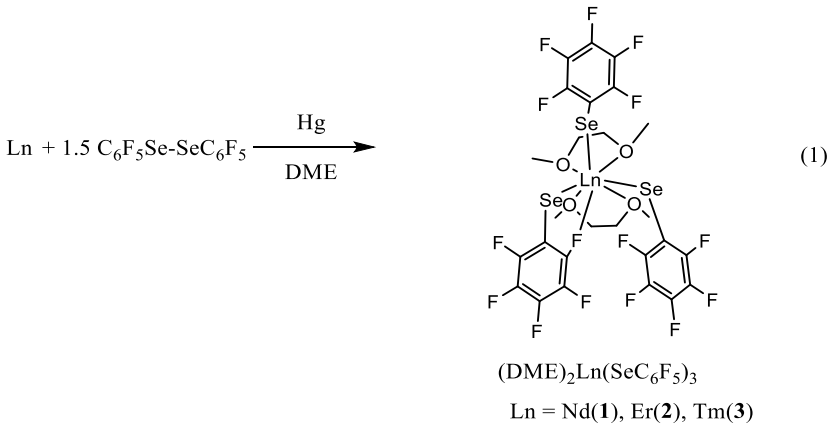

Scheme 1.1. Synthesis of $(DME)_2Ln(SeC_6F_5)_3$ (Ln = Nd **(1)**, Er (**2**), Tm (**3**))

Low temperature X-ray diffraction measurements reveal that all three compounds are isostructural. The crystallographic data and final R indices of **1** and **2** are summarized in Table 1.1, along with a unit cell determination of **3**, which is $P2_1/n$, a = 7.826(3) Å, b = 17.060(5) Å, c = 23.12(1) Å, β = 95.00(2)°, V = 3075.0(2) $Å^3$.

Table 1.1. Summary of crystallographic details for $(DME)_2Nd(SeC_6F_5)_3$ **(1)**, and $(DME)_2Er(SeC_6F_5)_3$ **(2)**

	1	**2**
empirical formula	$C_{26}H_{20}F_{15}O_4Se_3Nd$	$C_{26}H_{20}F_{15}O_4Se_3Er$
fw	1062.54	1085.56
crystal system	monoclinic	monoclinic
space group	$P2_1/n$	$P2_1/n$
a (Å)	7.9291(6)	7.8385(4)
b (Å)	17.1529(13)	17.0475(9)
c (Å)	23.2298(18)	23.1237(12)
α (deg)	90	90
β (deg)	94.5102(16)	95.0070(12)
γ (deg)	90	90
V ($Å^3$)	3149.6(4)	3078.2(3)
Z	4	4
D(calcd) (g/cm^3)	2.241	2.342
T (K)	100(2)	100(2)
abs coeff(mm^{-1})	5.238	6.399
$R(F)^b$ [I > 2σ(I)]	0.0297	0.0521
$R_w(F^2)^c$ [I > 2σ(I)]	0.0682	0.1086

The generalized ORTEP diagrams of **1** and **2** are shown in Figure 1.1 and Figure 1.2, respectively. The significant bond distances and angles are summarized in Table 1.2.

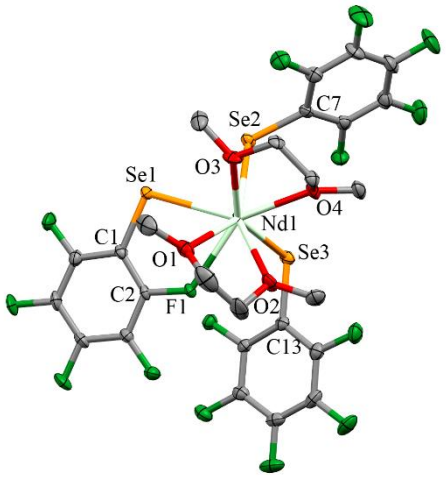

Figure 1.1. ORTEP diagram of $(DME)_2Nd(SeC_6F_5)_3$ (**1**), with orange Se, light green Nd, dark green F, red O, grey C, the H atoms removed for clarity and ellipsoids at the 50% probability level

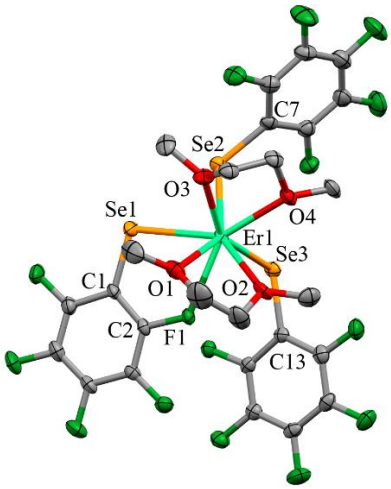

Figure 1.2. ORTEP diagram of $(DME)_2Er(SeC_6F_5)_3$ (**2**), with orange Se, bright green Er, dark green F, red O, grey C, the H atoms removed for clarity and ellipsoids at the 50% probability level

Table 1.2. Significant distances (Å) and angles (°) of **1** and **2**

1		**2**	
Nd(1)-O(1)	2.577(2)	Er(1)-O(1)	2.485(5)
Nd(1)-O(2)	2.482(2)	Er(1)-O(2)	2.408(5)
Nd(1)-O(3)	2.495(2)	Er(1)-O(3)	2.384(4)
Nd(1)-O(4)	2.498(2)	Er(1)-O(4)	2.385(4)
Nd(1)-Se(1)	2.9597(6)	Er(1)-Se(1)	2.8504(7)
Nd(1)-Se(2)	2.9539(4)	Er(1)-Se(2)	2.8776(7)
Nd(1)-Se(3)	2.9414(4)	Er(1)-Se(3)	2.8469(7)
Nd(1)-(F1)	2.6139(17)	Er(1)-(F1)	2.573(3)
C(1)-Se(1)-Nd(1)	99.55(9)	C(1)-Se(1)-Er(1)	99.70(19)
C(7)-Se(2)-Nd(1)	112.77(9)	C(7)-Se(2)-Er(1)	115.32(19)
C(13)-Se(3)-Nd(1)	108.80(9)	C(13)-Se(3)-Er(1)	110.48(19)
C(2)-F(1)-Nd(1)	128.15(16)	C(2)-F(1)-Er(1)	126.8(3)

Each Ln (III) is surrounded by three terminally bound SeC_6F_5 ligands and four oxygen donors from two DME molecules. There is also a dative interaction between Ln (III) and a fluorine atom at the ortho-position on one of the coordinating SeC_6F_5, resulting in an eight-coordinated structure.

A comparison of these selenolate structures with previously described phenoxides and thiolates is informative. All three compounds are monomers, and consistent with the fluorinated ligands withdrawing electron density from the Group 16 element and reducing the tendency of these anions to bridge metal centers. The metal-O(DME) bond

lengths are all consistent, and the Ln-E(C_6F_5) distances are also as expected.[11] The Ln-S and Ln-Se separations increase along with the covalent radius of the chalcogen, while the Ln-O distances are relatively short because of the highly ionic nature of the bond.[12]

The most significant structural difference within the groups is found in the dative interactions between Ln and F. In the phenoxide group there are no significant Ln-F dative interactions, with Ln-O-C angles that range from 129-180°.[10] An absence of Ln-F in these aryloxides has been rationalized in two ways. First, it can be argued that the electronegative O does not delocalize significant charge into the arene ring, so there is no electrostatic basis for a dative Ln-F bond. Second, there is a general consensus that in f-element compounds these obtuse Ln-O-C angles exist because the Ln-O bond is primarily ionic, and a wider angle minimizes repulsions between positive charges on the Ln and the ring carbon.[10]

Thiolates have considerably more acute Ln-S-C angles, and while dative Ln-F interactions in the fluorinated thiolates were noted, the interatomic separations were inconsistent with classic ionic bonding models that predict bond lengths by summing ionic radii.[13] In particular, the 2.881(2) Å Nd-F bond in $(DME)_2Nd(SC_6F_5)_3$[9a] and the 2.948(6) Å Er-F bond in $(DME)_2Er(SC_6F_5)_3$[8b] clearly show that ionic radii alone cannot be used to predict Ln-F separations, since the Nd(III) ion is larger[13] by 0.104 Å but the Nd-F separation is smaller than the Er-F separation by 0.06 Å. It appears in the thiolates that the Ln contraction leads to an increase in ligand-ligand repulsions, and that these forces have their most noticeable impact on the weakest bond, namely the dative Ln-F.

Selenolate behavior is altogether different. A comparison of the thiolates and selenolates reveals considerably shorter Ln-F separations in the selenolates (Nd-F = 2.614(2) Å in **1**, vs. 2.881(2) Å in $(DME)_2Nd(SC_6F_5)_3$,[9a] or Er-F = 2.573(3) Å in **2** vs. 2.948(6) Å in $(DME)_2Er(SC_6F_5)_3$[8b]). Note that in the selenolate compounds the Ln-F separations are now consistent with the changes in Ln ionic radii, with the greater Ln-F separation found for the metal with the larger ionic radius. This at first might seem inconsistent with the rationalization proposed to account for the thiolate structural features, given that in the thiolates the Ln-F separations were interpreted in terms of increasing ligand-ligand repulsions within the primary coordination sphere, and it might be reasonable to assume that the selenolates, with the larger group 16 donor, would be more congested. However, the longer Ln-Se bonds also increase the separation between arene rings, and this can lead to a reduction in ligand-ligand repulsions within the secondary coordination sphere. Stronger dative Ln-F interactions in the selenolates are then rationalized by considering the electronegativity of the Group 16 element, with the more electronegative S localizing electron density at the sulfur, and the less electronegative Se delocalizing more charge into the C_6F_5 ligand and thus onto the fluoride that then binds more strongly to the Ln. A stronger dative Ln-F interaction decreases the separation between the Ln ion and the arene ring, potentially impacting the magnitude of coupling between Ln* and ligand vibrational modes, possibly to the extent that ligand vibrations can quench NIR emission.

1.3 Spectroscopy and Calculation

Luminescent lanthanide ions can realize emissions from visible to near-infrared (NIR) regions. In collaboration with Dr. Ajith Kumar, the emission measurements and related calculations of the lanthanide materials were conducted.

Absorption spectra were recorded at room temperature using a Shimadzu UV-3600 double beam spectrophotometer with samples dissolved in THF at molar concentrations of 0.141 (Nd), 0.054 (Er), and 0.198 (Tm) mol/L.

Emission spectra of the powdered solid samples were obtained at 25ºC by exciting the Nd and Tm samples with the 808 nm band of a Ti-Sapphire laser and Er with a 980 nm diode laser. The emission was focused onto a 0.55 m monochromator (Jobin Yvon, Triax 550, Edison, NJ) and detected by a thermoelectrically cooled InGaAs detector. The signal was intensified with a lock-in amplifier (SR 850 DSP, Stanford Research System, Sunnyvale, CA) and processed with a computer controlled by SynerJY commercial software. To measure the decay time, the laser beam was modulated by a chopper, and the signal was collected on a digital oscilloscope.

Absorption spectra, with the standard spectral assignments for the characteristic absorption bands[14], and emission spectra for **1** - **3** are shown in Figure 1.3 to Figure 1.5, respectively.

The oscillator strengths of the observed transitions summarized in Table 1.3 (a, b, c) shows comparatively higher values relative to previously reported fluorinated thiolates[8b-d] and phenoxides.[8e,10]

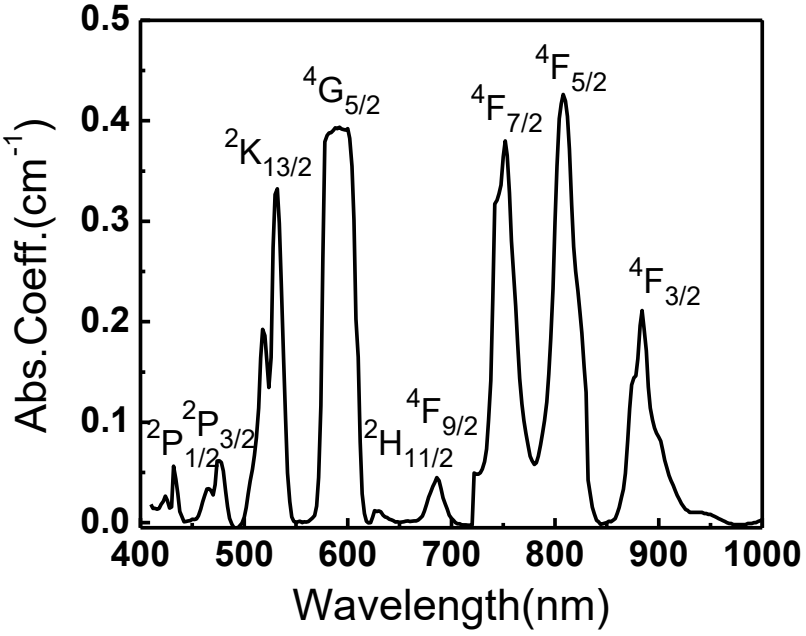

(a)

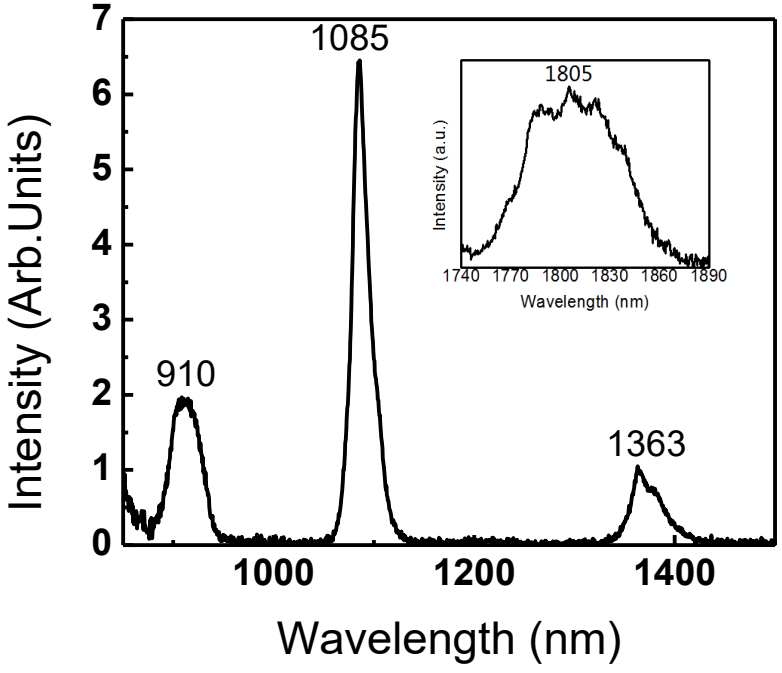

(b)

Figure 1.3. (a) Absorption and (b) emission spectra of $(DME)_2Nd(SeC_6F_5)_3$ (**1**)

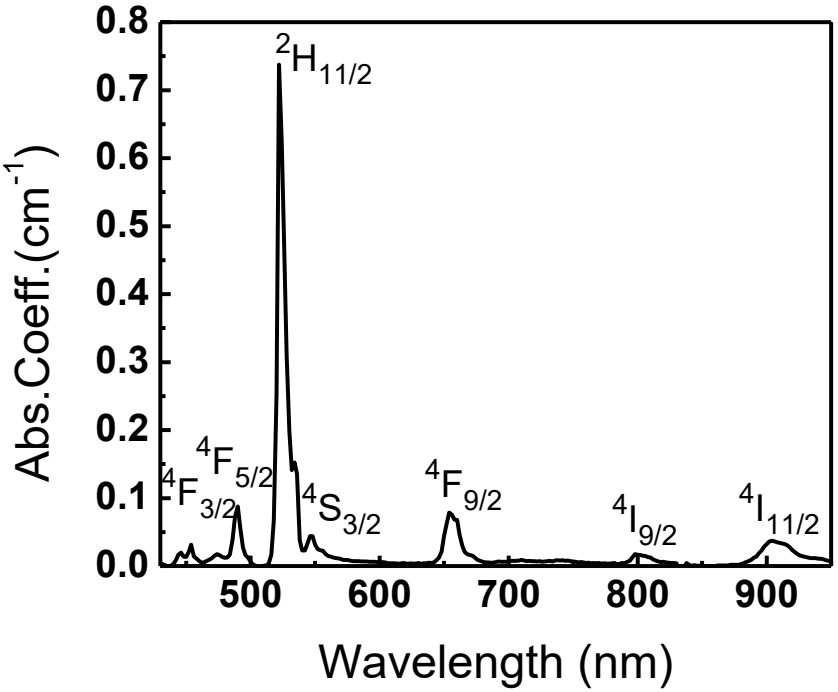

(a)

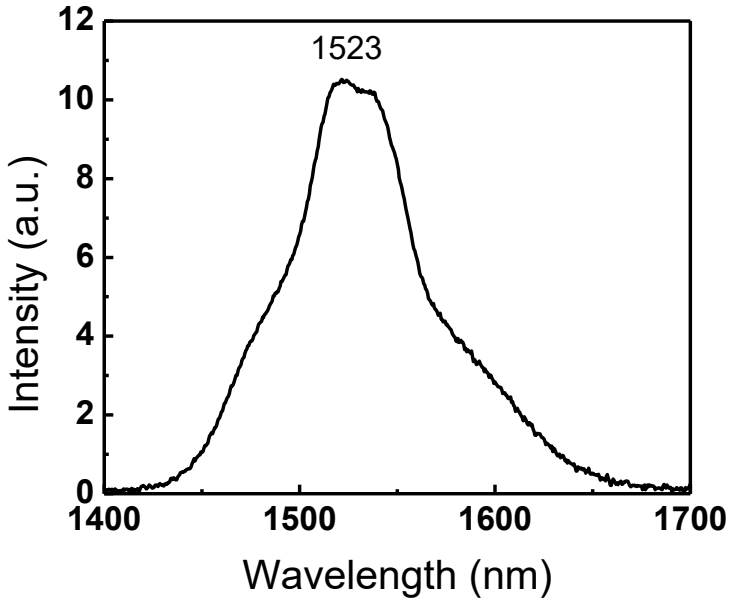

(b)

Figure 1.4. (a) Absorption and (b) emission spectra of $(DME)_2Er(SeC_6F_5)_3$ (**2**)

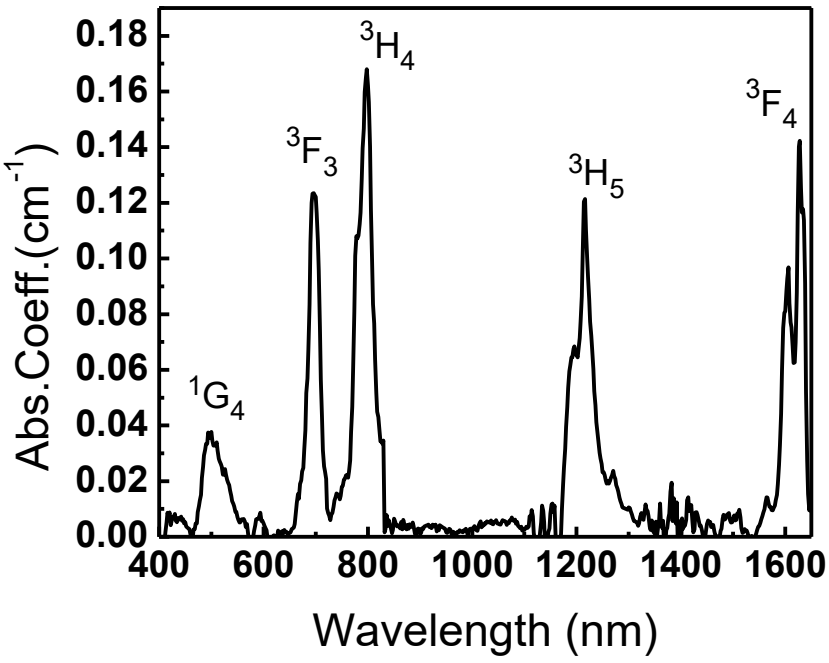

(a)

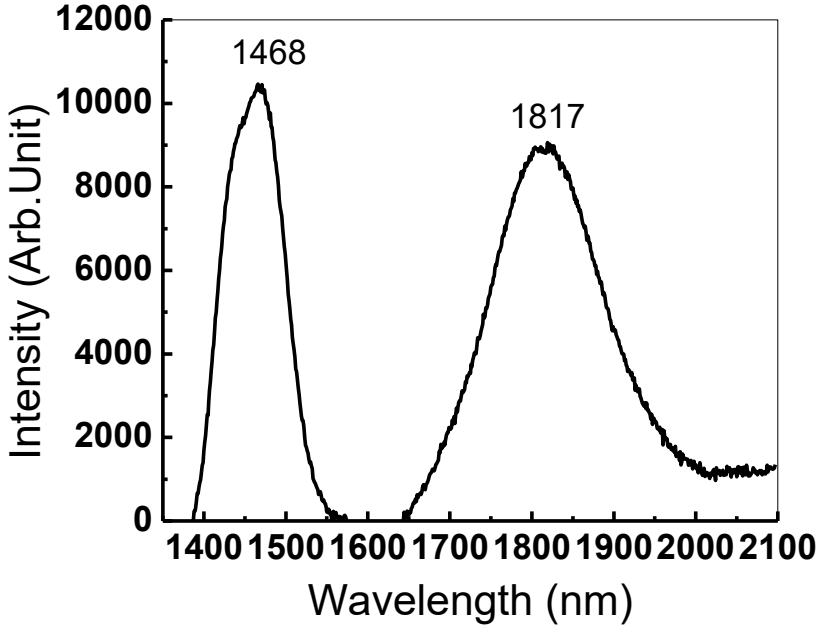

(b)

Figure 1.5. (a) Absorption and (b) emission spectra of $(DME)_2Tm(SeC_6F_5)_3$ (**3**)

Table 1.3. Experimental and calculated oscillator strengths of various transitions in:

(a) $(DME)_2Nd(SeC_6F_5)_3$ (**1**)

Transition (from $^4I_{9/2}$)	Wavelength (nm)	Mol.ext.coef. (L/mol· cm)	$f_{exp}(10^{-6})$	$f_{cal}(10^{-6})$
$^2P_{1/2}$	432.0	32.6	1.01	0.630
$^2P_{3/2}$	476.0	47.2	1.47	0.292
$^2K_{13/2}$	532.0	233	7.24	0.454
$^4G_{5/2}$	590.0	500	15.5	15.6
$^2H_{11/2}$	628.0	4.00	0.124	0.129
$^4F_{9/2}$	686.0	15.9	0.494	0.546
$^4F_{7/2}$+ $^4S_{3/2}$	751.0	182	5.65	5.93
$^2H_{9/2}$+ $^4F_{5/2}$	808.0	187	5.81	6.06
$^4F_{3/2}$	884.0	75.5	2.35	2.19

Judd-Ofelt parameters: Ω_2= 4.72×10^{-20} cm^2, Ω_4= 4.72×10^{-20} cm^2,Ω_6=4.33×10^{-20} cm^2

(b) $(DME)_2Er(SeC_6F_5)_3$ (**2**)

Transition (from $^4I_{15/2}$)	Wavelength (nm)	Mol.ext.coef. (L/mol·cm)	$f_{exp}(10^{-6})$	$f_{cal}(10^{-6})$
$^4I_{11/2}$	980.0	3.78	0.306	1.07
$^4I_{9/2}$	800.0	6.94	0.562	0.224
$^4F_{9/2}$	654.0	32.0	2.60	2.56
$^4S_{3/2}$	545.0	28.0	2.27	0.716
$^2H_{11/2}$	523.0	229	18.6	18.6
$^4F_{5/2}$	490.0	39.2	3.18	3.51
$^4F_{3/2}$	454.0	16.1	1.30	0.500

Judd-Ofelt parameters: Ω_2= 14.44×10^{-20} cm^2, Ω_4= 1.60×10^{-20} cm^2, Ω_6=1.96×10^{-20} cm^2

(c) $(DME)_2Tm(SeC_6F_5)_3$ (**3**)

Transition (from $^3H_6$)	Wavelength (nm)	Mol.ext.coef. (L/mol·cm)	$f_{exp}(10^{-6})$	$f_{cal}(10^{-6})$
$^1G_4$	496	0.192	1.62	1.83
$^3F_3$	696	0.626	1.66	1.61
$^3H_4$	799	0.858	2.24	2.11
$^3H_5$	1217	0.611	0.867	0.966
$^3F_4$	1626	0.727	0.433	0.409

Judd-Ofelt parameters: Ω_2= 2.6×10^{-20} cm^2, Ω_4= 1.7×10^{-20} cm^2, Ω_6=1.85×10^{-20} cm^2

For the Nd^{3+}, Er^{3+} and Tm^{3+} the metastable levels are $^4F_{3/2}$, $^4I_{13/2}$ and $^3H_4$ respectively. Their energy level diagrams are shown in Figure 1.6. Under 808 nm[15] excitation the Nd^{3+} compound **1** yields four emission bands at 910, 1085, 1363 and 1805 nm corresponding to the transitions from $^4F_{3/2}$ to $^4I_{9/2}$, $^4I_{11/2}$, $^4I_{13/2}$ and $^4I_{15/2}$ levels. The fluorescence branching ratio of the first three transitions are respectively 28, 56 and 15%, whereas the emission at 1805 nm is comparatively weak and was collected under different emission slit width settings. This relatively low energy emission is found only for a few materials, [4b,9d] because of the low phonon characteristics of the chalcogenolate ligands.

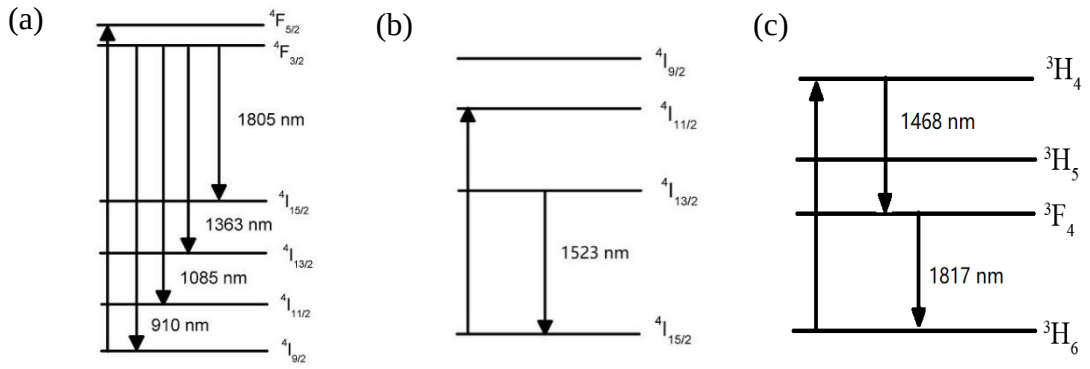

Figure 1.6. Energy level diagrams of (a) Nd, (b) Er, (c) Tm

Spectra for **2** and **3** are less complicated. Emission from the Er compound **2** was collected by exciting the $^4I_{11/2}$ level at 980 nm and the collected emission spectrum shows a broad band centered at 1523 nm with a spectral bandwidth (FWHM) of 80 nm. Similarly, under 808 nm excitation of the $^3H_4$ metastable level of Tm, the emission spectrum shows two bands at 1468 and 1817 nm corresponding to $^3H_4 \rightarrow {}^3F_4$ and $^3F_4 \rightarrow {}^3H_6$ transitions with respective fluorescence branching ratios of 35 and 65%.

All decay curves can be well fitted with a single exponential function as shown in Figure 1.7 for Nd, Er and Tm.

(a)

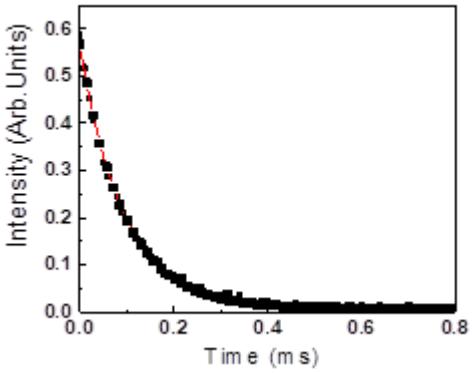

(b)

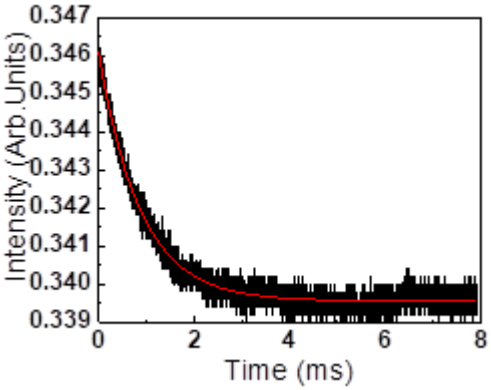

(c)

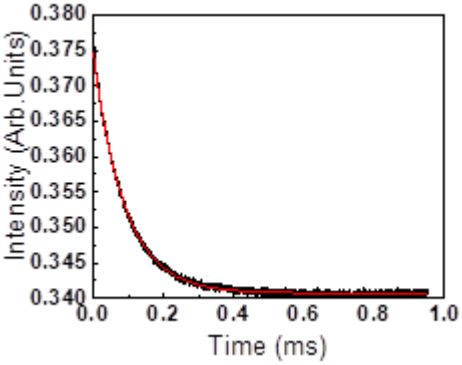

Figure 1.7. Fluorescence decay curves of (a) 1085 nm emission in $(DME)_2Nd(SeC_6F_5)_3$; (b) 1523 nm emission in $(DME)_2Er(SeC_6F_5)_3$; (c) 1468 nm emission in $(DME)_2Tm(SeC_6F_5)_3$.

For the $^4F_{3/2} \rightarrow {}^4I_{11/2}$ emission in Nd, the decay time obtained was 92 μs. With the measured fluorescence decay time, the quantum yield of the 1085 nm emission can be estimated from the ratio of the fluorescence decay time (τ_{fl}) to radiative or "natural" decay time (τ_r).[16] With a calculated radiative decay time of 453 μs following the Judd-Ofelt procedure,[16-17] a quantum efficiency of 20% is obtained for **1**. In compound **2**, a fluorescence decay time of 0.85 ms was obtained for the 1523 nm emission. The radiative quantum efficiency obtained is 16% corresponding to a radiative decay time of 5.3 ms. In **3** the 1468 nm emission yields a radiative quantum yield of 5.2% with the calculated radiative decay time of 1.7 ms and measured decay time of 0.089 ms. It should be noted that all the quantum efficiencies reported here are theoretically computed radiative quantum yields which are normally higher than the real experimentally measured values that have been reported in similar compounds in solid samples[18] and solutions.[19]

The quantum yield of Nd, Er and Tm with similar phenoxide and thiolate compounds are summarized in Table 1.4.

Table 1.4. Quantum efficiencies (%) for $(DME)_2Ln(EC_6F_5)_3$ (Ln = Nd, Er, Tm; E = O, S, Se)

Ln/E	**O**[10]	**S**	**Se**
Nd	2	9.3[8c]	20
Er	16	75[8b]	16
Tm	1.9	2.2[8d]	5.2

The Table 1.4 shows that the efficiencies for the Nd and Tm compounds are increasing in the order from Se > S > O, as expected given the increasingly low-phonon character of the ligands as they descend the periodic chart. Efficiency increases result both from the low vibrational frequency of the Ln-Se bond relative to Ln-S or Ln-O and because the longer Ln-Se bond increases the separation between Ln the arene rings, reducing the tendency of arene vibrations to quench Ln*. The efficiency of the Er compounds show a decrease on moving from S to Se, possibly because the shorter Ln-F distance in the SeC_6F_5 compounds that is allowing a particularly resonant arene ligand vibration to couple more effectively to the Er and significantly decrease the Er emission intensity and efficiency.

1.4 Conclusions

Fluorinated selenolate ligands form stable, easily crystallized compounds with both early and late lanthanides, and these compounds all have relatively short Ln-F dative interactions. With the low-phonon character of the Ln-Se bond, these compounds are exceptionally bright NIR emission sources.

References

(1) (a) Chan, E. M. Combinatorial approaches for developing upconverting nanomaterials: high-throughput screening, modeling, and applications. *Chem. Soc. Rev.* **2015**, *44*, 1653-1679.(b) Xiang, S.; Bao, D. X.; Wang, J.; Li, Y. C.; Zhao, X. Q. Luminescent lanthanide coordination compounds with pyridine-2,6-dicarboxylic acid. *J. Lumin.* **2017**, *186*, 273-282.(c) Brites, C. D. S.; Lima, P. P.; Silva, N. J. O.; Millan, A.; Amaral, V. S.; Palacio, F.; Carlos, L. D. Thermometry at the nanoscale using lanthanide-containing organic-inorganic hybrid materials. *J. Lumin.* **2013**, *133*, 230-232.(d) Di Bari, L.; Salvadori, P. Solution structure of chiral lanthanide complexes. *Coord. Chem. Rev.* **2005**, *249*, 2854-2879.(e) Dwivedi, Y.; Zilio, S. C. Advances in Rare Earth Spectroscopy and Applications. *J. Nanosci. Nanotechno.* **2014**, *14*, 1578-1596.(f) Bunzli, J. C. G. Review: Lanthanide coordination chemistry: from old concepts to coordination polymers. *J. Coord. Chem.* **2014**, *67*, 3706-3733.(g) Martinez-Gomez, N. C.; Vu, H. N.; Skovran, E. Lanthanide Chemistry: From Coordination in Chemical Complexes Shaping Our Technology to Coordination in Enzymes Shaping Bacterial Metabolism. *Inorg. Chem.* **2016**, *55*, 10083-10089.(h) Hackett, T. A.; Baldwin, D. J.; Paudyal, D. Electronic, magnetic, and magnetocrystalline anisotropy properties of light lanthanides. *J. Magn. Magn. Mater.* **2017**, *441*, 76-84.(i) Xia, Z. G.; Meijerink, A. Ce^{3+}-Doped garnet phosphors: composition modification, luminescence properties and applications. *Chem. Soc. Rev.* **2017**, *46*, 275-299.(j) Pointillart, F.; Cador, O.; Le Guennic, B.; Ouahab, L. Uncommon lanthanide ions in purely 4f Single Molecule Magnets. *Coord. Chem. Rev.* **2017**, *346*, 150-175.(k) Levason, W. Chemistry and applications of the lanthanides. *Coord. Chem. Rev.* **2017**, *340*, 1.

(2) (a) Thielemann, D. T.; Wagner, A. T.; Rosch, E.; Kolmel, D. K.; Heck, J. G.; Rudat, B.; Neumaier, M.; Feldmann, C.; Schepers, U.; Brase, S.; Roesky, P. W. Luminescent Cell-Penetrating Pentadecanuclear Lanthanide Clusters. *J. Am. Chem. Soc.* **2013**, *135*, 7454-7457.(b) Chan, W. T. K.; Wong, W. T. Recent development in lanthanide coordination compounds for biomedical imaging applications. *Polyhedron* **2014**, *83*, 150-158.(c) Bunzli, J. C. G. Lanthanide light for biology and medical diagnosis. *J. Lumin.* **2016**, *170*, 866-878.(d) Mihorianu, M.; Leonzio, M.; Monari, M.; Ravotto, L.; Ceroni, P.; Bettinelli, M.; Piccinelli, F. Structural and Spectroscopic Properties of New Chiral Quinoline-based Ln(III) Complexes. *Chemistryselect* **2016**, *1*, 1996-2003.(e) Goryacheva, O. A.; Beloglazova, N. V.; Vostrikova, A. M.; Pozharov, M. V.; Sobolev, A. M.; Goryacheva, I. Y. Lanthanide-to-quantum dot Forster resonance energy transfer (FRET): Application for immunoassay. *Talanta* **2017**, *164*, 377-385.(f) Zhang, Q.; Tian, X. H.; Zhou, H. P.; Wu, J. Y.; Tian, Y. P. Lighting the Way to See Inside Two-Photon Absorption Materials: Structure-Property Relationship and

Biological Imaging. *Materials* **2017**, *10*, 223-269.(g) Zeng, H. F.; Li, X. Y.; Sun, M. Y.; Wu, S. F.; Chen, H. F. Synthesis of Europium-Doped Fluorapatite Nanorods and Their Biomedical Applications in Drug Delivery. *Molecules* **2017**, *22*, 753-759.(h) Valencia, C.; Dujet, C.; Margathe, J. F.; Iturrioz, X.; Roux, T.; Trinquet, E.; Villa, P.; Hibert, M.; Dupuis, E.; Llorens-Cortes, C.; Bonnet, D. A Time-Resolved FRET Cell-Based Binding Assay for the Apelin Receptor. *Chemmedchem* **2017**, *12*, 925-931.

(3) (a) Sivakumar, S.; Reddy, M. L. P. Bright green luminescent molecular terbium plastic materials derived from 3,5-bis(perfluorobenzyloxy)benzoate. *J. Mater. Chem.* **2012**, *22*, 10852-10859.(b) Tan, M. C.; Naczynski, D. J.; Moghe, P. V.; Riman, R. E. Engineering the Design of Brightly-Emitting Luminescent Nanostructured Photonic Composite Systems. *Aust. J. Chem.* **2013**, *66*, 1008-1020.(c) Ye, H.; Li, Z.; Peng, Y.; Wang, C.; Li, T.; Zheng, Y.; Sapelkin, A.; Adamopoulos, G.; Hernández, I.; Wyatt, P. Organo-erbium systems for optical amplification at telecommunications wavelengths. *Nat. Mater.* **2014**, *13*, 382-386.(d) Peng, Y.; Hu, J. X.; Lu, H.; Wilson, R. M.; Motevalli, M.; Hernandez, I.; Gillin, W. P.; Wyatt, P. B.; Ye, H. Q. Functionalisation of ligands through click chemistry: long-lived NIR emission from organic Er(III) complexes with a perfluorinated core and a hydrogen-containing shell. *RSC Adv.* **2017**, *7*, 128-131.(e) Zhang, X. G.; Wu, Z. C.; Li, Y. C.; Xu, J. G.; Tian, L. Structure, energy level analysis and luminescent properties of a novel broadband blue-emitting phosphor $KBaYSi_2O_7$: Ce^{3+}. *Dyes Pigments* **2017**, *144*, 94-101.(f) Wang, S. S.; Xu, J.; Wang, J.; Wang, K. Y.; Dang, S.; Song, S. Y.; Liu, D.; Wang, C. Luminescence of samarium(III) bis-dithiocarbamate frameworks: codoped lanthanide emitters that cover visible and near-infrared domains. *J. Mater. Chem. C* **2017**, *5*, 6620-6628.(g) Qin, X.; Liu, X. W.; Huang, W.; Bettinelli, M.; Liu, X. G. Lanthanide-Activated Phosphors Based on 4f-5d Optical Transitions: Theoretical and Experimental Aspects. *Chem. Rev.* **2017**, *117*, 4488-4527.

(4) (a) Wachtler, M.; Speghini, A.; Gatterer, K.; Fritzer, H. P.; Ajo, D.; Bettinelli, M. Optical properties of rare-earth ions in lead germanate glasses. *J. Am. Ceram. Soc.* **1998**, *81*, 2045-2052.(b) Kornienko, A.; Moore, B. F.; Kumar, G. A.; Tan, M. C.; Riman, R. E.; Brik, M. G.; Emge, T. J.; Brennan, J. G. Highly NIR-Emissive Lanthanide Polyselenides. *Inorg. Chem.* **2011**, *50*, 9184-9190.(c) Trivedi, E. R.; Eliseeva, S. V.; Jankolovits, J.; Olmstead, M. M.; Petoud, S.; Pecoraro, V. L. Highly emitting near-infrared lanthanide "encapsulated sandwich" metallacrown complexes with excitation shifted toward lower energy. *J. Am. Chem. Soc.* **2014**, *136*, 1526-1534.(d) Pan, M.; Du, B. B.; Zhu, Y. X.; Yue, M. Q.; Wei, Z. W.; Su, C. Y. Highly Efficient Visible-to-NIR Luminescence of Lanthanide (III) Complexes with Zwitterionic Ligands Bearing Charge-Transfer Character: Beyond Triplet Sensitization. *Chem. Eur. J.* **2016**, *22*, 2440-2451.(e) Bünzli, J.-C. G. In *Handbook on the Physics and*

Chemistry of Rare Earths; Elsevier, **2016**; Vol. 50.(f) Zheng, Y. H.; Zhang, C. C.; Wang, Q. M. Prevailing paradigms in novel lanthanide optical probes from molecular complexes to hybrid materials. *Sensors Actuat. B-Chem.* **2017**, *245*, 622-640.

(5) (a) Bunzli, J. C. G. On the design of highly luminescent lanthanide complexes. *Coord. Chem. Rev.* **2015**, *293*, 19-47.(b) Zucchi, G.; Maury, O.; Thuery, P.; Gumy, F.; Bunzli, J. C. G.; Ephritikhine, M. 2,2 '-Bipyrimidine as Efficient Sensitizer of the Solid-State Luminescence of Lanthanide and Uranyl Ions from Visible to Near-Infrared. *Chem. Eur. J.* **2009**, *15*, 9686-9696.(c) Subhan, M. A.; Suzuki, T.; Fuyuhiro, A.; Kaizaki, S. Synthesis, X-ray structures and NIR chiroptical properties of a series of dinuclear lanthanide(III) complexes [Ln_2{μ-(S- or RS-pba)$_4$}(HBpz$_3$)$_2$]; novel configurational chirality due to non-bonding Ln···O interactions. *Dalton Trans.* **2003**, 3785-3791.(d) Kumar, G. A.; Riman, R. E.; Brennan, J. G. NIR emission from molecules and clusters with lanthanide-chalcogen bonds. *Coord. Chem. Rev.* **2014**, *273*, 111-124.(e) Li, F. F.; Li, C. G.; Liu, X. M.; Bai, T. Y.; Dong, W. J.; Zhang, X.; Shi, Z.; Feng, S. H. Microwave-assisted synthesis and up-down conversion luminescent properties of multicolor hydrophilic LaF_3:Ln^{3+} nanocrystals. *Dalton Trans.* **2013**, *42*, 2015-2022.(f) Sun, L. N.; Qiu, Y. N.; Liu, T.; Feng, J.; Deng, W.; Shi, L. Y. Visible-near-infrared luminescent lanthanide ternary complexes based on beta-diketonate using visible-light excitation. *Luminescence* **2015**, *30*, 1071-1076.(g) Echenique-Errandonea, E.; Oyarzabal, I.; Cepeda, J.; Sebastian, E. S.; Rodriguez-Dieguez, A.; Seco, J. M. Photoluminescence and magnetic analysis of a family of lanthanide(III) complexes based on diclofenac. *New J. Chem.* **2017**, *41*, 5467-5475.(h) Ilichev, V. A.; Blinova, L. I.; Rozhkov, A. V.; Balashova, T. V.; Rumyantcev, R. V.; Fukin, G. K.; Bochkarev, M. N. Fluorinated mercaptobenzothiazolates of lanthanides: Synthesis, structure and photoluminescence. *J. Mol. Struct.* **2017**, *1148*, 201-205.

(6) (a) Shi, M.; Li, F. Y.; Yi, T.; Zhang, D. Q.; Hu, H. M.; Huang, C. H. Tuning the triplet energy levels of pyrazolone ligands to match the $^5D_0$ level of europium(III). *Inorg. Chem.* **2005**, *44*, 8929-8936.(b) Holler, C. J.; Matthes, P. R.; Adlung, M.; Wickleder, C.; Muller-Buschbaum, K. Antenna- and Metal-Triggered Luminescence in Dense 1,3-Benzodinitrile Metal-Organic Frameworks $_\infty{}^3$[$LnCl_3$(1,3-Ph(CN)$_2$)], Ln = Eu, Tb. *Eur. J. Inorg. Chem.* **2012**, 5479-5484.(c) Karhunen, U.; Soikkeli, M.; Landenpera, S.; Soukka, T. Quantitative detection of well-based DNA array using switchable lanthanide luminescence. *Anal. Chim. Acta.* **2013**, *772*, 87-92.(d) Xu, H.; Sun, Q.; An, Z. F.; Wei, Y.; Liu, X. G. Electroluminescence from europium(III) complexes. *Coord. Chem. Rev.* **2015**, *293*, 228-249.

(7) (a) Hasegawa, Y.; Kimura, Y.; Murakoshi, K.; Wada, Y.; Kim, J. H.; Nakashima,

N.; Yamanaka, T.; Yanagida, S. Enhanced emission of deuterated tris(hexafluoroacetylacetonato)neodymium(III) complex in solution by suppression of radiationless transition via vibrational excitation. *J. Phys. Chem.* **1996**, *100*, 10201-10205.(b) Hebbink, G. A.; Reinhoudt, D. N.; van Veggel, F. C. J. M. Increased luminescent lifetimes of Ln^{3+} complexes emitting in the near-infrared as a result of deuteration. *Eur. J. Org. Chem.* **2001**, 4101-4106.(c) Browne, W. R.; Vos, J. G. The effect of deuteriation on the emission lifetime of inorganic compounds. *Coord. Chem. Rev.* **2001**, *219*, 761-787.(d) Glover, P. B.; Bassett, A. P.; Nockemann, P.; Kariuki, B. M.; Van Deun, R.; Pikramenou, Z. Fully fluorinated imidodiphosphinate shells for visible- and NIR-Emitting lanthanides: Hitherto unexpected effects of sensitizer fluorination on lanthanide emission properties. *Chem. Eur. J.* **2007**, *13*, 6308-6320.(e) Pitois, C.; Hult, A.; Lindgren, M. Lanthanide-cored fluorinated dendrimer complexes: synthesis and luminescence characterization. *J. Lumin.* **2005**, *111*, 265-283.(f) Hu, J. Y.; Ning, Y.; Meng, Y. S.; Zhang, J.; Wu, Z. Y.; Gao, S.; Zhang, J. L. Highly near-IR emissive ytterbium(III) complexes with unprecedented quantum yields. *Chem. Sci.* **2017**, *8*, 2702-2709.

(8) (a) Ilichev, V. A.; Rozhkov, A. V.; Rumyantcev, R. V.; Fukin, G. K.; Grishin, I. D.; Dmitriev, A. V.; Lypenko, D. A.; Maltsev, E. I.; Yablonskiy, A. N.; Andreev, B. A.; Bochkarev, M. N. LMCT facilitated room temperature phosphorescence and energy transfer in substituted thiophenolates of Gd and Yb. *Dalton Trans.* **2017**, *46*, 3041-3050.(b) Kumar, G. A.; Riman, R. E.; Torres, L. A. D.; Garcia, O. B.; Banerjee, S.; Kornienko, A.; Brennan, J. G. Chalcogenide-bound erbium complexes: Paradigm molecules for infrared fluorescence emission. *Chem. Mater.* **2005**, *17*, 5130-5135.(c) Kumar, G. A.; Riman, R. E.; Torres, L. A. D.; Banerjee, S.; Romanelli, A. D.; Emge, T. J.; Brennan, J. G. Near-infrared optical characteristics of chalcogenide-bound Nd^{3+} molecules and clusters. *Chem. Mater.* **2007**, *19*, 2937-2946.(d) Banerjee, S.; Kumar, G. A.; Emge, T. J.; Riman, R. E.; Brennan, J. G. Thiolate-bound thulium compounds: Synthesis, structure, and NIR emission. *Chem. Mater.* **2008**, *20*, 4367-4373.(e) Maleev, A. A.; Fagin, A. A.; Ilichev, V. A.; Lopatin, M. A.; Konev, A. N.; Samsonov, M. A.; Fukin, G. K.; Bochkarev, M. N. Lanthanide pentafluorophenolates. Synthesis, structure and luminescent properties. *J. Organomet. Chem.* **2013**, *747*, 126-132.

(9) (a) Banerjee, S.; Huebner, L.; Romanelli, M. D.; Kumar, G. A.; Riman, R. E.; Emge, T. J.; Brennan, J. G. Oxoselenido clusters of the lanthanides: Rational introduction of oxo ligands and near-IR emission from Nd(III). *J. Am. Chem. Soc.* **2005**, *127*, 15900-15906.(b) Kornienko, A.; Emge, T. J.; Kumar, G. A.; Riman, R. E.; Brennan, J. G. Lanthanide clusters with internal Ln ions: Highly emissive molecules with solid-state cores. *J. Am. Chem. Soc.* **2005**, *127*, 3501-3505.(c) Romanelli, M.; Kumar, G. A.; Emge, T. J.; Riman, R. E.; Brennan, J.

G. Intense near-IR emission from nanoscale lanthanoid fluoride clusters. *Angew. Chem. Int. Ed.* **2008**, *47*, 6049-6051.(d) Moore, B. F.; Kumar, G. A.; Tan, M. C.; Kohl, J.; Riman, R. E.; Brik, M. G.; Emge, T. J.; Brennan, J. G. Lanthanide Clusters with Chalcogen Encapsulated Ln: NIR Emission from Nanoscale $NdSe_x$. *J. Am. Chem. Soc.* **2011**, *133*, 373-378.(e) Banerjee, S.; Kumar, G. A.; Riman, R. E.; Emge, T. J.; Brennan, J. G. Oxoclusters of the lanthanides begin to resemble solid-state materials at very small cluster sizes: Structure and NIR emission from Nd(III). *J. Am. Chem. Soc.* **2007**, *129*, 5926-5931.(f) Kornienko, A.; Banerjee, S.; Kumar, G. A.; Riman, R. E.; Emge, T. J.; Brennan, J. G. Heterometallic chalcogenido clusters containing lanthanides and main group metals: Emissive precursors to ternary solid-state compounds. *J. Am. Chem. Soc.* **2005**, *127*, 14008-14014.

(10) Norton, K.; Kumar, G. A.; Dilks, J. L.; Emge, T. J.; Riman, R. E.; Brik, M. G.; Brennan, J. G. Lanthanide Compounds with Fluorinated Aryloxide Ligands: Near-Infrared Emission from Nd, Tm, and Er. *Inorg. Chem.* **2009**, *48*, 3573-3580.

(11) Hillier, A. C.; Liu, S. Y.; Sella, A.; Elsegood, M. R. J. Lanthanide chalcogenolate complexes: Synthesis and crystal structures of the isoleptic series $[Sm(Tp(Me,Me))_2ER]$ (E = O, S, Se, Te; Tp(Me,Me) = tris-3,5-dimethylpyrazolylborate). *Inorg. Chem.* **2000**, *39*, 2635-2644.

(12) Schomaker, V.; Stevenson, D. P. Some Revisions of the Covalent Radii and the Additivity Rule for the Lengths of Partially Ionic Single Covalent Bonds. *J. Am. Chem. Soc.* **1941**, *63*, 37-40.

(13) Shannon, R. D. Revised Effective Ionic Radii and Systematic Studies of Interatomic Distances in Halides and Chalcogenides. *Acta Crystallogr. Sect. A: Found. Crystallogr.* **1976**, *A32*, 751-767.

(14) (a) Krupke, W. F.; Gruber, J. B. Optical-Absorption Intensities of Rare-Earth Ions in Crystals: the Absorption Spectrum of Thulium Ethyl Sulfate. *Phys. Rev.* **1965**, *139*, 2008-2016.(b) Edvardsson, S.; Wolf, M.; Thomas, J. O. Sensitivity of Optical-Absorption Intensities for Rare-Earth Ions. *Phys. Rev. B* **1992**, *45*, 10918-10923.

(15) Ding, M. Y.; Xu, M.; Lu, C. H.; Xi, J. H.; Ji, Z. G.; Chen, D. Q. 808 nm NIR light excited single-band red upconversion emission in lanthanide-doped $KMnF_3$ nanocrystals. *J. Alloys Compd.* **2017**, *721*, 531-537.

(16) Judd, B. R. Optical Absorption Intensities of Rare-Earth Ions. *Phys. Rev.* **1962**, *127*, 750-761.

(17) Ofelt, G. S. Intensities of crystal spectra of rare-earth ions. *J. Chem. Phys.* **1962**,

37, 511-520.

(18) Batrice, R. J.; Ridenour, J. A.; Ayscue, R. L.; Bertke, J. A.; Knope, K. E. Synthesis, structure, and photoluminescent behaviour of molecular lanthanide-2-thiophenecarboxylate-2,2 ':6 ',2 "-terpyridine materials. *CrystEngComm* **2017**, *19*, 5300-5312.

(19) (a) Hasegawa, Y.; Ohkubo, T.; Sogabe, K.; Kawamura, Y.; Wada, Y.; Nakashima, N.; Yanagida, S. Luminescence of novel neodymium sulfonylaminate complexes in organic media. *Angew. Chem. Int. Ed.* **2000**, *39*, 357-360.(b) Aebischer, A.; Gumy, F.; Bunzli, J. C. G. Intrinsic quantum yields and radiative lifetimes of lanthanide tris(dipicolinates). *Phys. Chem. Chem. Phys.* **2009**, *11*, 1346-1353.

Chapter 2. Molecular Thorium Compounds with Dichalcogenide Ligands

2.1 Introduction

Understanding the complicated nature of bonding in actinide (An) systems remains one of the great challenges in inorganic chemistry, given our incomplete understanding of how much the radially extended 5f orbitals are involved in covalent interactions. In the quest to prepare and characterize appropriately insightful An molecules with significant covalent bonding character, ligands with less electronegative chalcogen (E; E = S, Se, Te) based anions are particularly attractive synthetic targets. Actinide compounds with An-E bonds are also appealing from a reactivity perspective, because these bonds are relatively weak and thus a potential source of controllable reactivity.

Compounds with An-E bonds are found with RE^-,[1] E^{2-},[1b-d,2] or $(E_n)^{2-}$ ligand systems, and of the three, the polychalcogenides (E_n^{2-}, n = 2,[2e-i,3] 3,[1g,2n,3b,4] 4,[2i,5] 5[6]) are the least well developed molecular class. Recent work has explored chemistry with sterically demanding ancillary ligands (i.e. silylamides,[1g,2h,3b-d,7] substituted cyclopentadienyls,[1k-p,2c,k,l,3e,6,8] pyrazolylborates,[1q,r,3f,9] branched alkoxides[1p]), because these ancillaries impart solubility in polar solvents that facilitates crystallization, and because their steric bulk inhibits ligand redistribution reactions. Control of steric properties within the primary and secondary coordination sphere in actinide molecules is critical to the

preparation of synthetically challenging motifs, i.e. the recent preparation of remarkable compounds with terminal An=E bonds.[3d,7d,10] In contrast, when it becomes interesting to prepare increasingly large polymetallic compounds in order to monitor size dependent physical properties,[11] sterically demanding ligands can be a liability, and it becomes advantageous to work with sterically undemanding ancillaries.

Polychalcogenide chemistry is particularly attractive because E-E bonds are readily reduced, providing chemists with a potential source of reactivity for rationally building larger clusters or heterometallic compounds. Actinide compounds with EE ligands can be prepared with less congested coordination environments, although success in this area has thus far been restricted to compounds of uranium. The first example of an actinide molecule with a dichalcogenide ligand was the uranyl dication $UO_2(thiocarbamate)_2(SS)^{2+}$ prepared by the thermal decomposition of a uranyl thiocarbamate methoxide precursor.[3a] This report was eventually followed by the successful synthesis of $[U(Se_2)_4]^{4-}$,[12] $[UO_2(SS)_3]^{4-}$,[13] and the imido analog $[(Bu_2bipyridine)U(NBu)_2I]_2Se_4$.[5]

Related chemistry with thorium is important, because diamagnetic Th(IV) affords an opportunity to probe solution structure, speciation, and reactivity, particularly with compounds of selenium, since the large NMR chemical shift dispersion of ^{77}Se has been useful[3d,14] for correlating solution and solid state structure/dynamics in both $Th(SeR)_4$ molecules and cubane clusters.[1b,s] This chapter outlines the synthesis and characterization of six dichalcogenido bridged thorium dimers, formed in the ligand

based redox reactions of thorium selenolates with elemental chalcogen. A powerful combination of ^{77}Se NMR and relativistic DFT calculations is used to show that the well-defined solid-state structures are maintained in solution, and an investigation into the thermal decomposition reactions of the halogenated materials shows that ThE_2, rather than ternary solid-state compounds, is produced.

2.2 Synthesis and Structure

Ligand based redox reactions of thorium halide/chalcogenolates with elemental E give high yields of bimetallic thorium compounds with bridging $(E_2)^{2-}$ ligands. Addition of elemental E to solutions of "$ThI_n(EPh)_{4-n}$" or "$ThX_n(SC_6F_5)_m(EPh)_{4-(n+m)}$" (E = S, Se; X = I, Br and n = 1 to 4) leads to the reduction of E to give $(E_2)^{2-}$, oxidation of EPh^- to give PhEEPh, and the formation of $(py)_6Th_2I_4(E_2)_2$ (Scheme 2.1) or $(py)_6Th_2X_2(SC_6F_5)_2(E_2)_2$ (Scheme 2.2).

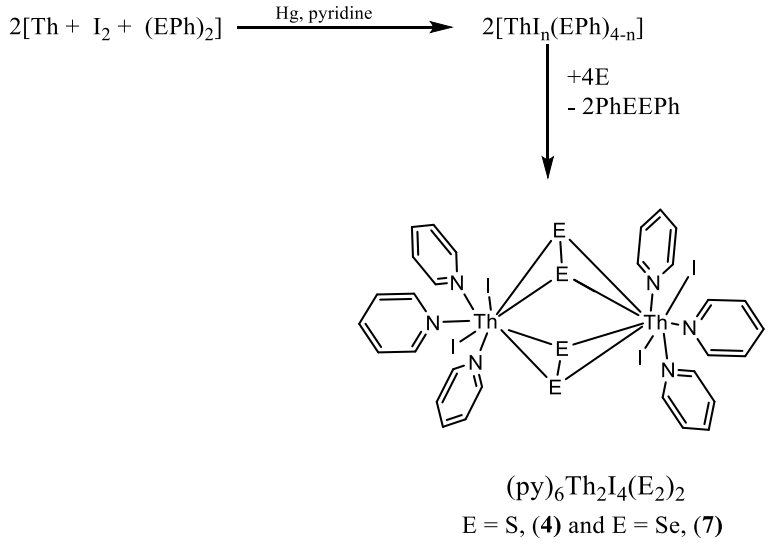

Scheme 2.1. Synthesis of dichalcogenido bridged thorium dimers with terminal iodides

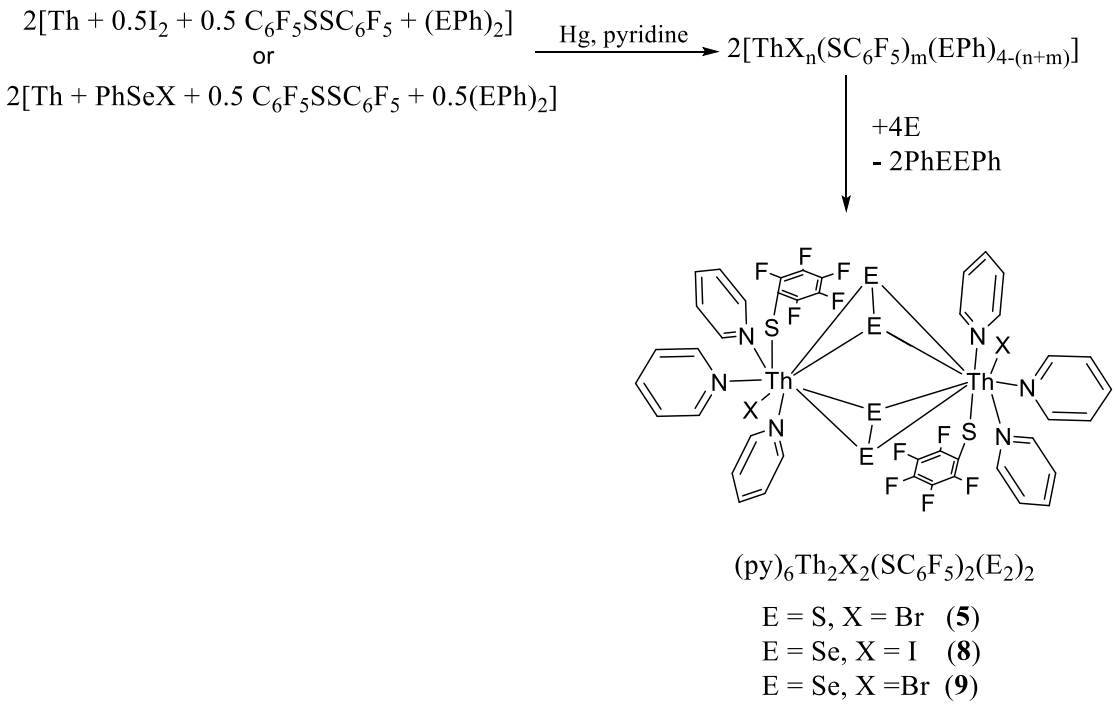

Scheme 2.2. Synthesis of dichalcogenido bridged thorium dimers with ancillary halides and fluorinated thiolates

A similar redox approach to the synthesis of the disulfido compounds in the presence of chloride ion led to formation of a product mixture, which includes $(py)_6Th_2Cl_2(SC_6F_5)_2S_4$ (**6**) and $(py)_4ThCl_4$ (**10**) (Scheme 2.3).

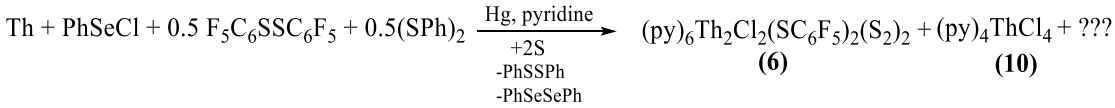

Scheme 2.3. Synthetic attempt to prepare disulfido bridged thorium dimer with terminally bound chloride and fluorothiolate ligands

Similarly, attempts to make a diselenido thorium dimer with terminal fluorothiolate and chloride led to the isolation of a crystalline mixture containing $(py)_4ThCl_4$ (**10**) and the thorium heterocubane $(py)_8Th_4Se_4(SePh)_4(SC_6F_5)_4$[1b] (Scheme 2.4).

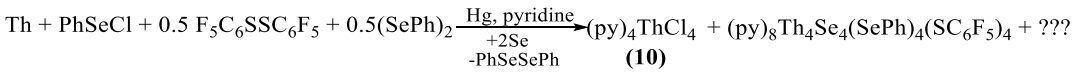

Scheme 2.4. Synthetic attempt to prepare diselenido bridged thorium dimer with terminally bound chloride and fluorothiolate ligands

Thermal ellipsoid diagrams for **4 - 9** are shown in Figures 2.1 - 2.6, respectively.

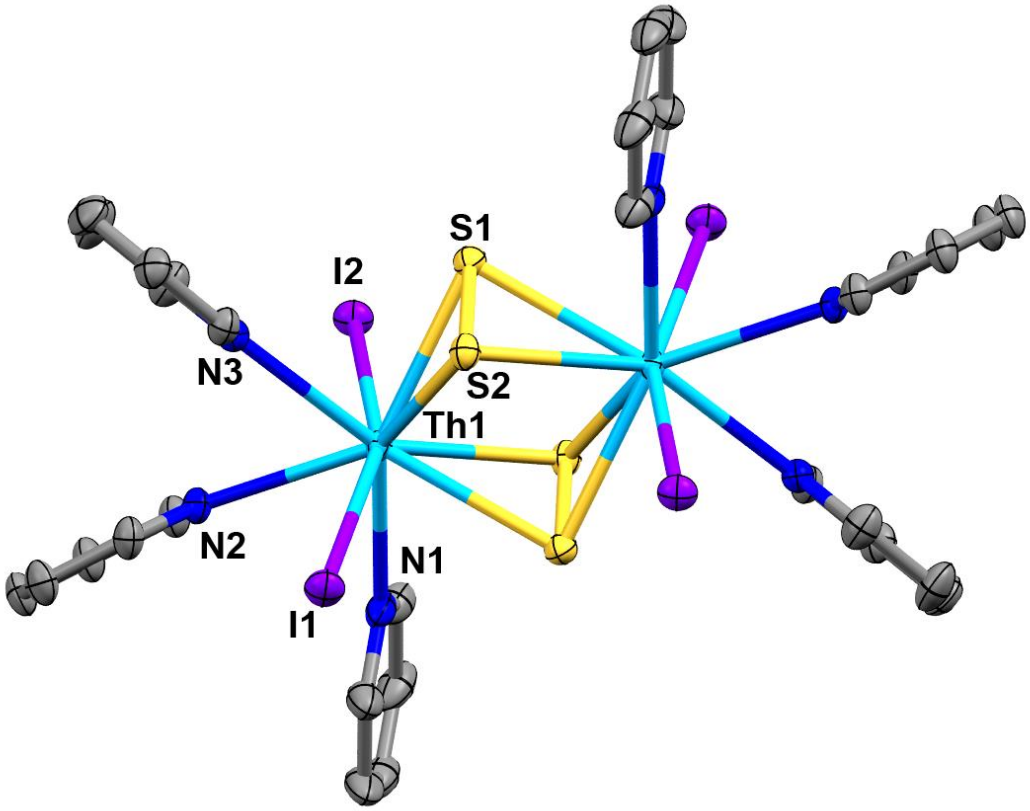

Figure 2.1. ORTEP diagram of $(py)_6Th_2I_4(S_2)_2$ **(4)**, with yellow S, purple I, light blue Th, dark blue N, grey C, the H atoms removed for clarity and ellipsoids at the 50% probability level

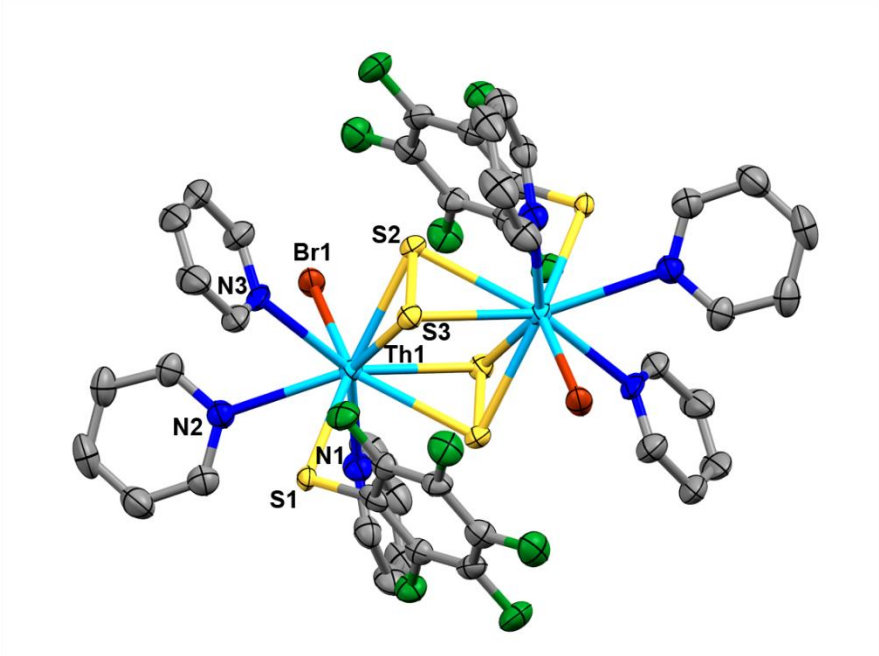

Figure 2.2 ORTEP diagram of $(py)_6Th_2Br_2(SC_6F_5)_2(S_2)_2$ **(5)**, with green F, yellow S, red Br, light blue Th, dark blue N, grey C, the H atoms removed for clarity, and ellipsoids at the 50% probability level

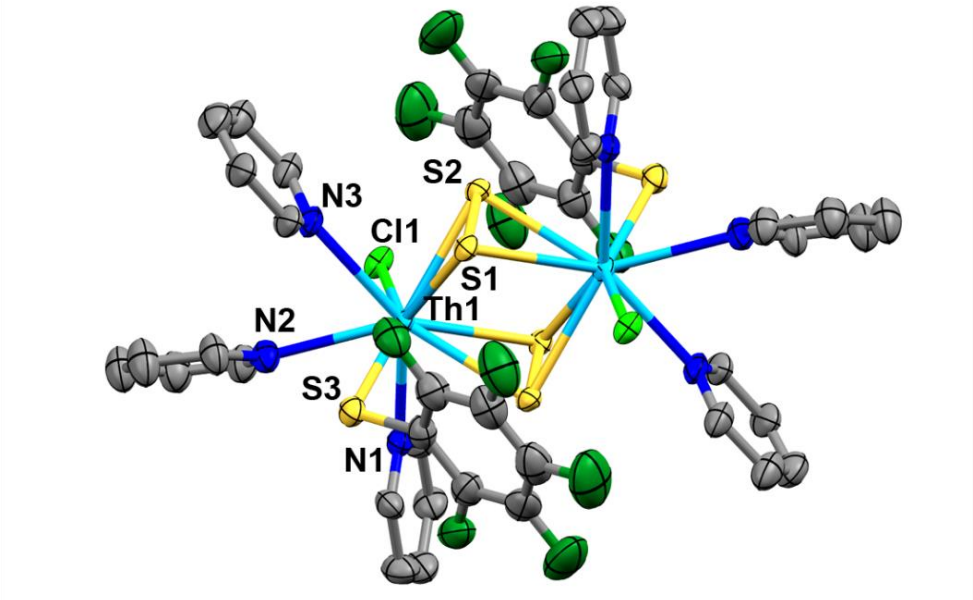

Figure 2.3. ORTEP diagram of $(py)_6Th_2Cl_2(SC_6F_5)_2(S_2)_2$ **(6)**, with dark green F, yellow S, light green Cl, light blue Th, dark blue N, grey C, the H atoms removed for clarity, and ellipsoids at the 50% probability level

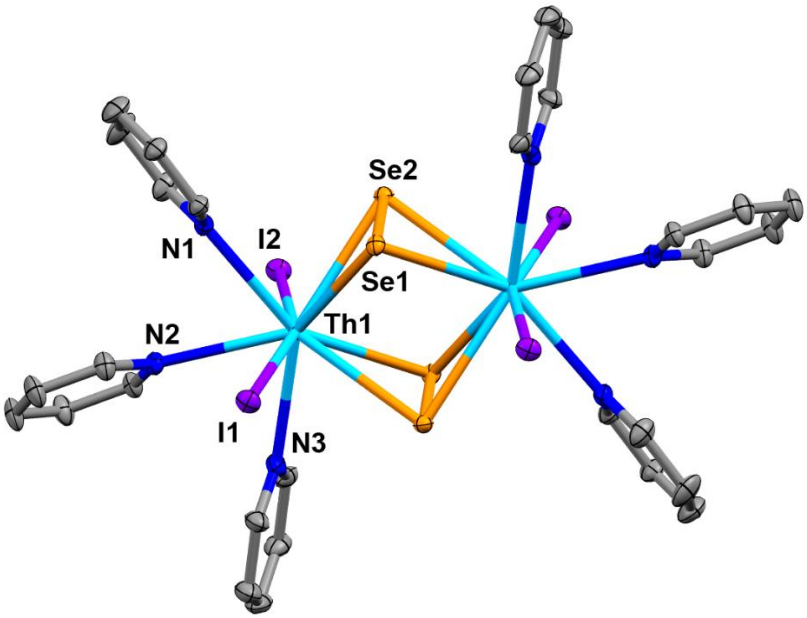

Figure 2.4. ORTEP diagram of $(py)_6Th_2I_4(Se_2)_2$ **(7)**, with orange Se, purple I, light blue Th, dark blue N, grey C, the H atoms removed for clarity and ellipsoids at the 50% probability level

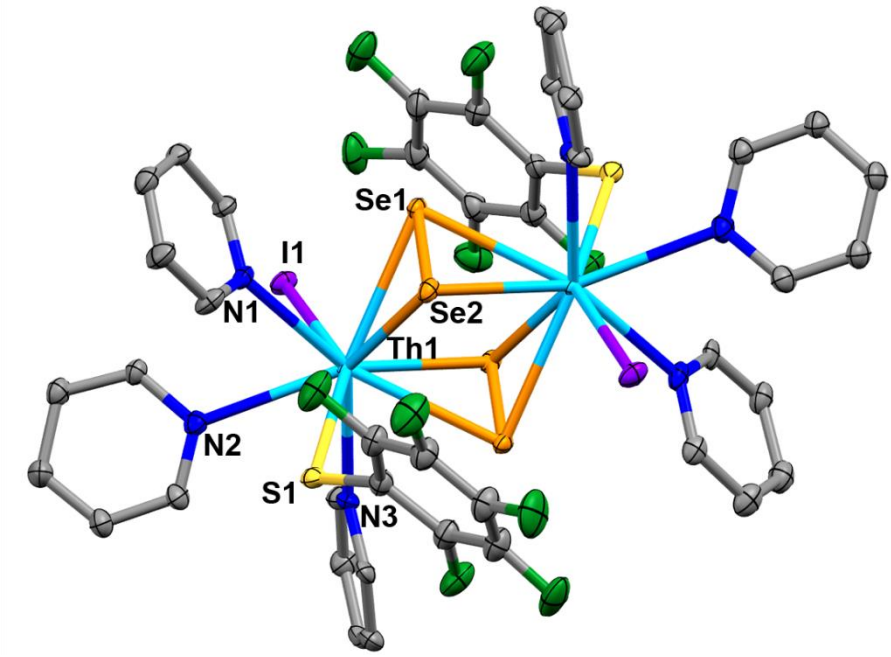

Figure 2.5. ORTEP diagram of $(py)_6Th_2I_2(SC_6F_5)_2(Se_2)_2$ **(8)**, with dark green F, yellow S, orange Se, purple I, light blue Th, dark blue N, grey C, the H atoms removed for clarity, and ellipsoids at the 50% probability level

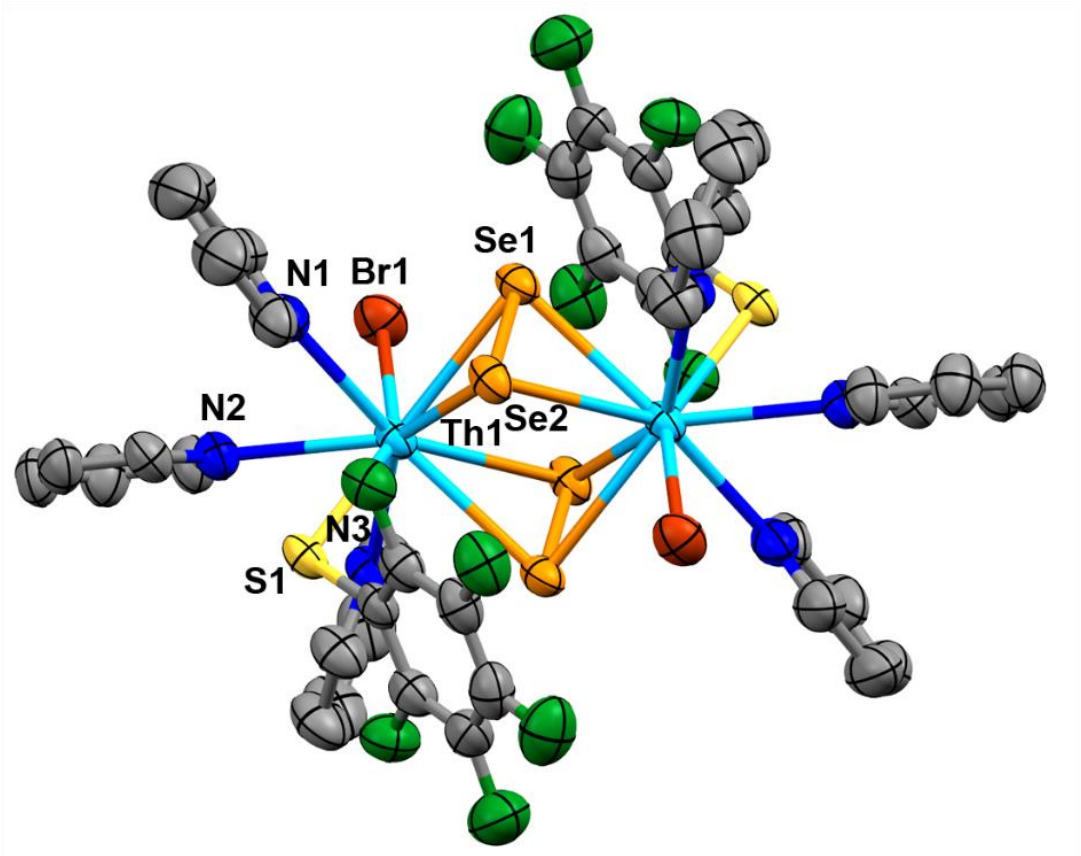

Figure 2.6. ORTEP diagram of $(py)_6Th_2Br_2(SC_6F_5)_2(Se_2)_2$ (**9**), with dark green F, yellow S, orange Se, red Br, light blue Th, dark blue N, grey C, the H atoms removed for clarity, and ellipsoids at the 50% probability level

Compounds **4** – **9** were characterized by spectroscopic methods and low-temperature single crystal X-ray diffraction. Crystallographic data and final R indices for compounds **4** – **9** are given in Table 2.1.

As reliable elemental analysis results are often difficult to obtain due to the loss of lattice solvent and the possibility of decomposition during the process, bulk phase purity for all compounds were determined by comparing observed diffraction patterns with profiles calculated from the respective single crystal results, shown in Figure 2.7-2.11.

Table 2.1. Crystallographic data for compounds **4 - 9**

	4	**5**	**6**	**7**	**8**	**9**
fw	1732.72	1624.98	1654.71	1920.32	1985.66	1970.78
crystal system	monoclinic	monoclinic	triclinic	monoclinic	triclinic	monoclinic
space group	$P2_1/n$	$P2_1/n$	$P\bar{1}$	$P2_1/n$	$P\bar{1}$	$P2_1/c$
a (Å)	11.621(1)	11.024 (2)	12.708(2)	11.836 (1)	12.113 (1)	12.030(1)
b (Å)	15.937(1)	18.599(2)	13.813(2)	16.059(1)	13.534(1)	21.717(2)
c (Å)	13.781(1)	12.161(2)	17.291(2)	13.707 (1)	18.620(2)	11.624(1)
α (deg)	90	90	94.060(4)	90	106.345(2)	90
β (deg)	90.128(1)	102.113(2)	100.923(3)	90.033(1)	100.024(2)	96.510(1)
γ (deg)	90	90	106.794(3)	90	100.3570	90
V ($Å^3$)	2552.6(3)	2438.3(4)	2827.8(6)	2605.3(3)	2798.8(4)	3017.5(4)
Z	2	2	2	2	2	2
D(calcd) (g/cm^3)	2.254	2.213	1.943	2.448	2.356	2.169
T (K)	120(2)	120(2)	120(2)	120(2)	120(2)	120(2)
abs coeff(mm^{-1})	8.438	8.065	5.644	10.901	9.160	8.802
$R(F)^b$ [$I > 2\sigma(I)$]	0.0313	0.0412	0.0509	0.0268	0.0521	0.0476
$R_w(F^2)^c$ [$I > 2\sigma(I)$]	0.0680	0.0473	0.1240	0.0614	0.1368	0.1294

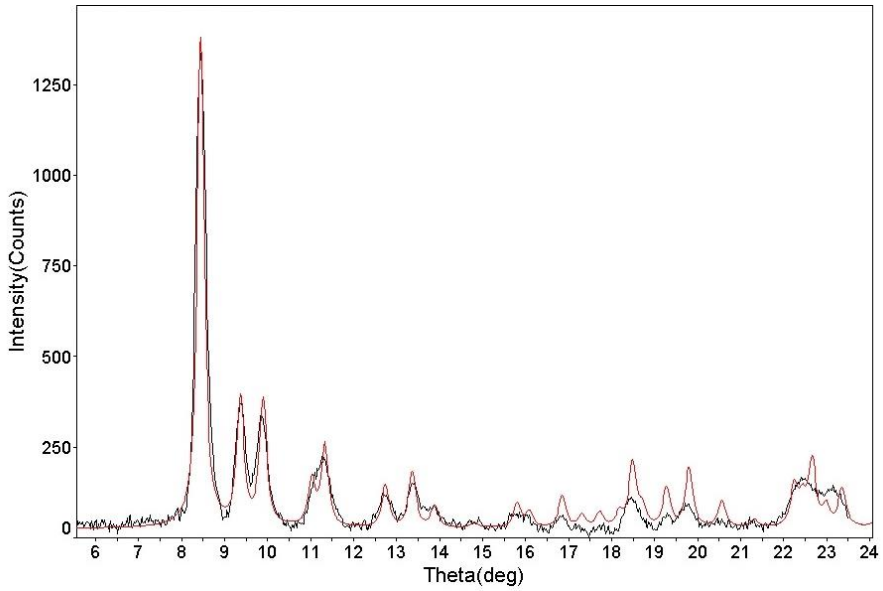

Figure 2.7. PXRD and calculated pattern from single crystal (in red) for $(py)_6Th_2I_4S_4$, **4**

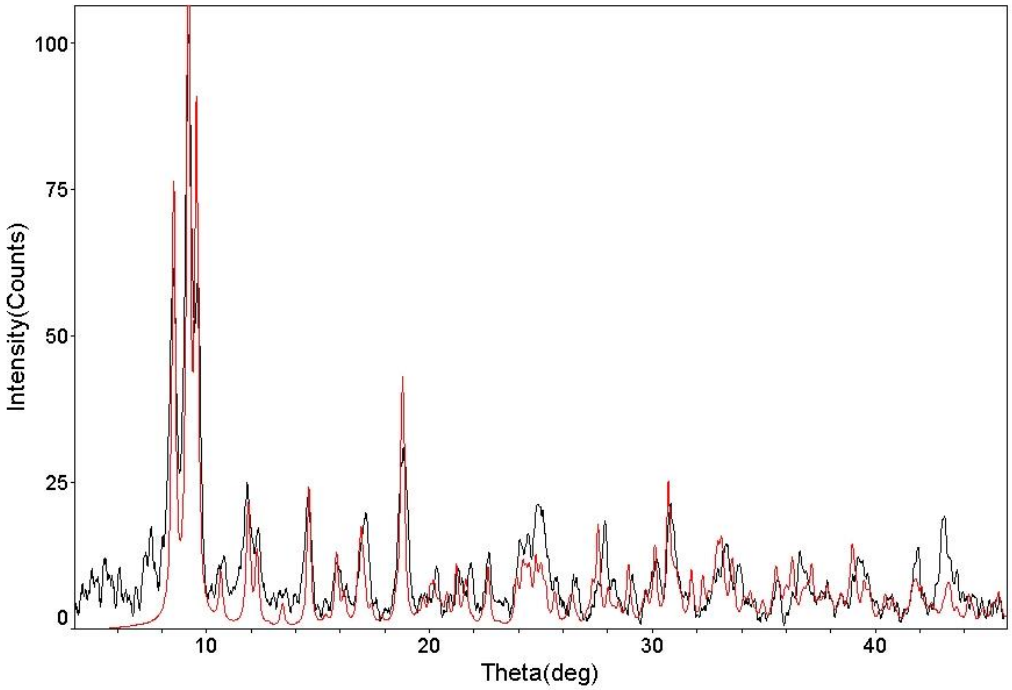

Figure 2.8. PXRD and calculated pattern from single crystal (in red) for $(py)_6Th_2Br_2(SC_6F_5)_2S_4$, **5**

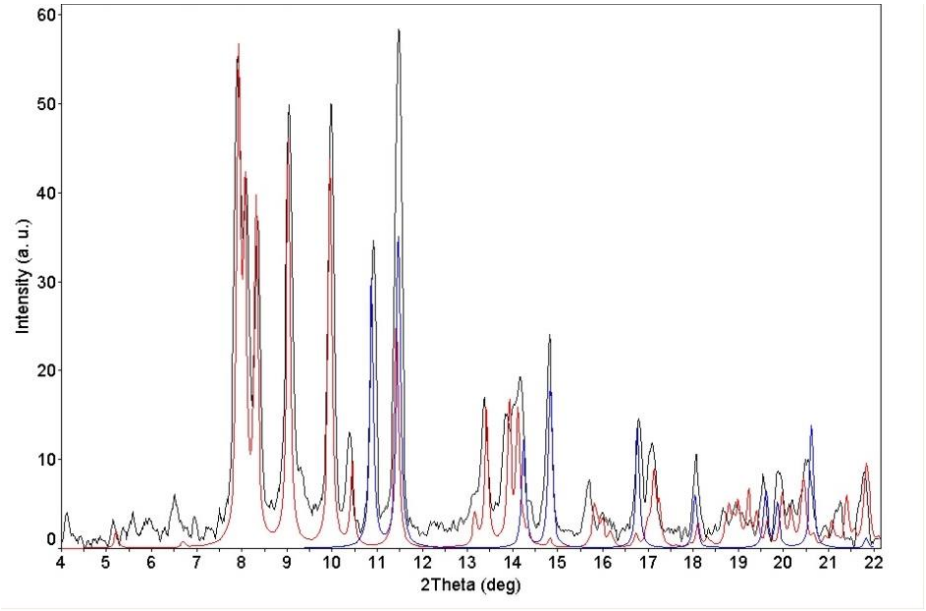

Figure 2.9. PXRD of crystalline products of the reaction (Scheme 2.3) and calculated patterns from single crystal for $(py)_6Th_2Cl_2(SC_6F_5)_2S_4$ (in red), **6** and $(py)_4ThCl_4$ (in blue), **10**

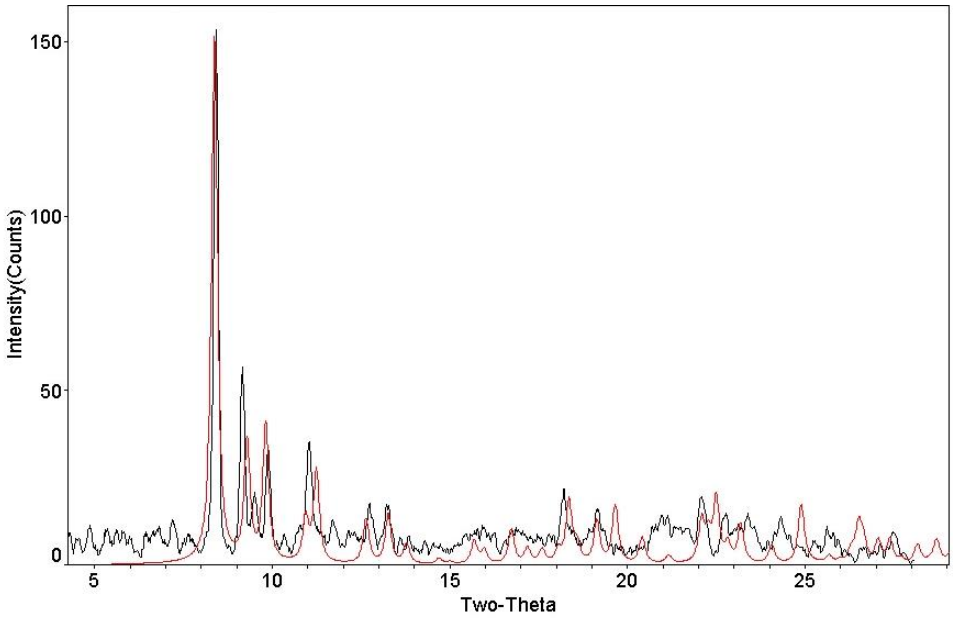

Figure 2.10. PXRD and calculated pattern from single crystal (in red) for $(py)_6Th_2I_4Se_4$, **7**

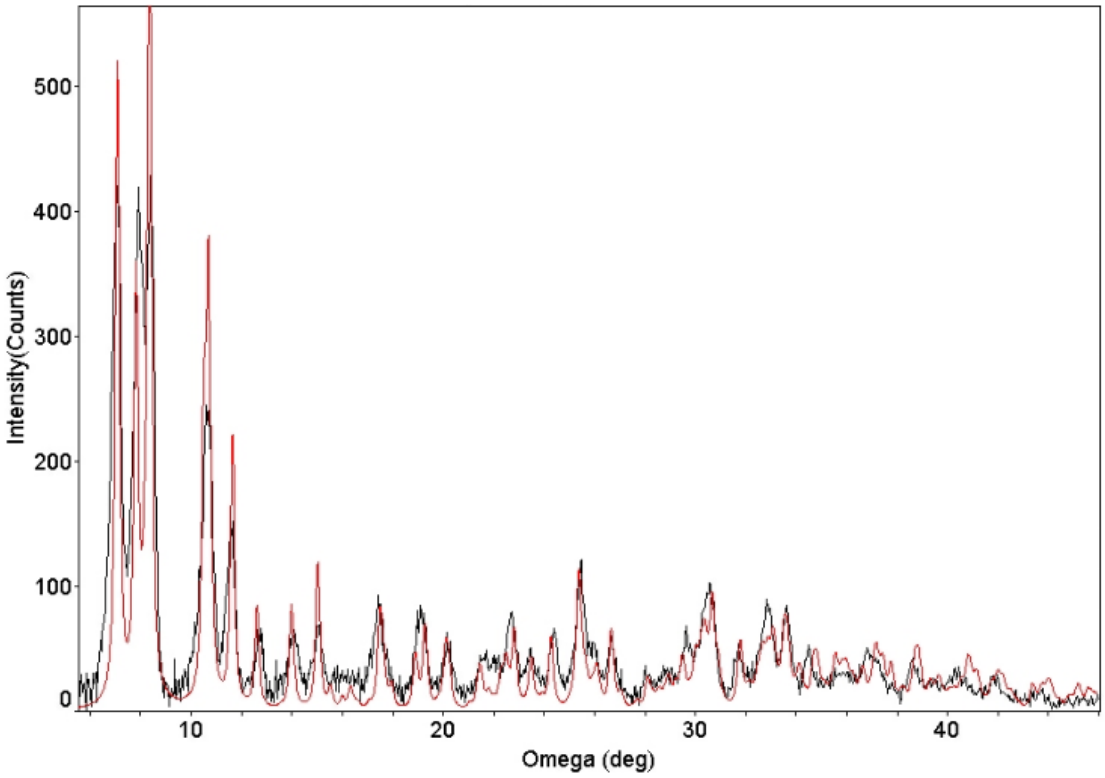

Figure 2.11. PXRD and calculated pattern from single crystal (in red) for $(py)_6Th_2Br_2(SC_6F_5)_2Se_4$, **9**

All six compounds **4** - **9** have similar structures containing a central $Th_2(\mu_2\text{-}E_2)_2$ core region, with the primary coordination sphere of each thorium saturated by two additional monodentate anions and three neutral pyridine ligands. These are the first examples of thorium compounds with bridging E_2^{2-} ligands. The molecular site symmetry of the individual dimer molecules for four of the six compounds is $P2_1/n$, with the exception being the chloride derivative **6** and iodide **9** with fluorothiolates that crystallizes in the space group P-1.

Thermal ellipsoid diagram for compound **10** is shown in Figure 2.12, and the crystallographic data and final R index for **10** are given in Table 2.2.

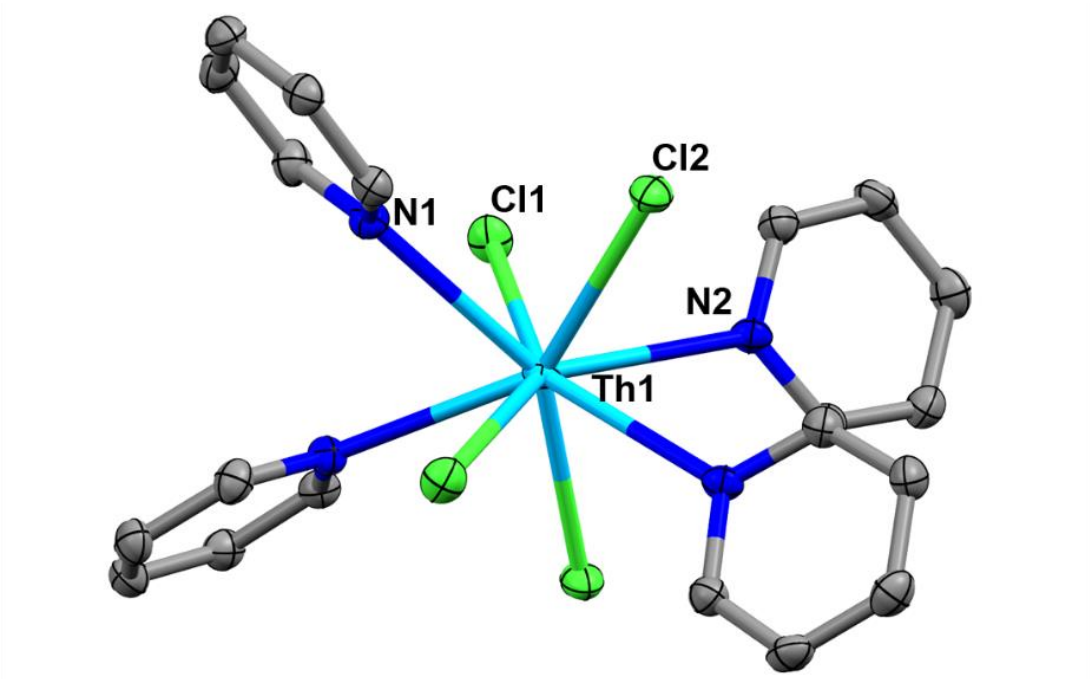

Figure 2.12. ORTEP diagram of $(py)_4ThCl_4$ **(10)**, with green Cl, light blue Th, dark blue N, grey C, the H atoms removed for clarity and ellipsoids at the 50% probability level

Table 2.2. Crystallographic data for $(py)_4ThCl_4$ (**10**)

empirical formula	$C_{20}H_{20}Cl_4N_4Th$	V (Å^3)	2288.1(5)
fw	690.24	Z	4
crystal system	monoclinic	D(calcd) (g/cm^3)	2.004
space group	C2/c	T (K)	120(2)
a (Å)	19.511(2)	abs coeff(mm^{-1})	6.999
b (Å)	9.5049(11)	R(F)^b [I > 2σ(I)]	0.0253
c (Å)	15.7056(18)	$R_w(F^2)^c$ [I > 2σ(I)]	0.0732
α (deg)	90		
β (deg)	128.2262(14)		
γ (deg)	90		

This structure has considerable literature precedence.[15]

Related compounds in the literature are limited. There exists a thorium dimer with two bridging sulfido ligands, $\{[\eta^5\text{-}1,2,4\text{-}(Me_3C)_3C_5H_2]_2Th\}_2(\mu\text{-}S)_2$ [2c] and there are two examples of monometallic thorium compounds with terminally bound $\eta^2\text{-}E_2$ units, namely $[Th(N(SiMe_3)_2)_3(Se_2)]^-$ [3d] and $Cp^*_2Th(DMAP)(S_2)$ [3e] (DMAP = 4-(dimethylamino)pyridine). In contrast, there is a more extensive uranium literature, including monometallic species with $\eta^2\text{-}E_2$ ligands,[1e,2e,3a-c,3f,g] and bimetallic compounds with one or two bridging E_2 ligands.[2b,e,h,i,3c,4]

Bond geometries for all six compounds summarized in Table 2.3 and Table 2.4 are consistent with prior literatures, with values reflecting the sizes of the atomic/ionic components. In all six compounds, there are three pyridine ligands bound to thorium(IV), with two of these pyridines (N(1), N(3)) having a Th-N bond lengths (2.68–2.72 Å) consistent with the wide range of previously reported Th-N(pyridine) bond lengths, i.e. 2.62–2.72 Å in monomeric $(py)_xTh(ER)_4$,[1a] (x = 3, 4; E = S, Se; R = Ph, C_6F_5), 2.63–2.71 Å in a group of cubane clusters,[1b,s] 2.730 Å in $(py)_2Th_2(\mu\text{-}OEt_2)_2(OEt_2)_6$.[16] Pyridines opposite to the E_2 bridges have a slightly longer Th-N(2) bond length (2.73-2.78 Å). The difference in Th-N(1), (3) and Th-N(2) bond lengths within one molecule are about 0.03 Å (compounds **4** and **6**), 0.09 (**5**), 0.01 Å (**7**), 0.07 Å (**8**), and 0.06 Å (**9**).

Table 2.3. Ranges of selected bond distances (Å) and bond angles (°) for **4 – 6** [a]

	$(py)_6Th_2I_4S_4$ $E_2=S_2$, X=I	$(py)_6Th_2Br_2(SC_6F_5)_2S_4$ $E_2=S_2$, X=Br	$(py)_6Th_2Cl_2(SC_6F_5)_2S_4$ $E_2=S_2$, X=Cl
Bond Length [a]	**4**	**5**	**6**
Th-N(1),N(3)	2.699(4), 2.702(4)	2.681(7), 2.688(6)	2.669-2.720(8)
Th-N(2)	2.736(4)	2.779(7)	2.727(8), 2.759(8)
Th-μ_2E_2	2.824-2.863(1)	2.852-2.879(2)	2.847-2.875(2)
Th-ηX	3.174(1), 3.179(1)	2.913(1)	2.738(8), 2.729(8)
Th-ηS(C_6F_5)	-	2.892(2)	2.894(3), 2.906(9)
E-E	2.076(1)	2.084(3)	2.088(3), 2.090(3)
S-C	-	1.733(9)	1.761(16), 1.765(11)
Bond Angles	**4**	**5**	**6**
Th-E-Th	88.59-89.00(<1)	90.3-91.12(<1)	89.09-89.95(<1)
N(1),N(3)-Th-X	87.76-88.34(3)	87.2-87.3(<1)	80.9-86.4(<1)
N(2)-Th-X	78.30(8)	77.54(19)	67.8-75.9(<1)
S-Th-X	-	144.0-145.12(<1)	148.0-149.0(<1)
E-Th-X(acute angle)	75.93-77.78(<1)	80.41-83.64(<1)	80.57-84.7(<1)
E-Th-X(obtuse angle)	118.01-120.34(<1)	121.65-125.82(<1)	122.39-126.5(3)
Th-S-C	-	97.4-107.7(<1)	110.3-110.4(<1)

a The ESD values are enclosed in parentheses. Refer to figures for N atom labels.

Table 2.4. Ranges of selected bond distances (Å) and bond angles (°) for **7 – 9** [a]

	$(py)_6Th_2I_4Se_4$ $E_2=Se_2$, X=I	$(py)_6Th_2I_2(SC_6F_5)_2Se_4$ $E_2=Se_2$, X=I	$(py)_6Th_2Br_2(SC_6F_5)_2Se_4E_2=Se_2$, X=Br
Bond Length	**7**	**8**	**9**
Th-N(1),N(3)	2.706(3), 2.710(3)	2.689-2.724(9)	2.684(6), 2.708(7)
Th-N(2)	2.726(3)	2.755(9), 2.789 (8)	2.775(6)
Th-μ_2E_2	2.971-3.005 (1)	2.985-3.016(1)	2.994-3.024(1)
Th-ηX	3.197(1), 3.201 (1)	3.194(1), 3.216(1)	2.920(2)
Th-η$S(C_6F_5)$	-	2.859(3), 2.911(4)	2.884(2)
E-E	2.343(1)	2.350(1), 2.345(1)	2.342(1)
S-C	-	1.782(8), 1.729(9)	1.718(8)
Bond Angles	**7**	**8**	**9**
Th-E-Th	86.71-87.04(3)	87.88-88.06(<1)	87.519-87.835(3)
N(1),N(3)-Th-X	82.28-86.61(3)	86.0-86.2(<1)	83.89-85.44(<1)
N(2)-Th-X	80.38(7)	83.3(<1)	76.68(3)
S-Th-X	-	146.94-159.0(<1)	147.22(4)
E-Th-X(acute angle)	74.70-74.96(<1)	69.2-72.7(<1)	77.03-80.05(<1)
E-Th-X(obtuse angle)	120.49-120.80(3)	115.1-118.6(<1)	121.96-125.39(<1)
Th-S-C	-	112.2-114.7(<1)	113.0(2)

a The ESD values are enclosed in parentheses. Refer to figures for N atom labels.

Thorium-sulfur(thiolate) distances are equally consistent with previous literature values: compare the Th-S(C_6F_5) in nine coordinate **5** (2.892(2) Å), **6** (avg. 2.900(9) Å), **8** (avg. 2.885(4) Å), and **9** (2.884(3) Å) with the Th-S(C_6F_5) bonds in the eight coordinate cubane clusters $(py)_8Th_4S_4(SPh)_4(SC_6F_5)_4$ (2.900(2) Å)[1b] and $(py)_8Th_4Se_4(SePh)_4(SC_6F_5)_4$ (2.889(2) Å)[1b] and the Th-S bonds in monometallic seven coordinate $(py)_3Th(SC_6F_5)_4$[1a] (2.811- 2.825(10) Å).

In all compounds the halide ligands are terminally bound. There are four iodides in **4** (3.174(1), 3.179(1)Å) and **7** (3.197(1), 3.201(1)Å), and two iodides in **8** (avg. 3.205(1) Å) with nearly identical Th-I bond lengths that are consistent with previously published Th-I distances, i.e. 3.172(1) Å in $(C_5Me_5)_2[^iPrNC(Me)N^iPr\text{-}k^2N,N']ThI$[17], 3.171(1) Å in $ThI_3[O(CH_2)_4I](THF)_3$,[18] and 3.226(1) Å in $ThI(OCH\ i\text{-}Pr_2)_3(py)_2$.[19] Similarly, complexes **5** and **9** contain terminal bromide ligands with Th-Br bond lengths that are also similar to previously reported examples, i.e. 2.895(1) Å in monomeric $(\eta^5\text{-}Cp)_2ThBr_2(THF)$,[20] or 2.885(2) Å in heterometallic $[(\eta^5\text{-}C_5Me_5)_2Th(Br)\text{-}N(mesityl)Cu(DMAP))]$.[21] In the single chloride derivative **6**, the Th-Cl bond lengths (avg. 2.733(8) Å) are again similar to literature values, i.e. 2.755(1) Å in monomeric $Th(TMTAA)Cl_2(THF)_2$[22] and 2.737(1) Å in ThCp*(TMTAA)Cl,[22] (TMTAA=Tetramethyl-tetra-aza-annulene) among others.[14c,21,23]

Disulfido bonds in **4**, **5**, and **6** are in the range 2.076-2.090(3) Å, consistent with the terminal SS unit in thorium disulfide complex $(\eta^5\text{-}C_5Me_5)_2ThS_2(DMAP)$, which contains a 2.088 Å[3e] sulfur-sulfur bond. Comparable distances[24] have also been noted

in uranium,[2e,f,h] lanthanide, [25,26] and transition metal chemistry.[27] Similarly, dimers **7**, **8**, and **9** contain Se-Se bonds within a narrow range of bond lengths (2.342-2.350(3) Å) that are almost identical to the 2.397(1) Å terminally bound diselenido ligand in [K(18-crown-6)][Th(η^2-E_2)(NR_2)$_3$],[3d] and fall within the range of expected values for diselenide moieties bound to lanthanides[28] and transition metals.[27h,29]

The molecular conformation of the [(py)$_3$ThX(SC_6F_5)E_2]$_2$ dimers **5**, **6**, **8**, and **9** can be viewed as having an equatorial plane containing the Th(IV) ions and the centroids of all the py ligands and the two μ_2-E_2 bridging ligands. In this scheme, the halide and SC_6F_5 ligands extend out of the equatorial plane, such that the X_2S_2 plane is nearly perpendicular to the equatorial plane. This motif makes available a variety of close contacts that are indicative of prevalent intramolecular hydrogen bonding to halogen, chalcogen and nitrogen acceptor atoms. Further, the py ligands are rotated around their Th-N bonds and this situation brings their α-H atoms into proximity with H-bond acceptors.

Table 2.5 summarized close contacts in the compounds **5**, **6**, **8** and **9**. The van der Waals radii sums (vdW)[30] are also included in Table 2.5 for comparison. In all of these compounds, intra-molecule interactions, which are indicated by distances shorter than vdW radii sums, are found for all α-H on py ligands. For example, in **5**, H(7)…F(5) for py(N1), H(12)…S(1) for py(N2), and H(21)…Br(1) for py(N3), are 0.21, 0.29, and 0.18 Å less than vdW, as shown in Figure 2.13; in **8**, H(11)…S(1) for py(N1), H(16)…S(1) for py(N2), and H(17)...S(1) for py(N3), are 0.18, 0.25, and 0.27 Å less than vdW; and

in **9**, H(7)…F(1) for py(N1), H(12)…S(1) for py(N2), and H(21)...Br(5) for py(N3), at 0.18, 0.27, and 0.10 Å less than vdW, respectively. Two of these are expected, since F and Br are good electronegative H-bond acceptors. As for H…S, the extreme shortness of this contact likely has both the electrostatic basis of the H-bond and the proximity basis of these two atoms more or less confined to a plane perpendicular to the above mentioned equatorial plane of the dimer. As mentioned earlier, Th(1)-N(2) bonds are much longer (0.09 Å in **5**, 0.07 Å in **8** and 0.06 Å in **9**) than Th(1)-N(1) and Th(1)-N(3), and it is consistent with py(N2) having a close contact on only one side of the ligand, versus py(N1) and py(N3) having close contacts on both sides of the py ligand. The situation in **6** is unique. H(12)…S(3) and H(16) …Cl(1) for py (N2) are 0.20 and 0.27 Å less than vdW, respectively. These close contacts from both sides of the py ligand are also consistent with the fact that the Th bound to N(2) is closer in the distance between Th bound to N(1) and N(3), namely, 2.727(8) versus 2.720(8) and 2.694(8) Å, when compared with **5**, **8** and **9**.

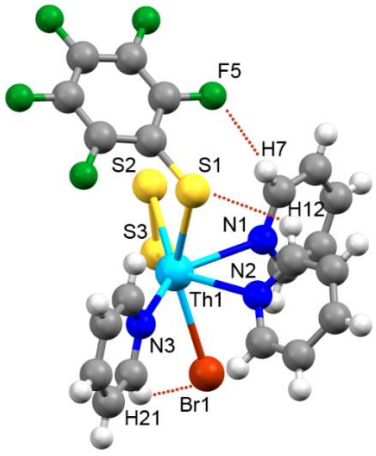

Figure 2.13. Asymmetric structural unit of compound **5**, with short contacts inside the molecule highlighted

Table 2.5. Summary of H…Y (Y = N, E, or X) distances (Å) in **5**, **6**, **8** and **9**, with values shorter than the sum of van der Waals radii [a] in bold

Compound	**5** [b]	**6** [c]	**8**	**9**
	$(py)_6Th_2Br_2(SC_6F_5)_2S_4$	$(py)_6Th_2Cl_2(SC_6F_5)_2S_4$	$(py)_6Th_2I_2(SC_6F_5)_2Se_4$	$(py)_6Th_2Br_2(SC_6F_5)_2Se_4$
Contacts from py(N1)	**H(7)…S(1) 2.95**	**H(7) … S(3) 2.80**	**H(11)…S(1) 2.82**	**H(7)…Se(2) 2.90**
	H(7)…F(5) 2.46	**H(7)…F(1) 2.54**	H(11)…F(1) 2.71	**H(7)…F(1) 2.49**
	H(11)…Br(1) 2.84	**H(11)…Cl(1) 2.82**	**H(7)…I(1) 3.06**	**H(11)…Br(1) 2.90**
Contacts from py(N2)	**H(12)…S(1) 2.71**	**H(12)…S(3) 2.80**	**H(16)…S(1) 2.75**	**H(12)…S(1) 2.73**
	H(12)…N(1) 2.91	H(12)…N(3) 2.86	H(16)…N(1) 2.75	**H(12)…N(1) 2.69**
	H(16)…Br(1) 3.01	**H(16)…Cl(1) 2.68**	**H(12)…I(1) 3.09**	**H(16)…Br(1) 3.00**
	H(16)…N(3) 2.76	H(16)…N(1) 2.89	**H(12)…N(3) 2.68**	**H(16)…N(3) 2.69**
Contacts from py(N3)	**H(17)…S(1) 2.78**	**H(17)…S(3) 3.09**	**H(17)…S(1) 2.73**	**H(21)…S(1) 2.82**
	H(17)…F(1) 2.67	H(17)…F(5) 2.99	**H(17)…F(5) 2.64**	**H(21)…F(5) 2.56**
	H(21)…Br(1) 2.87	**H(21)…Cl(1) 2.75**	H(21)…I(1) 3.28	**H(17)…Br(1) 2.95**
	H(21)…S(2) 3.27	H(21)…S(2) 3.54	**H(21)…Se(2) 2.96**	H(17)…Se(2) 3.14

[a] The van der Waals radii sum[30]: 2.75 Å for H…N, 3.00 Å for H…S, 3.10 Å for H…Se; 2.67 Å for H…F, 2.95 Å for H…Cl, 3.05 for H…Br and 3.18 for H…I. [b] S(1) is terminal atom, S(2) and S(3) are bridging atoms. [c] S(1) and S(2) are bridging atoms, S(3) is terminal atom.

If unit cell packing is viewed along crystallographic c-axis, the arrangement of neighboring molecules of **9** in the crystallographic ab plane is shown in Figure 2.14. A nearly one-dimensional (1D) void channel of coordinating py and solvate py molecules along the c-axis is sandwiched by [$Th_2Se_4Br_2(SC_6F_5)_2$] regions. There are also a few intermolecular interactions, i.e. H…F (2.508(1) Å) and H…Se (2.930(1) Å).

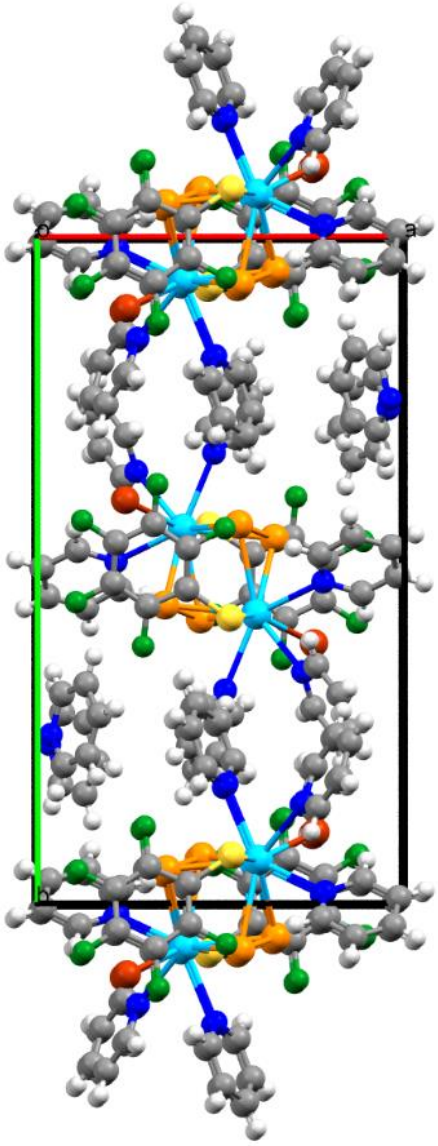

Figure 2.14. Arrangement of neighboring molecules of compound **9**, with green F, yellow S, orange Se, red Br, light blue Th, dark blue N, grey C, and white H atoms

2.3 DFT Calculations and ^{77}Se NMR Study of Solution Structures

^{77}Se NMR spectroscopy combined with relativistic DFT calculations and analysis of the measured chemical shifts provides unique insight into the solution structure of diselenido compounds **7**, **8**, and **9**. Establishing speciation for these molecules is important to fully understand the chemistry of the An-E bond and to realize the ultimate goal of being able to rationally design synthetic approaches to construct increasingly large cluster compounds. Solution and solid-state structures are not necessarily the same, given that strong bases such as pyridine can potentially fragment polymetallic compounds to give products with reduced nuclearity, as illustrated in ionic systems by the reaction of $(THF)_{14}Ln_{10}S_6(Se_2)_6I_6$ with pyridine to give $(py)_6Ln_2(Se_{0.2}S_{0.8})(Se_2)I_2$.[28a] In collaboration with Dr. Peter Hrobárik, we are able to further probe the solution structure with DFT calculation results.

The experimental ^{77}Se NMR shifts for complexes **7 - 9**, along with those computed for these and other hypothetical thorium dichalcogenide species that could potentially be present in pyridine-d_5 solution, are collected in Table 2.6. Compounds **7**, **8**, and **9** show a single ^{77}Se NMR resonance at 240, 336, and 308 ppm, respectively (Table 2.6), all in the range expected for diselenides bridging two Th(IV) ions.

Chemical shift calculations were done at the two-component ZORA relativistic level, including spin-orbit (SO) coupling, and using the user-customized hybrid PBE0-40HF functional, which was shown to perform very well for a series of monomeric Th selenolates, thorium cubanes and various organoselenides.[1s]

Table 2.6. Experimental and computed ^{77}Se NMR chemical shifts (in ppm vs. Me_2Se) in selected thorium diselenide complexes. DFT optimized Th-Se bond lengths, *d*(Th-Se) (in Å) and QTAIM delocalization indices of the Th-Se bonds, DI(Th-Se), are given as well

Compounds	d(Th-Se)	DI(Th-Se)	Calcd. $\delta(^{77}Se)^a$ [ppm]	Expt. $\delta(^{77}Se)^b$ [ppm]
$Th_2I_4(\mu_2\text{-}Se_2)_2$ (fully desolvated **7**)[c]	2.948	0.520	469	
$(py)_6Th_2I_4(\mu_2\text{-}Se_2)_2$ (**7**)	2.981	0.456	272	240
$(py)_6Th_2Br_4(\mu_2\text{-}Se_2)_2$	2.994	0.437	267	
$(py)_6Th_2Cl_4(\mu_2\text{-}Se_2)_2$	3.008	0.421	233	
$(py)_6Th_2I_2(SC_6F_5)_2(\mu_2\text{-}Se_2)_2$ (**8**)	2.993	0.443	328	336
$(py)_6Th_2Br_2(SC_6F_5)_2(\mu_2\text{-}Se_2)_2$ (**9**)	2.997	0.436	318	308
$(py)_3ThI_2(\mu_2\text{-}Se_2)$	2.775	0.794	656	
$(py)_4ThI_2(\mu_2\text{-}Se_2)$	2.796	0.738	497	
$(py)_3ThI(SC_6F_5)(\mu_2\text{-}Se_2)$	2.788	0.770	678	
$(py)_4ThI(SC_6F_5)(\mu_2\text{-}Se_2)$	2.804	0.725	520	
$[K(18\text{-crown-6})]Th(Se_2)(NR_2)_3$	2.914	0.529	273	302[3e]

[a] 2c-ZORA(SO)/PBE0-40HF/TZ2P results using a COSMO solvation model (cf. Computational Details). Note that the trends in ^{77}Se NMR shifts are dominated by paramagnetic shielding contribution; [b] NMR spectra recorded in pyridine-d_5 at room temperature; [c] This compound has not been prepared.

The investigated structures were fully optimized at the DFT level (PBE0-D3(BJ)/ECP/def2-TZVP) using quasi-relativistic small-core pseudopotentials for thorium and iodine, along with atom-pairwise corrections for dispersion forces (see Computational Details). Table 2.7 summarizes the DFT optimized bond-lengths in selected thorium dichalcogenide complexes. There is an excellent agreement between X-ray and DFT optimized structures of complexes **4 - 9**, with differences in Th−E, E−E and Th−X (E = S or Se; X = Cl, Br or I) bond lengths of less than 0.03 Å. Interestingly, one pyridine molecule on each Th atom opposite to the E_2^{2-} bridges (equatorial position with respect to the Th_2X_2 plane) has notably longer Th−N bond length than the others (by more than 0.07 Å), consistent with the Th−N bond asymmetry observed for axial and equatorial nitrogen atoms in solid-state structures of **4 - 9**, although this inequality is less pronounced in X-ray structures of complexes **4** and **7**. Energy decomposition analysis (EDA) suggests that the longer Th−N_{py} bonds in the equatorial position have an electronic origin resulting from weaker Th-N orbital attractive interactions rather than from steric effects (the latter is comparable with that for axial Th-N_{py} bonds). In addition, similar Th−N bond asymmetry for equatorial and axial pyridine ligands is computed for isoelectronic group 4 (Ti, Zr, Hf) congeners of complex **7**, showing that this phenomenon is not related to Th(5f) orbitals but to a trans influence of bridging E_2^{2-} moieties, and it also appears in monomeric Th dichalcogenide species (i.e. Th-N bonds in the *trans* position to the centroid of E_2^{2-} ligands are elongated more than those in the *cis* position). Adding more pyridine ligands to the first Th coordination sphere in

$(py)_6Th_2I_4$ $(\mu_2\text{-}Se_2)_2$ and $(py)_4ThI_4(\mu_2\text{-}Se_2)$ and optimization of these structures at the DFT level results in detachment of these extra py molecules from the metal center, demonstrating the saturated metal coordination environment in isolated dichalcogenide complexes **4 - 9**. In contrast, removal of pyridine ligands leads to somewhat shorter Th–E bonds and elongated E–E contacts (Table 2.7).

Table 2.7. DFT optimized bond lengths (Å) in selected thorium dichalcogenide complexes (E = S, Se; X = Br, I) [a,b]

	d(Th–E)	*d*(E–E)	*d*(Th–N_{eq})	*d*(Th–N_{axial})	*d*(Th–X)	*d*(Th–S_{Ar})
$(py)_6Th_2I_4(S_2)_2$ (**4**)	2.828	2.074	2.787	2.710	3.162	-
$(py)_6Th_2Br_2(SC_6F_5)_2(S_2)_2$ (**5**)	2.843	2.072	2.783	2.700	2.900	2.869
$(py)_6Th_2Cl_2(SC_6F_5)_2(S_2)_2$ (**6**)	2.849	2.072	2.785	2.693	2.710	2.883
$Th_2I_4(Se_2)_2$ (fully desolvated **7**)	2.948	2.379	-	-	2.948	-
$(py)_6Th_2I_4(Se_2)_2$ (**7**)	2.981	2.343	2.791	2.713	3.172	-
$(py)_6Th_2Br_4(Se_2)_2$	2.994	2.344	2.817	2.701	2.910	-
$(py)_6Th_2Cl_4(Se_2)_2$	3.008	2.347	2.843	2.690	2.720	-
$(py)_6Th_2I_2(SC_6F_5)_2(Se_2)_2$ (**8**)	2.993	2.339	2.779	2.714	3.161	2.860
$(py)_6Th_2Br_2(SC_6F_5)_2(Se_2)_2$ (**9**)	2.997	2.338	2.784	2.702	2.905	2.881
	d(Th–E)	*d*(E–E)	*d*(Th–N_{trans})	*d*(Th–N_{cis})	*d*(Th–X)	*d*(Th–S_{Ar})
$(py)_3ThI_2(\mu_2\text{-}Se_2)$	2.775	2.356	2.755	2.641	3.080	-
$(py)_4ThI_2(\mu_2\text{-}Se_2)$	2.796	2.350	2.789	2.622	3.160	-
$(py)_3ThI_2(SC_6F_5)(\mu_2\text{-}Se_2)$	2.788	2.356	2.737	2.649	3.086	2.804
$(py)_4ThI_2(SC_6F_5)(\mu_2\text{-}Se_2)$	2.804	2.350	2.769	2.625	3.168	2.805

[a] PBE0-D3(BJ)/ECP/def2-TZVP results (cf. Computational Details in main text); [b] Averaged values over chemically equivalent bonds. The py ligands in dimeric structures possess two locations with respect to the plane containing two Th(IV) ions and the centroid of the two μ_2-E_2 bridging ligands (see Table S52). In monomeric species, these positions can be viewed as nearly *trans* and *cis* with respect to the centroid of Th-Se_2 bonds.

Experimentally observed ^{77}Se NMR shifts for pyridine-d_5 solutions of complexes **7 - 9** match very well with the DFT computed values and are consistent with the dimeric structures being maintained in solution. Not surprisingly, "desolvated" species (with no pyridine ligands attached to thorium) are absent in solution; these hypothetical molecules are computed to be deshielded by about 200 ppm relative to their pyridine solvated congeners (Table 2.6), but no ^{77}Se resonance signal in the region 350-1000 ppm was detected. Similarly, ^{77}Se NMR shifts for corresponding monomeric Th species with terminal dichalcogenide ligands are predicted to appear within the range 490-680 ppm (depending on the number of coordinated py molecules; Table 2.6), excluding thus the dissociation of dimers in solution. We note further that although ^{77}Se NMR shifts observed herein for dimeric structures resemble the value measured for a thorium complex with the "terminal" Se_2^{2-} ligand, [K(18-crown-6)][Th(Se_2)(NR_2)$_3$] (δ(^{77}Se) = 302 ppm in pyridine-d_5),[3d] this coincidence can be attributed to the anionic nature of the latter, which is reflected in its elongated Th-Se bonds and reduced Th-Se covalency as compared to neutral mononuclear Th diselenides (Table 2.6). Replacing iodide ligands with lighter Br^- or Cl^- leads to slightly longer Th–Se distances that is also reflected in small but notable upfield ^{77}Se shifts, as is also evident from experimental data for complexes **8** and **9**. This can be rationalized by stronger π-donating abilities within the row $I^- < Br^- < Cl^-$, which in turn weakens the Th–Se bond covalency in mixed Th chalcogenide-halide complexes as going up the halogen group, and might be the reason for lower stability of dimeric Th_2E_4 species with terminal Cl^- ligands.

2.4 UV-Vis Absorption Spectra

In contrast to colorless compounds **4** - **6**, complexes **7** - **9** are yellow to yellow-orange in the solid-state as well as in pyridine solution. The UV-Vis absorption spectrum of compound **7** is given in Figure 2.15, showing the strongest absorption band at about 310 nm, followed by intense absorption without a distinct maximum reaching a plateau at about 400 nm and the steadily decreasing absorption within the wavelength range of 400-500 nm. To understand the nature of the electronic transitions, we performed time-dependent DFT calculations of excitation energies (Table 2.8 and Figure 2.16) for isostructural compounds **4** (colorless) and **7** (yellow). The profile of the TD-DFT simulated absorption spectrum of **7** agrees well with experiment and allows thus assignment of the most intense bands (Table 2.8 and Figure 2.17).

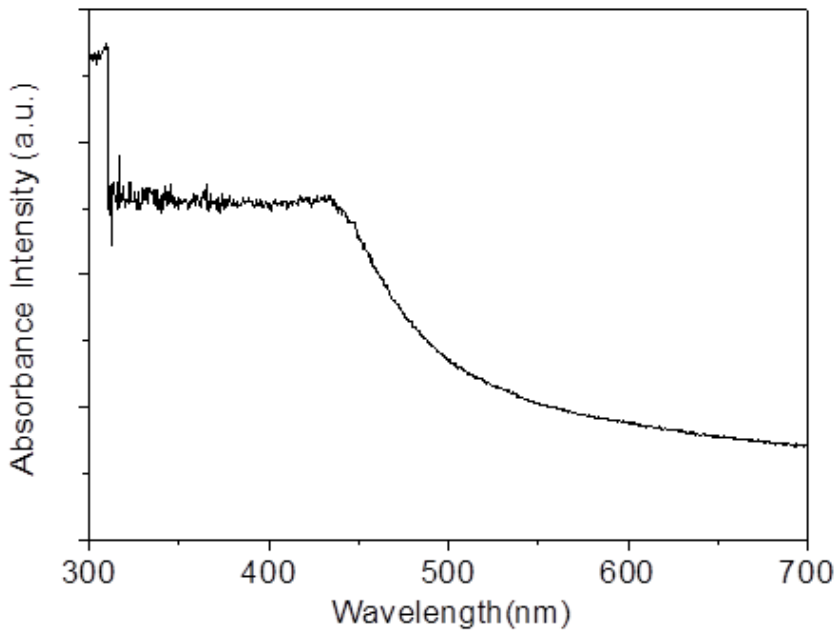

Figure 2.15. UV-Vis spectrum for compound **7**

Table 2.8. Calculated vertical excitation energies and oscillator strengths for the lowest ten and three most intense electronic transitions in complex **7**

Excited state #	Character of transition (dominant contributions)		Energy (eV)	Wavelength (nm)	Oscillator strength
1	100%	HOMO→LUMO	2.510	494	0.000
2	100%	HOMO→LUMO+1	2.725	455	0.000
3	99%	HOMO-1→LUMO	2.749	451	0.000
4	99%	HOMO→LUMO+2	2.799	443	0.000
5	98%	**HOMO→LUMO+3**	**2.857**	**434**	**0.006**
6	47% 45%	**HOMO-2→LUMO** **HOMO-1→LUMO+1**	**2.945**	**421**	**0.008**
7	100%	HOMO→LUMO+6	2.952	420	0.000
8	54% 25% 20%	HOMO-1→LUMO+1 HOMO-2→LUMO HOMO→LUMO+4	2.967	418	0.003
9	69% 27%	HOMO→LUMO+4 HOMO-2→LUMO	2.995	414	0.001
10	99%	HOMO→LUMO+5	3.032	409	0.000
13	95%	**HOMO-1→LUMO+3**	**3.131**	**396**	**0.0303**
19	95%	**HOMO-1→LUMO+7**	**3.407**	**364**	**0.0193**
59	62% 10%	**HOMO-1→LUMO+13** **HOMO-1→LUMO+17**	**4.013**	**310**	**0.0407**

[a] ZORA-SR/PBE0-10HF/TZ2P results

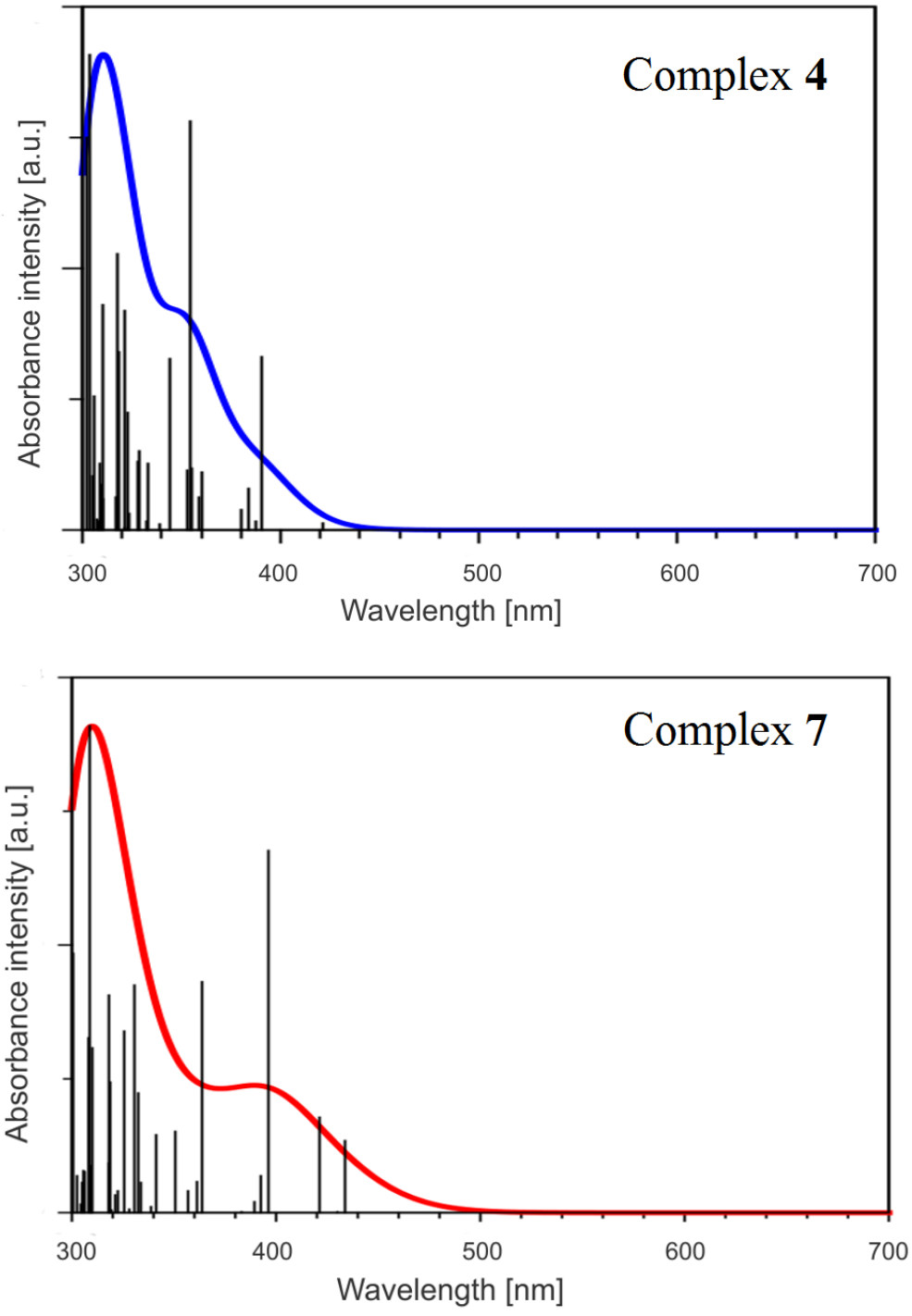

Figure 2.16. TD-DFT calculated UV-Vis absorption spectra for complexes **4** and **7** in pyridine (ZORA-SR/PBE0-10HF/TZ2P/COSMO results taking into account the lowest 75 excitations). Spectra were convoluted with a Gaussian profile having a full width at half-maximum (fwhm) equal to 0.20 eV

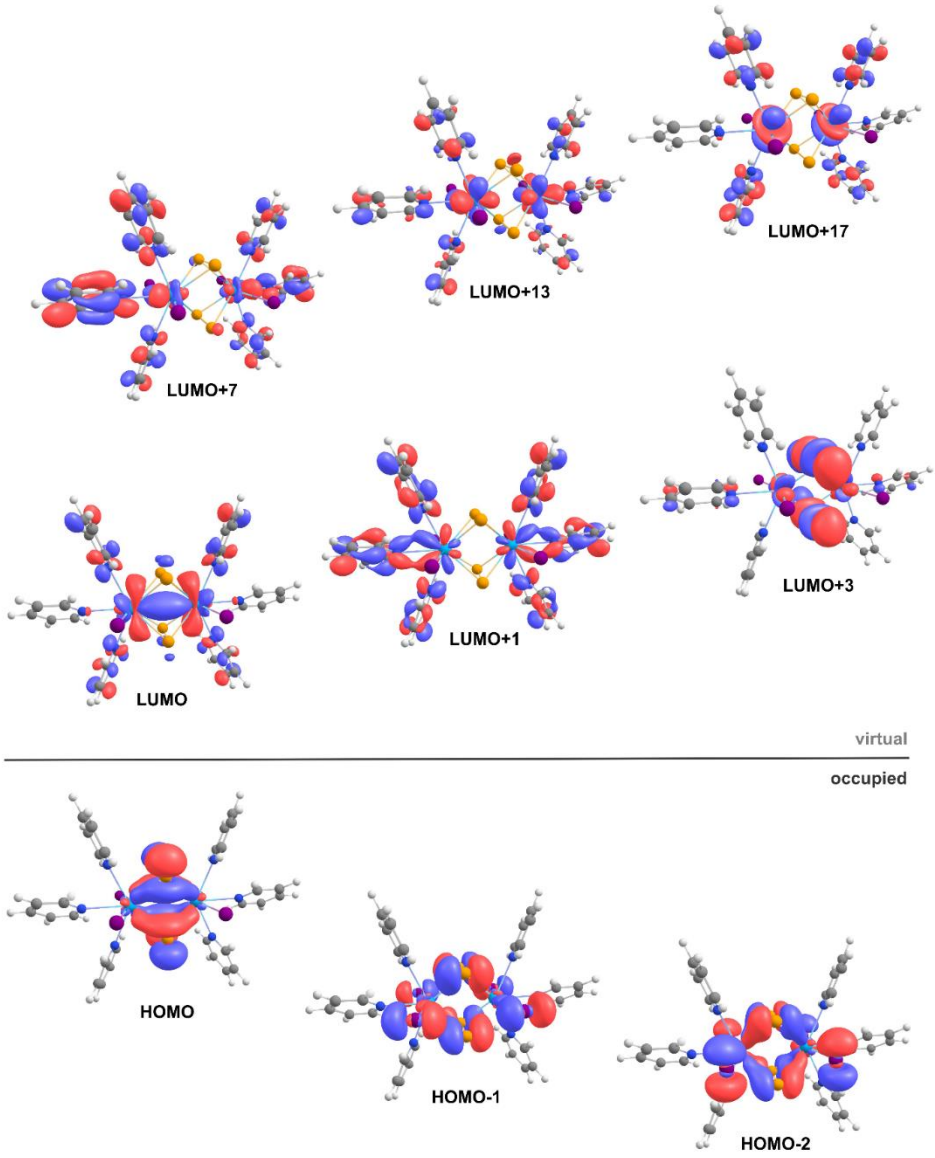

Figure 2.17. Relevant occupied and unoccupied MOs (isosurface plots ±0.03 au) involved in intense (f_{osc} > 0.005) electronic transitions of **7**

Hence, it is clear that the strongest peak in the UV region (~310 nm) can be primarily assigned to excitations from nonbonding lone pairs on the bridging selenium atoms (HOMO-1) to predominantly metal-centered MOs with a large Th(5f) contribution (LUMO+13, LUMO+17), followed by less intense excitations from the Se lone pairs to pyridine ligands (~350 nm, HOMO-1 → LUMO+7

transition). The absorption in the visible (violet) region (370-410 nm) is primarily related to transitions from the Th-Se bonding MOs (HOMO, HOMO-2) and non-bonding Se lone pairs (HOMO-1) to selenium antibonding MOs (LUMO+3). Since the latter excitation energies corresponding to the $n(E_2^{2-})\rightarrow\pi^*(E_2^{2-})$ transition are shifted hypsochromically in disulfide complexes, these appear as colorless. We note in passing that the yellow color is also observed for some lanthanide di- and tri-selenide complexes[28a,31] that can be similarly related to $n(Se_2^{2-})\rightarrow\pi^*(Se_2^{2-})$ transitions, and that the behavior of related telluride compounds[32] are also consistent with this interpretation.

2.5 Thermolysis

Thermolysis[1a,33] of carefully designed molecular precursors is potentially useful as a low temperature synthesis approach to metastable solid-state materials, with compounds **4** and **7** presenting an opportunity to explore the low-temperature preparation of ternary solid-state materials. Of the two, the I/SeSe combination found in **7** was the most promising candidate to form a ternary phase at elevated temperatures because of the relative electronegativity of I and Se. Compounds with fluorinated thiolate ligands are complicated by the tendency of Th to abstract F and form ThF_4, and the more electronegative sulfur in **4** favors the formation of ThS_2 rather than ThI_2S or ThI_2(SS). Thermolysis of **7** was performed at the same conditions as for previously reported[1a] $(py)_3Th(SePh)_4$. The PXRD analysis revealed that $ThSe_2$[34] is the only solid-state product, with no evidence for the formation of any ternary ThISe phases. The

surface morphology of the resulting powder of the thermal residual is shown in Figure 2.18 by SEM.

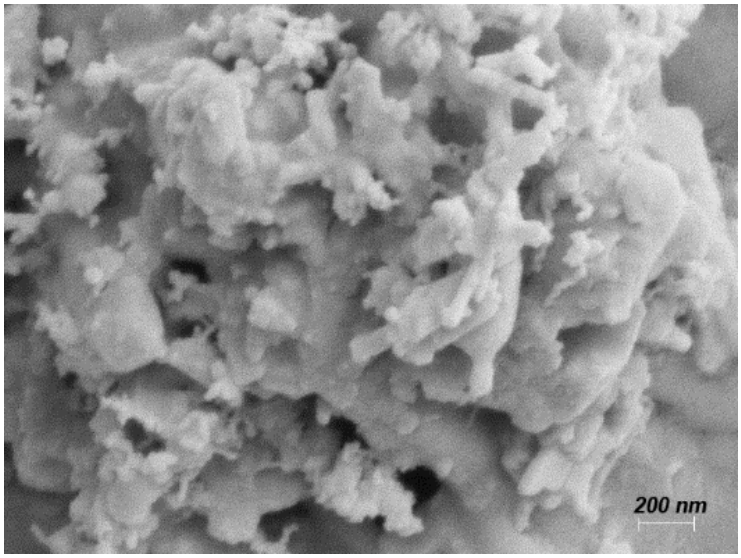

Figure 2.18. SEM images of $ThSe_2$ (in 200 nm scale) obtained from the thermolysis of compound **7**

This $ThSe_2$ stoichiometry was also confirmed by Energy Dispersive X-ray Spectroscopy (EDS) (Figure 2.19), with trace (< 3%) iodide present.

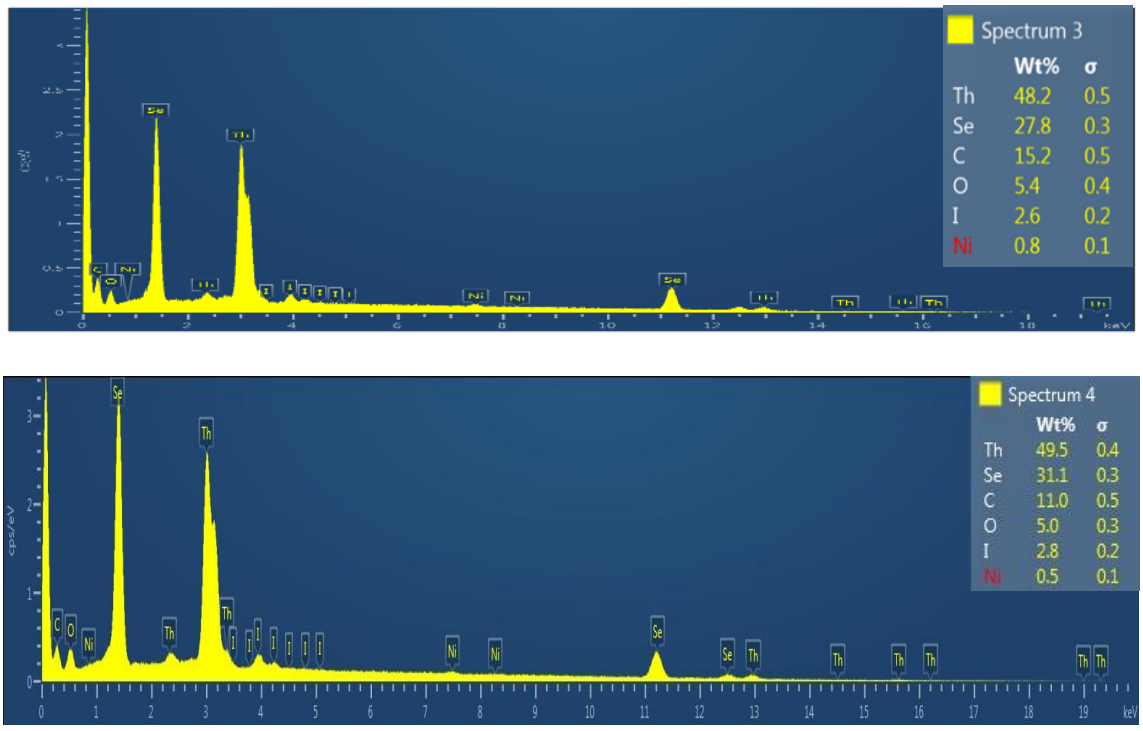

Figure 2.19. EDS analysis of thermolysis product of compound **7**

GC/MS analysis of the volatile products identified both pyridine and elemental iodine (Scheme 2.5).

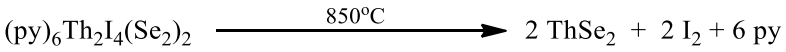

Scheme 2.5. Thermal decomposition of compound **7**

2.6 Conclusions

Remarkably simple chalcogen-rich molecular Th dimers containing E_2^{2-} (E = S, Se) bridging ligands can be prepared with a range of sterically undemanding ancillary ligands, including both halogens and fluorinated thiolates. These compounds are fundamentally important starting materials for our ultimate goal of rationally approaching increasingly large actinide and heterometallic actinide/transition metal cluster compounds. The solution ^{77}Se NMR spectra are consistent with the dimeric structure being maintained in pyridine solution. Thermolysis of the dimer containing both I^- and Se_2^{2-} ligands resulted in reductive cleavage of the Se–Se bond, oxidative elimination of I_2 and the formation of solid-state $ThSe_2$.

Reference

(1) (a) Rehe, D.; Kornienko, A. Y.; Emge, T. J.; Brennan, J. G. Thorium Compounds with Bonds to Sulfur or Selenium: Synthesis, Structure, and Thermolysis. *Inorg. Chem.* **2016**, *55*, 6961-6967.(b) Stuber, M. A.; Kornienko, A. Y.; Emge, T. J.; Brennan, J. G. Tetrametallic Thorium Compounds with Th_4E_4 (E = S, Se) Cubane Cores. *Inorg. Chem.* **2017**, *56*, 10247-10256.(c) Arliguie, T.; Thuery, P.; Le Floch, P.; Mezailles, N.; Ephritikhine, M. A homoleptic SPS-based complex and a double-cubane-type sulfur cluster of an actinide element. *Polyhedron* **2009**, *28*, 1578-1582.(d) Gaunt, A. J.; Scott, B. L.; Neu, M. P. U(IV) chalcogenolates synthesized via oxidation of uranium metal by dichalcogenides. *Inorg. Chem.* **2006**, *45*, 7401-7407.(e) Siladke, N. A.; Ziller, J. W.; Evans, W. J. Insertion, Isomerization, and Cascade Reactivity of the Tethered Silylalkyl Uranium Metallocene $(\eta^5\text{-}C_5Me_4SiMe_2CH_2\text{-}\kappa C)_2U$. *J. Am. Chem. Soc.* **2011**, *133*, 3507-3516.(f) Tang, Y. X.; Deng, J. Y.; Li, W. L.; Malyi, O. I.; Zhang, Y. Y.; Zhou, X. R.; Pan, S. W.; Wei, J. Q.; Cai, Y. R.; Chen, Z.; Chen, X. D. Water-Soluble Sericin Protein Enabling Stable Solid-Electrolyte Interphase for Fast Charging High Voltage Battery Electrode. *Adv. Mater.* **2017**, *29*, 1701828.(g) Smiles, D. E.; Wu, G.; Hayton, T. W. Synthesis, Electrochemistry, and Reactivity of the Actinide Trisulfides [K(18-crown-6)][$An(\eta^3\text{-}S_3)(NR_2)_3$] (An = U, Th; R = $SiMe_3$). *Inorg. Chem.* **2016**, *55*, 9150-9153.(h) Franke, S. M.; Rosenzweig, M. W.; Heinemann, F. W.; Meyer, K. Reactivity of uranium(III) with H_2E (E = S, Se, Te): synthesis of a series of mononuclear and dinuclear uranium(IV) hydrochalcogenido complexes. *Chem. Sci.* **2015**, *6*, 275-282.(i) Gaunt, A. J.; Scott, B. L.; Neu, M. P. A molecular actinide-tellurium bond and comparison of bonding in $[M^{III}\{N(TeP\textit{i}Pr_2)_2\}_3]$ (M = U, La). *Angew. Chem. Int. Ed.* **2006**, *45*, 1638-1641.(j) Jones, R. G.; Karmas, G.; Martin Jr., G. A.; Gilman, H. Organic compounds of Uranium. II. Uranium (IV) amides, alkoxides and mercaptides. *J. Am. Chem. Soc.* **1956**, *78*, 4285-4286.(k) Zhou, E. W.; Ren, W. S.; Hou, G. H.; Zi, G. F.; Fang, D. C.; Walter, M. D. Small Molecule Activation Mediated by a Thorium Terminal Imido Metallocene. *Organometallics* **2015**, *34*, 3637-3647.(l) Evans, W. J.; Takase, M. K.; Ziller, J. W.; DiPasquale, A. G.; Rheingold, A. L. Reductive Reactivity of the Tetravalent Uranium Complex $[\eta^5\text{-}C_5Me_5)(\eta^8\text{-}C_8H_8)U]_2(\mu\text{-}\eta^3\text{:}\eta^3\text{-}C_8H_8)$. *Organometallics* **2009**, *28*, 236-243.(m) Ren, W. S.; Zi, G. F.; Walter, M. D. Synthesis, Structure, and Reactivity of a Thorium Metallocene Containing a 2,2'-Bipyridyl Ligand. *Organometallics* **2012**, *31*, 672-679.(n) Leverd, P. C.; Ephritikhine, M.; Lance, M.; Vigner, J.; Nierlich, M. Triscyclopentadienyl uranium thiolates and selenolates. *J. Organomet. Chem.* **1996**, *507*, 229-237.(o) Evans, W. J.; Miller, K. A.; Ziller, J. W.; DiPasquale, A. G.; Heroux, K. J.; Rheingold, A. L. Formation of $(C_5Me_5)_2U(EPh)Me$,$(C_5Me_5)_2U(EPh)_2$, and $(C_5Me_5)_2U(\eta^2\text{-}TeC_6H_4)$ from $(C_5Me_5)_2UMe_2$ and PhEEPh (E = S, Se, Te).

Organometallics **2007**, *26*, 4287-4293.(p) Thomson, R. K.; Graves, C. R.; Scott, B. L.; Kiplinger, J. L. Synthesis and Molecular Structure of $(C_5Me_5)_2U(O^tBu)(SePh)$: A Mixed-Ligand Alkoxide-Selenide Uranium(IV) Metallocene Complex Resulting from *tert*-Butoxy-Trimethylsilane Elimination. *J. Chem. Crystallogr.* **2011**, *41*, 1241-1244.(q) Domingos, A.; Dematos, A. P.; Santos, I. Synthesis and Characterization of the Uranium Alkylthiolate Complex $U(Spr^i)_2(HBPz_3)_2$. *Polyhedron* **1992**, *11*, 1601-1606.(r) Matson, E. M.; Breshears, A. T.; Kiernicki, J. J.; Newell, B. S.; Fanwick, P. E.; Shores, M. P.; Walensky, J. R.; Bartt, S. C. Trivalent Uranium Phenylchalcogenide Complexes: Exploring the Bonding and Reactivity with CS_2 in the Tp^*_2UEPh Series (E = O, S, Se, Te). *Inorg. Chem.* **2014**, *53*, 12977-12985.(s) Ringgold, M.; Rehe, D.; Hrobarik, P.; Kornienko, A. Y.; Emge, T. J.; Brennan, J. G. Thorium Cubanes-Synthesis, Solid-State and Solution Structures, Thermolysis, and Chalcogen Exchange Reactions. *Inorg. Chem.* **2018**, *57*, 7129-7141.

(2) (a) Benaud, O.; Berthet, J. C.; Thuery, P.; Ephritikhine, M. CCDC 958676. *CSD Commun.* **2013**.(b) Lam, O. P.; Heinemann, F. W.; Meyer, K. Activation of elemental S, Se and Te with uranium(III): bridging U-E-U (E = S, Se) and diamond-core complexes $U\text{-}(E)_2\text{-}U$ (E = O, S, Se, Te). *Chem. Sci.* **2011**, *2*, 1538-1547.(c) Ren, W. S.; Zi, G. F.; Fang, D. C.; Walter, M. D. Thorium Oxo and Sulfido Metallocenes: Synthesis, Structure, Reactivity, and Computational Studies. *J. Am. Chem. Soc.* **2011**, *133*, 13183-13196.(d) Chatelain, L.; White, S.; Scopelliti, R.; Mazzanti, M. Isolation of a Star-Shaped Uranium(V/VI) Cluster from the Anaerobic Photochemical Reduction of Uranyl(VI). *Angew. Chem. Int. Ed.* **2016**, *55*, 14323-14327.(e) Camp, C.; Antunes, M. A.; Garcia, G.; Ciofini, I.; Santos, I. C.; Pecaut, J.; Almeida, M.; Marcalo, J.; Mazzanti, M. Two-electron versus one-electron reduction of chalcogens by uranium(III): synthesis of a terminal U(V) persulfide complex. *Chem. Sci.* **2014**, *5*, 841-846.(f) Gardner, B. M.; King, D. M.; Tuna, F.; Wooles, A. J.; Chilton, N. F.; Liddle, S. T. Assessing crystal field and magnetic interactions in diuranium-μ-chalcogenide triamidoamine complexes with $U^{IV}\text{-E-}U^{IV}$ cores (E = S, Se, Te): implications for determining the presence or absence of actinide-actinide magnetic exchange. *Chem. Sci.* **2017**, *8*, 6207-6217.(g) Arnold, P. L.; Stevens, C. J.; Bell, N. L.; Lord, R. M.; Goldberg, J. M.; Nichol, G. S.; Love, J. B. Multi-electron reduction of sulfur and carbon disulfide using binuclear uranium(III) borohydride complexes. *Chem. Sci.* **2017**, *8*, 3609-3617.(h) Brown, J. L.; Wu, G.; Hayton, T. W. Chalcogen Atom Transfer to Uranium(III): Synthesis and Characterization of $[(R_2N)_3U]_2(\mu\text{-E})$ and $[(R_2N)_3U]_2(\mu\text{-}\eta^2\text{:}\eta^2\text{-}S_2)$ (R = $SiMe_3$; E = S, Se, Te). *Organometallics* **2013**, *32*, 1193-1198.(i) Franke, S. M.; Heinemann, F. W.; Meyer, K. Reactivity of uranium(IV) bridged chalcogenido complexes $U^{IV}\text{-E-}U^{IV}$ (E = S. Se) with elemental sulfur and selenium: synthesis of polychalcogenido-bridged uranium complexes. *Chem. Sci.* **2014**, *5*, 942-950.(j) Avens, L. R.; Barnhart, D. M.; Burns, C. J.; Mckee, S. D.; Smith, W. H.

Oxidation Chemistry of a Uranium(III) Aryloxide. *Inorg. Chem.* **1994**, *33*, 4245-4254.(k) Clark, D. L.; Gordon, J. C.; Huffman, J. G.; Watkin, J. G.; Zwick, B. D. Preparation of Mono-Pentamethylcyclopentadienyl Uranium(IV) Sulfido Clusters through Oxidation of $(\eta\text{-}C_5Me_5)_3U_3(\mu_3\text{-}S)(\mu_2\text{-}I)_3I_3$. *New J. Chem.* **1995**, *19*, 495-502.(l) Evans, W. J.; Montalvo, E.; Ziller, J. W.; DiPasquale, A. G.; Rheingold, A. L. Uranium Metallocene Complexes of the 1,3,4,6,7,8-Hexahydro-2*H*-pyrimido[1,2-a]pyrimidinato Ligand, $(hpp)^-$. *Inorg. Chem.* **2010**, *49*, 222-228.(m) Thevenin, T. L.; Wilmarth, W. R.; Peterson, J. R.; Haire, R. G. New Ternary Trans-Uranium Compounds: Chalcogenide Halides. *Mater. Res. Bull.* **1988**, *23*, 851-855.(n) Groom, C. R.; Bruno, I. J.; Lightfoot, M. P.; Ward, S. C. The Cambridge Structural Database. *Acta Crystallogr B* **2016**, *72*, 171-179.

(3) (a) Perry, D. L.; Zalkin, A.; Ruben, H.; Templeton, D. H. Synthesis, Characterization, and Structure of a Uranyl Complex with a Disulfide Ligand, Bis(di-n-Propylammonium) Disulfidobis(di-n-Propylthiocarbamato)dioxouranate(VI). *Inorg. Chem.* **1982**, *21*, 237-240.(b) Smiles, D. E.; Wu, G.; Hayton, T. W. Reversible Chalcogen-Atom Transfer to a Terminal Uranium Sulfide. *Inorg. Chem.* **2014**, *53*, 12683-12685.(c) Smiles, D. E.; Wu, G.; Hayton, T. W. Reactivity of $[U(CH_2SiMe_2NSiMe_3)(NR_2)_2]$ (R = $SiMe_3$) with elemental chalcogens: towards a better understanding of chalcogen atom transfer in the actinides. *New J. Chem.* **2015**, *39*, 7563-7566.(d) Smiles, D. E.; Wu, G.; Hrobarik, P.; Hayton, T. W. Use of ^{77}Se and ^{125}Te NMR Spectroscopy to Probe Covalency of the Actinide-Chalcogen Bonding in $[Th(E_n)\{N(SiMe_3)_2\}_3]^-$ (E = Se, Te; n=1, 2) and Their Oxo-Uranium(VI) Congeners. *J. Am. Chem. Soc.* **2016**, *138*, 814-825.(e) Yang, P. K.; Zhou, E. W.; Fang, B.; Hou, G. H.; Zi, G. F.; Walter, M. D. Preparation of $(\eta^5\text{-}C_5Me_5)_2Th(bipy)$ and Its Reactivity toward Small Molecules. *Organometallics* **2016**, *35*, 2129-2139.(f) Matson, E. M.; Goshert, M. D.; Kiernicki, J. J.; Newell, B. S.; Fanwick, P. E.; Shores, M. P.; Walensky, J. R.; Bart, S. C. Synthesis of Terminal Uranium(IV) Disulfido and Diselenido Compounds by Activation of Elemental Sulfur and Selenium. *Chem. Eur. J.* **2013**, *19*, 16176-16180.(g) Grant, D. J.; Weng, Z. H.; Jouffret, L. J.; Burns, P. C.; Gagliardi, L. Synthesis of a Uranyl Persulfide Complex and Quantum Chemical Studies of Formation and Topologies of Hypothetical Uranyl Persulfide Cage Clusters. *Inorg. Chem.* **2012**, *51*, 7801-7809.

(4) Andrez, J.; Pecaut, J.; Scopelliti, R.; Kefalidis, C. E.; Maron, L.; Rosenzweig, M. W.; Meyere, K.; Mazzanti, M. Synthesis and reactivity of a terminal uranium(IV) sulfide supported by siloxide ligands. *Chem. Sci.* **2016**, *7*, 5846-5856.

(5) Spencer, L. P.; Yang, P.; Scott, B. L.; Batista, E. R.; Boncella, J. M. Oxidative

Addition to U(V)-U(V) Dimers: Facile Routes to Uranium(VI) Bis(imido) Complexes. *Inorg. Chem.* **2009**, *48*, 11615-11623.

(6) Wrobleski, D. A.; Cromer, D. T.; Ortiz, J. V.; Rauchfuss, T. B.; Ryan, R. R.; Sattelberger, A. P. Preparation and Characterization of the First Organoactinide Polysulfide $(\eta^5\text{-}C_5Me_5)_2ThS5$. A Unique Example of the Twist-Boat Conformation of the MS_5 Ring. *J. Am. Chem. Soc.* **1986**, *108*, 174-175.

(7) (a) Smiles, D. E.; Wu, G.; Kaltsoyannis, N.; Hayton, T. W. Thorium-ligand multiple bonds via reductive deprotection of a trityl group. *Chem. Sci.* **2015**, *6*, 3891-3899.(b) Clark, D. L.; Miller, M. M.; Watkin, J. G. Synthesis, Characterization, and X-Ray Structure of the Uranium Thiolate Complex $U(S\text{-}2,6\text{-}Me_2C_6H_3)[N(SiMe_3)_2]_3$. *Inorg. Chem.* **1993**, *32*, 772-774.(c) Roger, M.; Barros, N.; Arliguie, T.; Thuery, P.; Maron, L.; Ephritikhine, M. $U(SMes^*)_n$, (n=3, 4) and $Ln(SMes^*)_3$ (Ln = La, Ce, Pr, Nd): Lanthanide(III)/actinide(III) differentiation in agostic interactions and an unprecedented η^3 Ligation mode of the arylthiolate ligand, from X-ray diffraction and DFT analysis. *J. Am. Chem. Soc.* **2006**, *128*, 8790-8802.(d) Brown, J. L.; Fortier, S.; Lewis, R. A.; Wu, G.; Hayton, T. W. A Complete Family of Terminal Uranium Chalcogenides, $[U(E)(N\{SiMe_3\}_2)_3]^-$ (E = O, S, Se, Te). *J. Am. Chem. Soc.* **2012**, *134*, 15468-15475.

(8) (a) Zhang, L.; Fang, B.; Hou, G.; Ai, L.; Ding, W.; Walter, M. D.; Zi, G. Intrinsic reactivity of a uranium metallacyclopropene toward unsaturated organic molecules. *Dalton Trans.* **2016**, *45*, 16441-16452.(b) Montalvo, E.; Miller, K. A.; Ziller, J. W.; Evans, W. J. Reactivity of Tuck-in and Tuck-over Uranium Metallocene Complexes. *Organometallics* **2010**, *29*, 4159-4170.(c) Barnea, E.; Andrea, T.; Kapon, M.; Eisen, M. S. Formation of inclusion organoactinide complexes with boron-containing macrocycles. *J. Am. Chem. Soc.* **2004**, *126*, 5066-5067.(d) Zhang, L.; Hou, G.; Zi, G.; Ding, W.; Walter, M. D. Preparation of a uranium metallacyclocumulene and its reactivity towards unsaturated organic molecules *Dalton Trans.* **2017**, *46*, 3716-3728.(e) Ren, W. S.; Song, H. B.; Zi, G. F.; Walter, M. D. A bipyridyl thorium metallocene: synthesis, structure and reactivity. *Dalton Trans.* **2012**, *41*, 5965-5973.(f) Graves, C. R.; Scott, B. L.; Morris, D. E.; Kiplinger, J. L. Selenate and tellurate complexes of pentavalent uranium. *Chem. Commun.* **2009**, 776-778.(g) Zalkin, A.; Brennan, J. G. A Trivalent-Uranium Thioether Coordination Compound. *Acta Crystallogr. C* **1985**, *41*, 1295-1297.(h) Brennan, J. G.; Andersen, R. A.; Zalkin, A. Chemistry of Trivalent Uranium Metallocenes: Electron-Transfer Reactions with Carbon Disulfide. Formation of $[(RC_5H_4)_3U]_2[\mu\text{-}\eta^1, \eta^2\text{-}CS_2]$. *Inorg. Chem.* **1986**, *25*, 1756-1760.(i) Siladke, N. A.; LeDuc, J.; Ziller, J. W.; Evans, W. J. Synthesis and Insertion Chemistry of Mixed Tether Uranium Metallocene Complexes. *Chem. Eur. J.* **2012**, *18*, 14820-14827.(j) Fang, B.;

Ren, W. S.; Hou, G. H.; Zi, G. F.; Fang, D. C.; Maron, L.; Walter, M. D. An Actinide Metallacyclopropene Complex: Synthesis, Structure, Reactivity, and Computational Studies. *J. Am. Chem. Soc.* **2014**, *136*, 17249-17261.(k) Evans, W. J.; Walensky, J. R.; Ziller, J. W. Reaction Chemistry of the U^{3+} Metallocene Amidinate $(C_5Me_5)_2[^iPrNC(Me)N^iPr]U$ Including the Isolation of a Uranium Complex of a Monodentate Acetate. *Inorg. Chem.* **2010**, *49*, 1743-1749.(l) Ventelon, L.; Lescop, C.; Arliguie, T.; Leverd, P. C.; Lance, M.; Nierlich, M.; Ephritikhine, M. Synthesis and X-ray crystal structure of [Na(18-crown-6)][$U(Cp^*)_2(SBu^t)(S)$], the first f-element compound containing a metal-sulfur double bond. *Chem. Commun.* **1999**, 659-660.(m) Lin, Z. R.; Brock, C. P.; Marks, T. J. Synthesis, Structural Characterization, and Properties of the Organothorium Alkylthiolate Complex $[(CH_3)_5C_5]_2Th(SCH_2CH_2CH_3)_2$. *Inorg. Chim. Acta* **1988**, *141*, 145-149.(n) Arliguie, T.; Blug, M.; Le Floch, P.; Mezailles, N.; Thuery, P.; Ephritikhine, M. Organouranium complexes with phosphinine-based SPS pincer ligands. Variations with the substituent at the phosphorus atom. *Organometallics* **2008**, *27*, 4158-4165.(o) Tourneux, J. C.; Berthet, J. C.; Thuery, P.; Mezailles, N.; Le Floch, P.; Ephritikhine, M. Easy access to uranium nucleophilic carbene complexes. *Dalton Trans.* **2010**, *39*, 2494-2496.(p) Fang, B.; Zhang, L.; Hou, G.; Zi, G.; Fang, D.-C.; Walter, M. D. Experimental and Computational Studies on an Actinide Metallacyclocumulene Complex. *Organometallics* **2015**, *34*, 5669-5681.(q) Cao, Y.; Kobayashi, N.; Zhang, Y. W.; Ohnuma, S.; Masumoto, H. Enhanced spin-dependent charge transport of Co-(Al-fluoride) granular nanocomposite by co-separate sputtering. *J. Appl. Phys.* **2017**, *122*, 133903.(r) Kiernicki, J. J.; Staun, S. L.; Zeller, M.; Bart, S. C. A Uranium(IV) Triamide Species with Bronsted Basic Ligand Character: Metal Ligand Cooperativity in the f Block. *Organometallics* **2017**, *36*, 665-672.(s) Formanuik, A.; Ortu, F.; Inman, C. J.; Kerridge, A.; Castro, L.; Maron, L.; Mills, D. P. Concomitant Carboxylate and Oxalate Formation From the Activation of CO_2 by a Thorium(III) Complex. *Chem. Eur. J.* **2016**, *22*, 17976-17979.(t) Tourneux, J. C.; Berthet, J. C.; Cantat, T.; Thuery, P.; Mezailles, N.; Le Floch, P.; Ephritikhine, M. Uranium(IV) Nucleophilic Carbene Complexes. *Organometallics* **2011**, *30*, 2957-2971.(u) Roger, M.; Belkhiri, L.; Thuery, P.; Arliguie, T.; Fourmigue, M.; Boucekkine, A.; Ephritikhine, M. Lanthanide(III)/actinide(III) differentiation in mixed cyclopentadienyl/dithiolene compounds from X-ray diffraction and density functional theory analysis. *Organometallics* **2005**, *24*, 4940-4952.(v) Arliguie, T.; Lescop, C.; Ventelon, L.; Leverd, P. C.; Thuery, P.; Nierlich, M.; Ephritikhine, M. C-H and C-S bond cleavage in uranium(III) thiolato complexes. *Organometallics* **2001**, *20*, 3698-3703.(w) Evans, W. J.; Miller, K. A.; Kozimor, S. A.; Ziller, J. W.; DiPasquale, A. G.; Rheingold, A. L. Actinide hydride complexes as multielectron reductants: Analogous reduction chemistry from $[(C_5Me_5)_2UH]_2$, $[(C_5Me_5)_2UH_2]_2$, and $[(C_5Me_5)_2ThH_2]_2$. *Organometallics* **2007**,

26, 3568-3576.(x) Ren, W. S.; Lukens, W. W.; Zi, G. F.; Maron, L.; Walter, M. D. Is the bipyridyl thorium metallocene a low-valent thorium complex? A combined experimental and computational study. *Chem. Sci.* **2013**, *4*, 1168-1174.(y) Lescop, C.; Arliguie, T.; Lance, M.; Nierlich, M.; Ephritikhine, M. Bispentamethylcyclopentadienyl uranium(IV) thiolate compounds. Synthesis and reactions with CO_2 and CS_2. *J. Organomet. Chem.* **1999**, *580*, 137-144.(z) Mehdoui, T.; Berthet, J. C.; Thuery, P.; Ephritikhine, M. CCDC 958639. *CSD Commun.* **2014**.(aa) Evans, W. J.; Miller, K. A.; Hillman, W. R.; Ziller, J. W. Two-electron reductive reactivity of trivalent uranium tetraphenylborate complexes of $(C_5Me_5)^{1-}$ and $(C_5Me_4H)^{1-}$. *J. Organomet. Chem.* **2007**, *692*, 3649-3654.(ab) Roger, M.; Belkhiri, L.; Arliguie, T.; Thuery, P.; Boucekkine, A.; Ephritikhine, M. Uranium and lanthanide complexes with the 2-mercapto benzothiazolate ligand: Evidence for a specific covalent binding site in the differentiation of isostructural lanthanide(III) and actinide(III) compounds. *Organometallics* **2008**, *27*, 33-42.(ac) Graves, C. R.; Scott, B. L.; Morris, D. E.; Kiplinger, J. L. Facile access to pentavalent uranium organometallics: One-electron oxidation of Uranium(IV) imido complexes with copper(I) salts. *J. Am. Chem. Soc.* **2007**, *129*, 11914-11915.(ad) Kiernicki, J. J.; Fanwick, P. E.; Bart, S. C. Utility of a redox-active pyridine(diimine) chelate in facilitating two electron oxidative addition chemistry at uranium. *Chem. Commun.* **2014**, *50*, 8189-8192.

(9) Campello, M. P. C.; Domingos, A.; Galvao, A.; de Matos, A. P.; Santos, I. Derivative chemistry of $[UCl_2\{B(pz)_4\}_2]$: stability of complexes containing the fragments $[U\{B(pz)_4\}_2]$ and $[U\{HB(pz)_3\}_2]$. *J. Organomet. Chem.* **1999**, *579*, 5-17.

(10) (a) Smiles, D. E.; Wu, G.; Hayton, T. W. Synthesis of Uranium-Ligand Multiple Bonds by Cleavage of a Trityl Protecting Group. *J. Am. Chem. Soc.* **2014**, *136*, 96-99.(b) Brown, J. L.; Fortier, S.; Wu, G.; Kaltsoyannis, N.; Hayton, T. W. Synthesis and Spectroscopic and Computational Characterization of the Chalcogenido-Substituted Analogues of the Uranyl Ion, $[OUE]^{2+}$ (E = S, Se). *J. Am. Chem. Soc.* **2013**, *135*, 5352-5355.

(11) (a) Choi, C. L.; Alivisatos, A. P. From Artificial Atoms to Nanocrystal Molecules: Preparation and Properties of More Complex Nanostructures. *Annu Rev Phys Chem* **2010**, *61*, 369-389.(b) Salunkhe, A. B.; Khot, V. M.; Pawar, S. H. Magnetic Hyperthermia with Magnetic Nanoparticles: A Status Review. *Curr. Top. Med. Chem.* **2014**, *14*, 572-594.(c) Ubale, A. U.; Choudhari, D. M.; Kantale, J. S.; Mitkari, V. N.; Nikam, M. S.; Gawande, W. J.; Patil, P. P. Synthesis of nanostructured Cu_xS thin films by chemical route at room temperature and investigation of their size dependent physical properties. *J. Alloys Compd.* **2011**, *509*, 9249-9254.

(12) Sutorik, A. C.; Kanatzidis, M. G. Synthesis of $[U(Se_2)_4]^{4-}$ - the First Homoleptic Actinide Polychalcogenide Complex. *J. Am. Chem. Soc.* **1991**, *113*, 7754-7755.

(13) Sutorik, A. C.; Kanatzidis, M. G. Isolation of the polysulfide complex $[(UO_2)(S_2)_3]^{4-}$ from the in situ formation and subsequent reaction of uranyl cations in molten alkali metal polysulfide salts. *Polyhedron* **1997**, *16*, 3921-3927.

(14) (a) Behrle, A. C.; Levin, J. R.; Kim, J. E.; Drewett, J. M.; Barnes, C. L.; Schelter, E. J.; Walensky, J. R. Stabilization of M-IV = Ti, Zr, Hf, Ce, and Th using a selenium bis(phenolate) ligand. *Dalton Trans.* **2015**, *44*, 2693-2702.(b) Crawford, M. J.; Karaghiosoff, K.; Mayer, P. The Homoleptic $U(NCSe)_8^{4-}$ Anion in $(Pr_4N)_4U(NCSe)_8 \cdot 2CFCl_3$ and $Th(NCSe)_4(OP(NMe_2)_3)_4 \cdot 0.5CH_3CN \cdot 0.5H_2O$: First Structurally Characterised Actinide Isoselenocyanates. *Z. Anorg. Allg. Chem.* **2010**, *636*, 1903-1906.(c) Settineri, N. S.; Garner, M. E.; Arnold, J. A Thorium Chalcogenolate Series Generated by Atom Insertion into Thorium-Carbon Bonds. *J. Am. Chem. Soc.* **2017**, *139*, 6261-6269.

(15) (a) Gotthelf, G.; Stuber, M. A.; Kornienko, A. Y.; Emge, T. J.; Brennan, J. G. Organosoluble tetravalent actinide di- and trifluorides. *Chem. Commun.* **2018**, *54*, 12018-12020.(b) Cooper, O. J.; Mills, D. P.; Lewis, W.; Blake, A. J.; Liddle, S. T. Reactivity of the uranium(IV) carbene complex $[U(BIPM^{TMS})(Cl)(\mu\text{-}Cl)_2Li(THF)_2]$ (BIPMTMS = $\{C(PPh_2NSiMe_3)_2\}$) towards carbonyl and heteroallene substrates: metallo-Wittig, adduct formation, C–F bond activation, and [2 + 2]-cycloaddition reactions. *Dalton Trans.* **2014**, *43*, 14275-14283.(c) Berthet, J. C.; Thuery, P.; Ephritikhine, M. CCDC 959209. *CSD Commun.* **2013**.(d) Siffredi, G.; Berthet, J. C.; Thuery, P.; Ephritikhine, M. CCDC 958347. *CSD Commun.* **2013**.

(16) Barnhart, D. M.; Clark, D. L.; Gordon, J. C.; Huffman, J. C.; Watkin, J. G. Oligomerization of Metal-Oxygen Bonds in Thorium Alkoxide Chemistry: X-Ray Crystal Structures of $Th_4(O\text{-}i\text{-}Pr)_{16}(py)_2$ and $Th_2(OCHEt_2)_8(py)_2$. *Inorg. Chem.* **1994**, *33*, 3939-3944.

(17) Evans, W. J.; Walensky, J. R.; Ziller, J. W. Reactivity of Methyl Groups in Actinide Metallocene Amidinate and Triazenido Complexes with Silver and Copper Salts. *Organometallics* **2010**, *29*, 101-107.

(18) Travia, N. E.; Monreal, M. J.; Scott, B. L.; Kiplinger, J. L. Thorium-mediated ring-opening of tetrahydrofuran and the development of a new thorium starting material: preparation and chemistry of $ThI_4(DME)_2$. *Dalton Trans.* **2012**, *41*, 14514-14523.

(19) Barnhart, D. M.; Clark, D. L.; Gordon, J. C.; Huffman, J. C.; Watkin, J. G.; Zwick, B. D. Solution Study of the Ambient-Temperature Monomer-Dimer Equilibrium $Th_2(OR)_8 \rightleftharpoons 2Th(OR)_4$ (R=CH-*i*-Pr_2)$_4$(quin)and X-Ray Crystal-Structures of Th2(OCH-*i*-Pr_2)$_8$, Th(OCH-*i*-Pr_2)$_4$(quin), and ThI(OCH-*i*-Pr_2)$_3$(py)$_2$. *Inorg. Chem.* **1995**, *34*, 5416-5423.

(20) Edelman, M. A.; Hitchcock, P. B.; Hu, J.; Lappert, M. F. Organoactinide Chemistry.II. The Chemistry of Some Novel Cyclopentadienylthorium Complexes. *New J. Chem.* **1995**, *19*, 481-489.

(21) Yang, P.; Zhou, E.; Hou, G.; Zi, G.; Ding, W.; Walter, M. D. Experimental and Computational Studies on the Formation of Thorium-Copper Heterobimetallics. *Chem. Eur. J.* **2016**, *22*, 13845-13849.

(22) Hohloch, S.; Garner, M. E.; Parker, B. F.; Arnold, J. New supporting ligands in actinide chemistry: tetramethyltetraazaannulene complexes with thorium and uranium. *Dalton Trans.* **2017**, *46*, 13768-13782.

(23) (a) Cantat, T.; Scott, B. L.; Kiplinger, J. L. Convenient access to the anhydrous thorium tetrachloride complexes $ThCl_4(DME)_2$, $ThCl_4$(1,4-dioxane)$_2$ and $ThCl_4(THF)_{3.5}$ using commercially available and inexpensive starting materials. *Chem. Commun.* **2010**, *46*, 919-921.(b) Ward, A. L.; Lukens, W. W.; Lu, C. C.; Arnold, J. Photochemical Route to Actinide-Transition Metal Bonds: Synthesis, Characterization and Reactivity of a Series of Thorium and Uranium Heterobimetallic Complexes. *J. Am. Chem. Soc.* **2014**, *136*, 3647-3654.(c) Fang, B.; Hou, G.; Zi, G.; Ding, W.; Walter, M. D. Steric and Electronic Influences of Internal Alkynes on the Formation of Thorium Metallacycles: A Combined Experimental and Computational Study. *Organometallics* **2016**, *35*, 1384-1391.(d) Rickard, C. E. F.; Woollard, D. C. Structure of Tetrachlorotetrakis(Diphenyl Sulfoxide)Thorium(IV). *Acta Crystallogr B* **1980**, *36*, 292-294.(e) Moloy, K. G.; Marks, T. J.; Day, V. W. Carbon-Monoxide Activation by Organoactinides. η^2-Acyl-CO Coupling and the Formation of Metal-Bound Ketenes. *J. Am. Chem. Soc.* **1983**, *105*, 5696-5698.(f) Mora, E.; Maria, L.; Biswas, B.; Camp, C.; Santos, I. C.; Pecaut, J.; Cruz, A.; Carretas, J. M.; Marcalo, J.; Mazzanti, M. Diamine Bis(phenolate) as Supporting Ligands in Organoactinide(IV) Chemistry. Synthesis, Structural Characterization, and Reactivity of Stable Dialkyl Derivatives. *Organometallics* **2013**, *32*, 1409-1422.(g) Stobbe, B. C.; Powell, D. R.; Thomson, R. K. Schiff base thorium(IV) and uranium(IV) chloro complexes: synthesis, substitution and oxidation chemistry. *Dalton Trans.* **2017**, *46*, 4888-4892.(h) Karmel, I. S. R.; Fridman, N.; Eisen, M. S. Actinide Amidinate Complexes with a Dimethylamine Side Arm: Synthesis, Structural Characterization, and Reactivity. *Organometallics* **2015**, *34*, 636-643.

(24) Alvarez, S.; Hoffmann, R.; Mealli, C. A Bonding Quandary-or-A Demonstration of the Fact That Scientists Are Not Born With Logic. *Chem. Eur. J.* **2009**, *15*, 8358-8373.

(25) (a) Fagin, A. A.; Kuznetsova, O. V.; Balashova, T. V.; Cherkasov, A. V.; Fukin, G. K.; Bochkarev, M. N. Iodide-sulfides of dysprosium: Elucidation of the pathway to lanthanide iodide-sulfide-nitride clusters. *Inorg. Chim. Acta* **2018**, *469*, 227-230.(b) Zhang, Z. X.; Zhang, L. X.; Li, Y. R.; Hong, L. C.; Chen, Z. X.; Zhou, X. G. Activation of Bis(guanidinate)lanthanide Alkyl and Aryl Complexes on Elemental Sulfur: Synthesis and Characterization of Bis(guanidinate)lanthanide Thiolates and Disulfides. *Inorg. Chem.* **2010**, *49*, 5715-5722.

(26) (a) Melman, J. H.; Fitzgerald, M.; Freedman, D.; Emge, T. J.; Brennan, J. G. Chalcogen-rich lanthanide clusters from lanthanide halide starting materials: A new approach to the low-temperature synthesis of LnS_x solids from molecular precursors. *J. Am. Chem. Soc.* **1999**, *121*, 10247-10248.(b) Fitzgerald, M.; Emge, T. J.; Brennan, J. G. Chalcogen-rich lanthanide clusters with fluorinated thiolate ligands. *Inorg. Chem.* **2002**, *41*, 3528-3532.

(27) (a) Brunner, H.; Meier, W.; Wachter, J.; Guggolz, E.; Zahn, T.; Ziegler, M. L. Investigation into the Reactivity of the Metal-Metal Triple Bond in $[Cp'(CO)_2M]_2$(Cp'=η^5-C_5Me_5; M=Mo,W) vs. Elemental Sulfur. Formation of Different $Cp'_2M_2S_4$ Isomers and Crystal Structures of $Cp'_2Mo_2(\mu\text{-}S_2)(\mu\text{-}S)_2$ and $Cp'_2(CO)_2W_2(\mu\text{-}S)_2S$. *Organometallics* **1982**, *1*, 1107-1113.(b) Fedin, V. P.; Muller, A.; Filipek, K.; Rohlfing, R.; Bogge, H.; Vorovets, A. V.; Dziegielewski, J. O. Extrusion of Molecular Clusters from Solid-State Materials - Synthesis by Application of γ-Irradiation - Molecular and Crystal-Structure of $(H_9O_4)(Et_4N)[MO_3S_7Br_6]$. *Inorg. Chim. Acta* **1994**, *223*, 5-7.(c) Bar-Nahum, I.; York, J. T.; Young, V. G.; Tolman, W. B. Novel reactivity of side-on (disulfido)dicopper complexes supported by Bi- and tridentate nitrogen donors: Impact of axial coordination. *Angew. Chem. Int. Ed.* **2008**, *47*, 533-536.(d) Kubas, G. J.; Ryan, R. R.; Kubatmartin, K. A. Cleavage of SO_2 on (η^5-$C_5Me_5)_2Mo_2(\mu\text{-}S_2)(\mu\text{-}S)_2$ to Form S_8 and a Thiosulfate Complex, (η^5-$C_5Me_5)_2Mo_2(\mu\text{-}S_2)(\mu\text{-}S)(\mu\text{-}SSO_3)$ - Possible Role in Homogeneous Hydrogenation of SO_2 Catalyzed by Mo-S Complexes. *J. Am. Chem. Soc.* **1989**, *111*, 7823-7832.(e) Fujisawa, K.; Morooka, Y.; Kitajima, N. Formation of a μ-η^2:η^2-Disulfide Dinuclear Copper(II) Complex by Thermal-Decomposition of a Thiolate Complex via C-S Bond-Cleavage. *J. Chem. Soc. Chem. Commun.* **1994**, 623-624.(f) Helton, M. E.; Maiti, D.; Zakharov, L. N.; Rheingold, A. L.; Porco, J. A.; Karlin, K. D. A μ-η^2:η^2-disulfide dicopper(II) complex from reaction of S_8 with a copper(I) precursor: Reactivity of the bound disulfur moiety. *Angew. Chem. Int. Ed.* **2006**, *45*, 1138-1141.(g) Kajita, Y.; Matsumoto, J.; Takahashi,

I.; Hirota, S.; Funahashi, Y.; Ozawa, T.; Masuda, H. Syntheses, characterization, and reactivities of (μ-η^2:η^2)-disulfido)dicopper(II) complexes with N-alkylated *cis*, *cis*-1,3,5-triaminocyclohexane derivatives. *Eur. J. Inorg. Chem.* **2008**, 3977-3986.(h) Ryu, S.; Whang, D.; Kim, H. J.; Kim, K.; Yoshida, M.; Hashimoto, K.; Tatsumi, K. Novel disulfido- and diselenido-bridged zirconium and hafnium porphyrin dimers with unusual coordination geometries: $[M(TPP)]_2(\mu$-η^2-$Q_2)_2$ (M=Zr, Hf; Q=S, Se). *Inorg. Chem.* **1997**, *36*, 4607-4609.

(28) (a) Huebner, L.; Kornienko, A.; Emge, T. J.; Brennan, J. G. Lanthanide clusters with internal Ln: Fragmentation and the formation of dimers with bridging Se^{2-} and Se_2^{2-} ligands. *Inorg. Chem.* **2005**, *44*, 5118-5122.(b) Kornienko, A. Y.; Emge, T. J.; Brennan, J. G. Chalcogen-rich lanthanide clusters: Cluster reactivity and the influence of ancillary ligands on structure. *J. Am. Chem. Soc.* **2001**, *123*, 11933-11939.

(29) (a) Yao, S. L.; Xiong, Y.; Zhang, X. H.; Schlangen, M.; Schwarz, H.; Milsmann, C.; Driess, M. Facile Dissociation of $[(LNi^{II})_2E_2]$ Dichalcogenides: Evidence for $[LNi^{II}E_2]$ Superselenides and Supertellurides in Solution. *Angew. Chem. Int. Ed.* **2009**, *48*, 4551-4554.(b) Wu, D. H.; Xu, B. H.; Li, Y. Z.; Yan, H. Diruthenium half-sandwich complexes containing one μ-E_2 (E = S, Se) unit and two chelating 1,2-dicarba-closo-dodecaborane-1,2-dithiolate ligands: Reactivity studies with methyl acetylene carboxylates. *Organometallics* **2007**, *26*, 6300-6306.(c) Fedin, V. P.; Sokolov, M. N.; Gerasko, O. A.; Virovets, A. V.; Podberezskaya, N. V.; Fedorov, V. Y. Triangular $M_3Se_7^{4+}$ and $M_3Se_4^{4+}$Complexes (M = Mo, W). An X-Ray Study of $Mo_3Se_7(Et_2NCS_2)_4$ and $W_3Se_7(Et_2NCS_2)_4$ *Inorg. Chim. Acta* **1991**, *187*, 81-90.

(30) Bondi, A. Van der Waals Volumes and Radii. *J. Phys.Chem.* **1964**, *68*, 441-451.

(31) (a) Kornienko, A.; Melman, J. H.; Hall, G.; Emge, T. J.; Brennan, J. G. Chalcogen Rich Lanthanide Clusters from Halide Starting Materials (II): Selenido Compounds. *Inorg. Chem.* **2002**, *41*, 121-126.(b) Kornienko, A.; Moore, B. F.; Kumar, G. A.; Tan, M.-C.; Riman, R. E.; Brik, M. G.; Emge, T. J.; Brennan, J. G. Highly NIR-Emissive Lanthanide Polyselenides. *Inorg. Chem.* **2011**, *50*, 9184-9190.(c) Kornienko, A.; Emge, T. J.; Kumar, G. A.; Riman, R. E.; Brennan, J. G. Lanthanide Clusters with Internal Ln Ions: Highly Emissive Molecules with Solid-State Cores. *J. Am. Chem. Soc.* **2005**, *127*, 3501-3505.(d) Moore, B. F.; Kumar, G. A.; Tan, M.-C.; Kohl, J.; Riman, R. E.; Brik, M. G.; Emge, T. J.; Brennan, J. G. Lanthanide Clusters with Chalcogen Encapsulated Ln: NIR Emission from Nanoscale $NdSe_x$. *J. Am. Chem. Soc.* **2011**, *133*, 373-378.

(32) Freedman, D.; Emge, T. J.; Brennan, J. G. Chalcogen-Rich Lanthanide Clusters: Compounds with Te2-, (TeTe)2-, TePh, TeTePh,

(TeTeTe(Ph)TeTe)5-, and [(TeTe)4TePh]9- Ligands; Single Source Precursors to Solid-State Lanthanide Tellurides. *Inorg. Chem.* **2002**, *41*, 492-500.

(33) (a) Bueyuekyazi, M.; Fischer, T.; Yu, P.; Coll, M.; Mathur, S. A cobalt(II) heteroarylalkenolate precursor for homogeneous Co_3O_4 coatings by atomic layer deposition *Dalton Trans.* **2017**, *46*, 12996-13001.(b) Jamil, A.; Schlaefer, J.; Goenuellue, Y.; Lepcha, A.; Mathur, S. Precursor-Derived Rare Earth Metal Pyrochlores: $Nd_2Sn_2O_7$ Nanofibers and Thin Films As Efficient Photoabsorbers. *Cryst. Growth Des.* **2016**, *16*, 5260-5267.(c) Lee, J.; Brewer, M.; Berardini, M.; Brennan, J. G. Trivalent Lanthanide Chalcogenolates - Synthesis, Structure, and Thermolysis Chemistry. *Inorg. Chem.* **1995**, *34*, 3215-3219.(d) Fuhrmann, D.; Dietrich, S.; Krautscheid, H. Copper Zinc Thiolate Complexes as Potential Molecular Precursors for Copper Zinc Tin Sulfide (CZTS). *Chem. Eur. J.* **2017**, *23*, 3338-3346.(e) Gaber, A. A. M.; Wentrup, C. Pyrolysis of hydrazine derivatives and related compounds with N-N single bonds. *J. Anal. Appl. Pyrol.* **2017**, *125*, 258-278.(f) Holligan, K.; Rogler, P.; Rehe, D.; Pamula, M.; Kornienko, A. Y.; Emge, T. J.; Krogh-Jespersen, K.; Brennan, J. G. Copper, Indium, Tin, and Lead Complexes with Fluorinated Selenolate Ligands: Precursors to MSe_x. *Inorg. Chem.* **2015**, *54*, 8896-8904.

(34) D'Eye, R. W. M. The crystal structures of $ThSe_2$ and Th_7Se_{12} *J. Chem. Soc.* **1953**, 1670-1672.

Chapter 3. Thorium Chalcogenolates with Different Neutral Donor Ligands

3.1 Introduction

Interest in the chemistry of actinide ions bound to softer chalcogen (E; E = S, Se or Te) based ligands is in part motivated by the desire to design materials with maximum covalent contributions to stability. A growing number of new actinide chalcogenolate complexes has been published in the past decade and most of the research focused on uranium species.[1] Thorium chemistry is relatively unexplored, as only a few molecular thorium compounds containing Th-E bonds have been reported.[2]

It would be valuable to develop a series of thorium chalcogenolate complexes with various neutral donor ligands in which the chalcogenolate (ER; R = C_6H_5, C_6F_5) is the only coordinated anion (Scheme 3.1), as it may help to understand how the bonding between thorium and chalcogen may impact the structure and stability of these materials. It can also help to understand the influence of the neutral donor ligand on the final structures of the resulting actinide compounds.

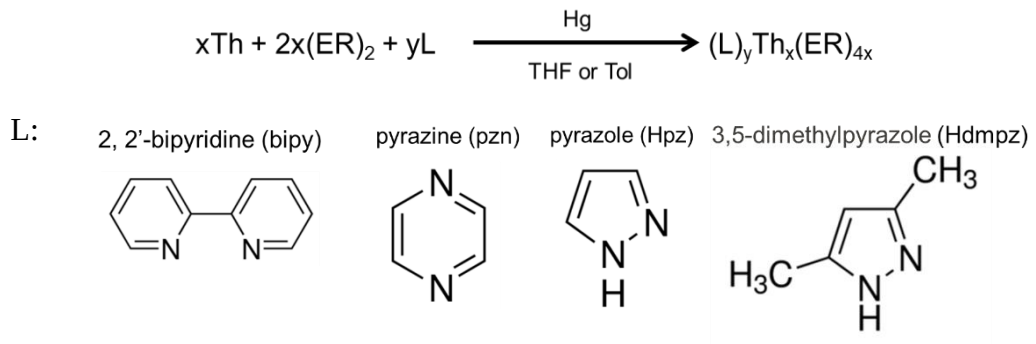

Scheme 3.1. Synthesis of molecular thorium chalcogenolate compounds

2,2'-Bipyridine (bipy) is a widely known bidentate neutral ligand in coordination chemistry. It has been extensively used to form stable metal complexes due to its strong chelating effect and ease of functionalization.[3] In actinide chemistry, there are some examples of uranium compounds with bipy,[4] but no thorium analogs.

Pyrazine (pzn) can act as a neutral donor ligand and coordinate to metal ions through two nitrogen atoms, and it has been used as a bridging ligand because of its ability to yield one-dimensional linear chains or two-dimensional layer compounds.[5] However, it can also act as a monodentate terminal group, and some complexes[6] even contain both bridging and terminal pyrazine ligands.

Pyrazole (Hpz) can coordinate to metal through one nitrogen atom as a monodentate ligand. When deprotonated, it coordinates through both nitrogen atoms as a bidentate ligand, to form pyrazolate anion (pz^-). In addition, the nucleophilicity of the nitrogen atoms and their steric accessibility may be varied through appropriate substitution on the heterocyclic ring.[7] This feature makes pyrazole and pyrazole-derived ligands, including 3,5-dimethylpyrazole (Hdmpz), $HB(pz)_3^-$ (Tp^-), and $HB(dmpz)_3^-$ (Tp^{*-}), extremely versatile in organometallic chemistry. While a majority of the complexes are based on transitional metal centers with steric bulky ligands, actinide complexes with pyrazole-derived ligands are limited,[8] and few thorium examples have been reported,[9] all of which contain the Tp ligand.

This chapter outlines synthesis and characterizations of a series of thorium perfluorothiolates with different neutral donor ligands, including bipy, pzn, Hpz and

Hdmpz. A thorium dimer with -SePh and a thorium cluster with SeC_6F_5 have also been obtained with pyrazole-based ligands in toluene solution.

3.2 Thorium Chalcogenolate with Bipyridine Ligand

Metal Th reacts with $(SC_6F_5)_2$ and bipy in THF solution to form the bis-bipy chelate thorium monomer $(bipy)_2Th(SC_6F_5)_4$ (**11**). Trace amount of mercury was added as a catalyst to reduce the reaction time. The product was characterized by conventional methods and low-temperature single-crystal X-ray diffraction. Figures 3.1 shows the ORTEP diagram of the molecular structure of **11**. Selected crystallographic details are given in Table 3.1.

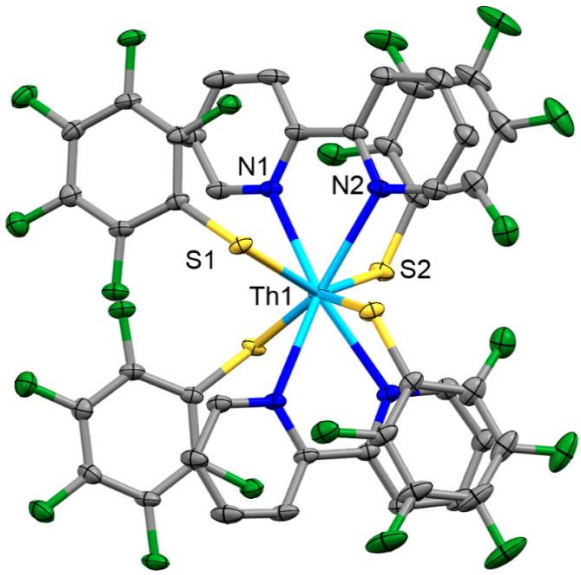

Figure 3.1. ORTEP diagram of $(bipy)_2Th(SC_6F_5)_4$ (**11**), with yellow S, green F, light blue Th, dark blue N, grey C, the H atoms removed for clarity and ellipsoids at the 50% probability level.

Table 3.1. Crystallographic data for $(bipy)_2Th(SC_6F_5)_4$ (**11**)

empirical formula	$C_{52}H_{32}F_{20}N_4O_2S_4Th$	V (Å^3)	5191.9(4)
fw	1485.09	Z	4
crystal system	monoclinic	D(calcd) (g/cm^3)	1.900
space group	C2/c	T (K)	100(2)
a (Å)	26.2472(11)	abs coeff(mm^{-1})	3.153
b (Å)	12.5980(5)	$R(F)^b$ [I > 2σ(I)]	0.0290
c (Å)	17.2129(7)	$R_w(F^2)^c$ [I > 2σ(I)]	0.0643
α (deg)	90		
β (deg)	114.1892(7)		
γ (deg)	90		

In order to confirm the purity of the compound **11**, PXRD was used for characterization and the result is shown in Figure 3.2. Comparison of the experimentally determined PXRD profile with the calculated pattern from the single crystal data indicates high purity of the bulk material.

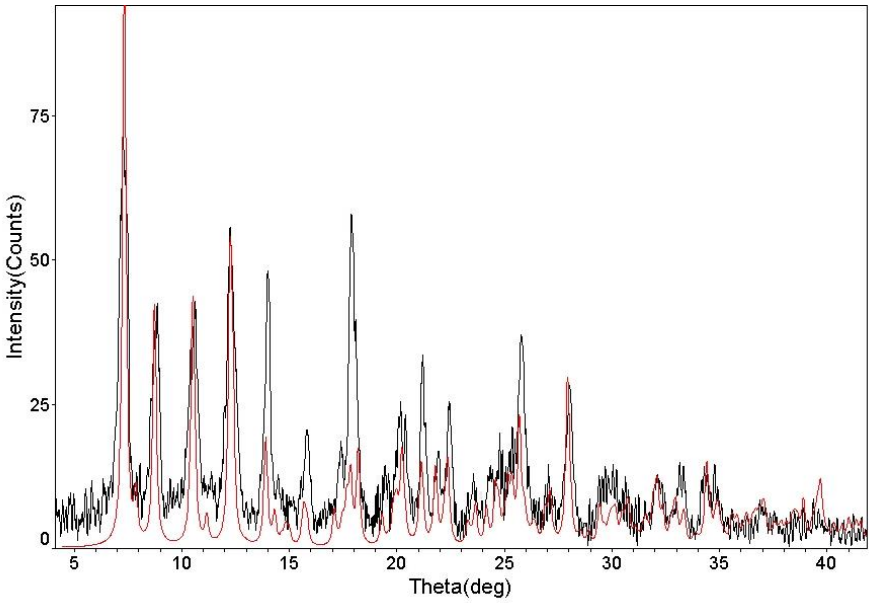

Figure 3.2. PXRD and calculated pattern from single crystal (in red) for $(bipy)_2Th(SC_6F_5)_4$ (**11**)

In this complex, the Th atom is bound to two 2, 2'-bipy neutral ligand and four $SC_6F_5^-$ anions, forming an eight-coordinate geometry. The average Th-S bond length is 2.858 Å, and in good agreement with recently reported monomeric chalcogenolates, such as 2.84 – 2.85 Å in the pyridine derivative $(py)_4Th(SPh)_4$, [2h] and is slightly longer than the 2.81 - 2.82 Å found in 7-coordinate $(py)_4Th(SC_6F_5)_4$. [2h] The average Th-N bond length (2.629 Å) is also in the range (2.3 – 2.8 Å) of An-N bond lengths in the reported actinide compounds containing py and bipy. The distance between the aromatic ring in 2, 2'-bipy and the SC_6F_5 ring is 3.519 Å and 3.643 Å, indicating the existence of face to face π...π stacking interactions.[10]

3.3 Thorium Chalcogenolate with Pyrazine Ligand

The reaction of metallic Th with stoichiometric $(SC_6F_5)_2$ and pyrazine in toluene solution gives a $(pzn)_4Th_2(SC_6F_5)_8$ (**12**) dimer. Trace amount of mercury was added to reduce the reaction time. The product was characterized by low-temperature single-crystal X-ray diffraction. Selected crystallographic details are given in Table 3.2.

Table 3.2. Crystallographic data for $(pzn)_4Th_2(SC_6F_5)_8$ (**12**)

empirical formula	$C_{85}H_{40}F_{40}N_8S_8Th_2$	V (Å^3)	4580(2)
fw	2653.81	Z	4
crystal system	triclinic	D(calcd) (g/cm^3)	2.072
space group	P-1	T (K)	100(2)
a (Å)	14.941(3)	abs coeff(mm^{-1})	3.570
b (Å)	15.150(3)	$R(F)^b$ [I > 2σ(I)]	0.0725
c (Å)	23.122(8)	$R_w(F^2)^c$ [I > 2σ(I)]	0.1655
α (deg)	81.771(15)		
β (deg)	77.580(15)		
γ (deg)	63.817(8)		

ORTEP diagram of the molecular structure of **12** is shown in Figures 3.3.

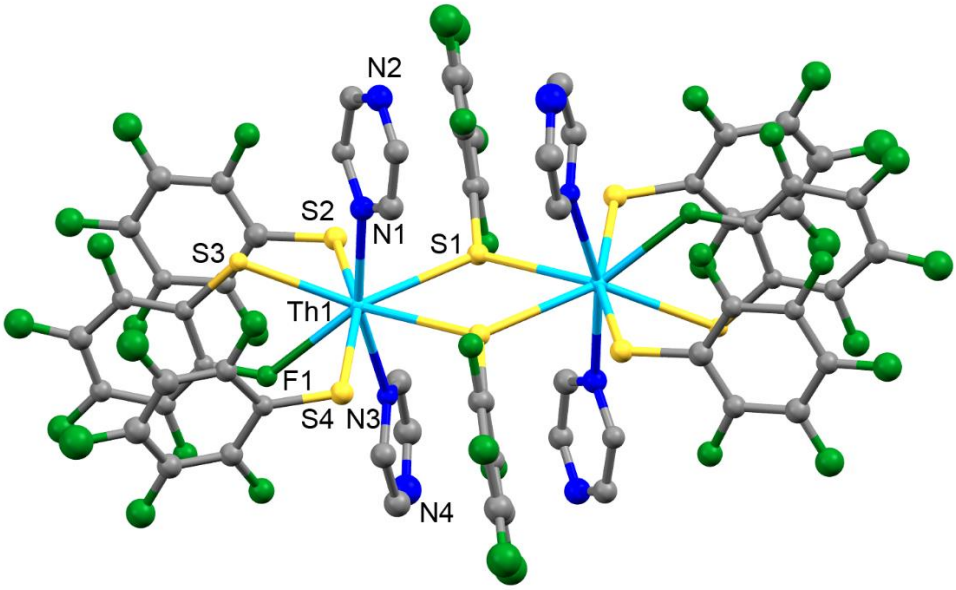

Figure 3.3. ORTEP diagram of $(pzn)_4Th_2(SC_6F_5)_8$ (**12**), with yellow S, green F, light blue Th, dark blue N, grey C, the H atoms removed for clarity and ellipsoids at the 50% probability level.

This compound contains two bridging SC_6F_5 entities, and is the first example of actinide dimer bridged by SC_6F_5. Each Th atom has two terminal pyrazines and three terminal SC_6F_5 ligands. A dative Th-F (2.660 Å) bond is formed to complete coordination sphere on Th metal, resulting in an eight-coordinate structure. Three SC_6F_5 groups are nearly parallel to each other, the distance between the two neighboring aromatic rings are 3.607 Å and 3.777 Å, possibly making intramolecular π...π interactions[10]. The average bond length between Th and S from bridging SC_6F_5 is 2.972 Å, while that between Th and S from terminal thiolate ligand is 2.803 Å, both are consistent with the reported Th-S bond length in the literature.[11] The average Th-N bond length is 2.618 Å and there is no bridging pyrazine in the structure.

3.4 Thorium Chalcogenolates with Pyrazole-derived ligands

Direct synthesis of thorium metal, $(SePh)_2$ or $(SC_6F_5)_2$ ligands and pyrazole (Hpz) in toluene results in two compounds $(Hpz)_4(pz)_2Th_2(SePh)_6$ (**13**) and $(Hpz)_4(pz)Th(SC_6F_5)_3$ (**14**). Replacing Hpz with 3,5-dimethylpyrazole (Hdmpz) in the reaction also results in two compounds $(Hdmpz)_4(dmpz)_2Th_2(SC_6F_5)_6$ (**15**) and $(Hdmpz)_2(dmpz)_2Th(SC_6F_5)_2$ (**16**). Addition of catalytic amount of mercury reduces the reaction completion time.

All these compounds were characterized by low-temperature single-crystal X-ray diffraction. Figures 3.4 - 3.7 show ORTEP diagrams of the molecular structures of **13** - **16**, respectively.

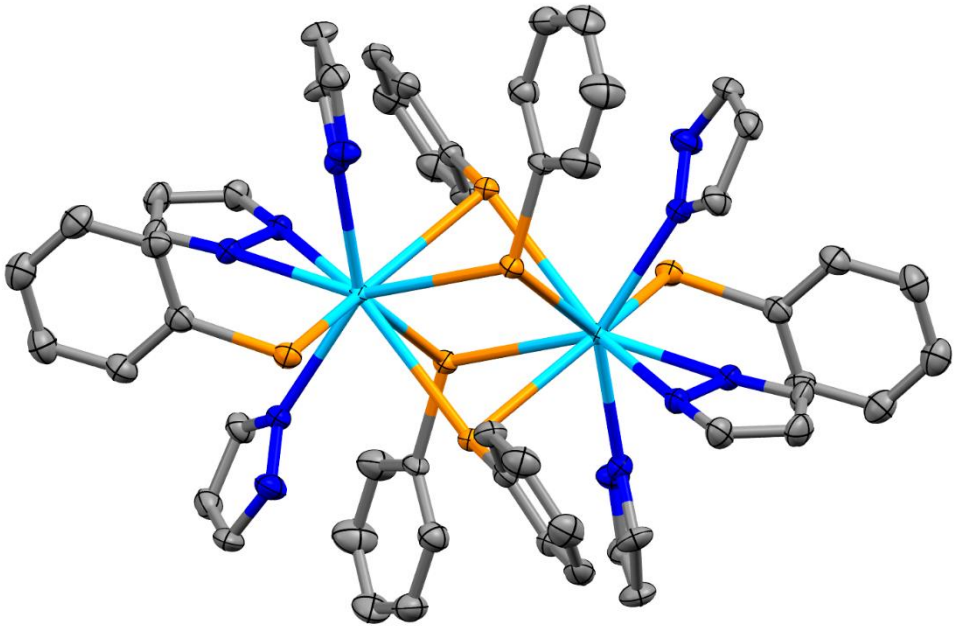

Figure 3.4. ORTEP diagram of $(Hpz)_4(pz)_2Th_2(SePh)_6$ (**13**), with orange Se, light blue Th, dark blue N, grey C, the H atoms removed for clarity and ellipsoids at the 50% probability level.

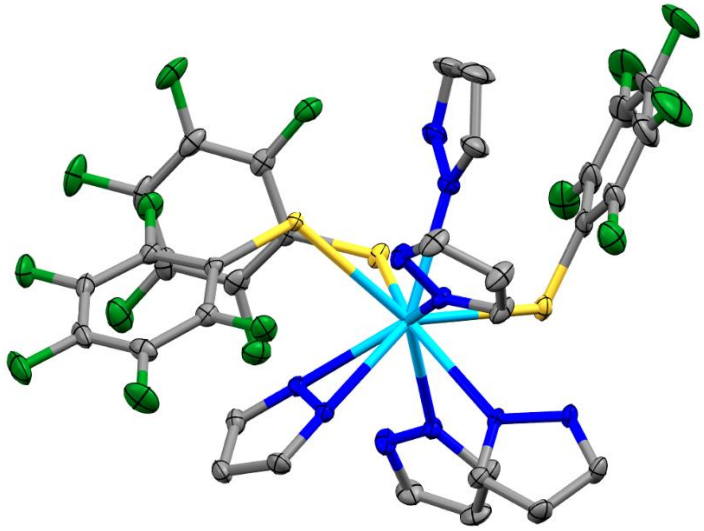

Figure 3.5. ORTEP diagram of $(Hpz)_4(pz)Th(SC_6F_5)_3$ (**14**), with yellow S, green F, light blue Th, dark blue N, grey C, the H atoms removed for clarity and ellipsoids at the 50% probability level.

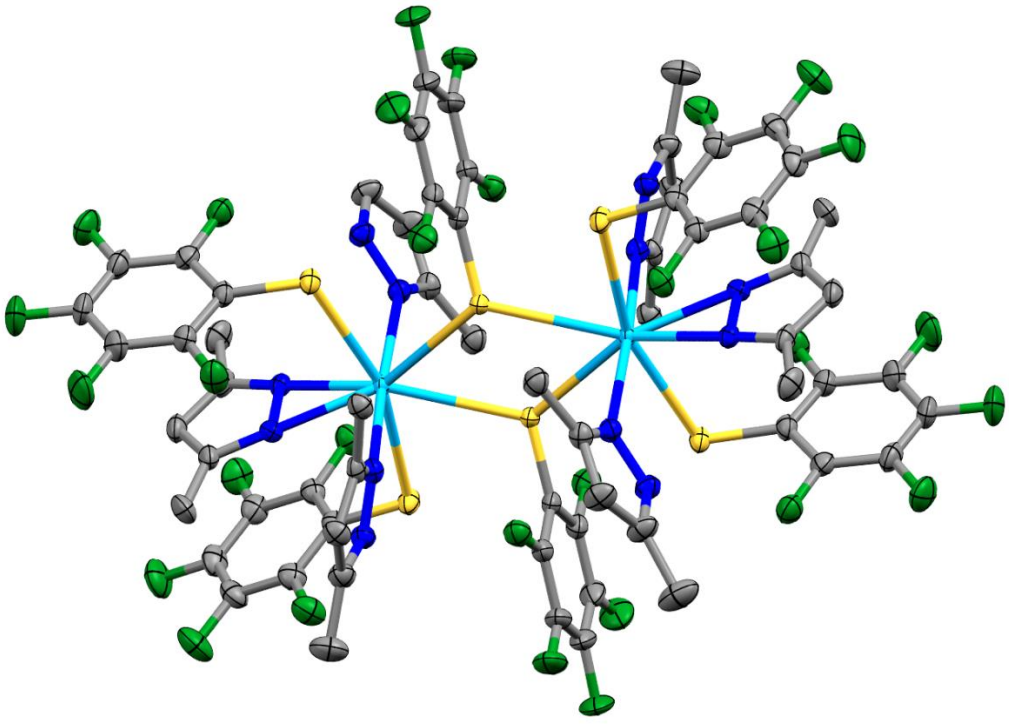

Figure 3.6. ORTEP diagram of $(Hpz)_4(pz)Th(SC_6F_5)_3$ (**15**), with yellow S, green F, light blue Th, dark blue N, grey C, the H atoms removed for clarity and ellipsoids at the 50% probability level.

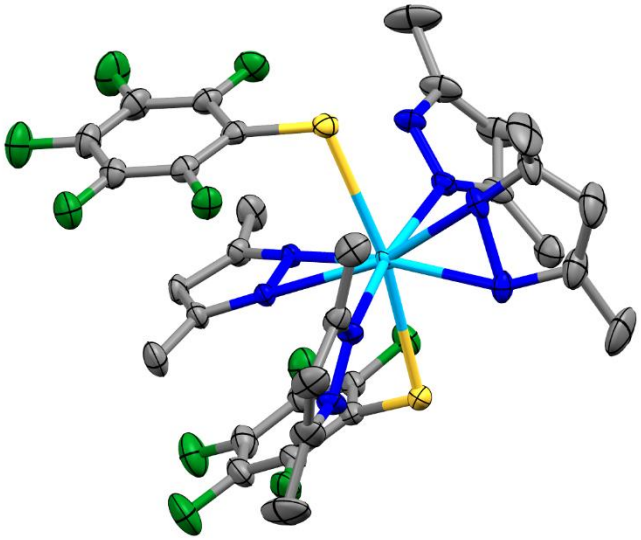

Figure 3.7. ORTEP diagram of $(Hdmpz)_2(dmpz)_2Th(SC_6F_5)_2$ (**16**), with yellow S, green F, light blue Th, dark blue N, grey C, the H atoms removed for clarity and ellipsoids at the 50% probability level.

These structures contain bidentate anionic pyrazolate (pz) and monodentate neutral Hpz ligands (compounds **13** and **14**) or bidentate 3,5-dimethylpyrazolate (dmpz) and monodentate Hdmpz ligands (compounds **15** and **16**). It is likely that the binding potential of Hpz and pz (or Hdmpz and dmpz) and also that of chalcogenolates SC_6F_5 and SePh are all on the same order of magnitude, since all compounds (**13 – 16**) are readily obtained. Furthermore, the observed intramolecular interactions, especially hydrogen bonds involving the F atoms, and π...π interactions involving neighboring pairs or triplets of these aromatic ligands, are expected to provide robust molecular properties based upon these chemically adjustable geometries.

Selected crystallographic details are given in Table 3.3.

Table 3.3. Crystallographic data for compounds **13 - 16**

Compound	**13**	**14**	**15**	**16**
fw	1806.91	1260.93	2782.35	1011.79
crystal system	triclinic	orthorhombic	triclinic	monoclinic
space group	Pī	Pbca	Pī	C2c
a (Å)	11.191(1)	23.707(2)	14.523 (1)	17.364(1)
b (Å)	12.080(1)	13.607(1)	14.579 (1)	19.534(2)
c (Å)	12.828(1)	27.726(2)	15.666(1)	11.430(1)
α (deg)	113.411(2)	90	74.037(1)	90
β (deg)	101.438(3)	90	85.330(1)	98.813(1)
γ (deg)	108.012(2)	90	60.278(1)	90
V ($Å^3$)	1407.2(3)	8944.2(10)	2763.5(4)	3830.9(5)
Z	1	8	4	4
D(calcd) (g/cm^3)	2.132	1.883	1.672	1.754
T (K)	100(2)	100(2)	120(2)	120(2)
abs coeff(mm^{-1})	9.026	3.581	2.905	4.085
$R(F)^b$ [I > 2σ(I)]	0.0404	0.0287	0.0377	0.0325
$R_w(F^2)^c$ [I > 2σ(I)]	0.0892	0.0567	0.0820	0.0765

As reliable elemental analysis results are often difficult to obtain due to the loss of lattice solvent and the possibility of decomposition during the process, bulk phase purity for all compounds were determined by PXRD, as shown in Figure 3.8-3.11.

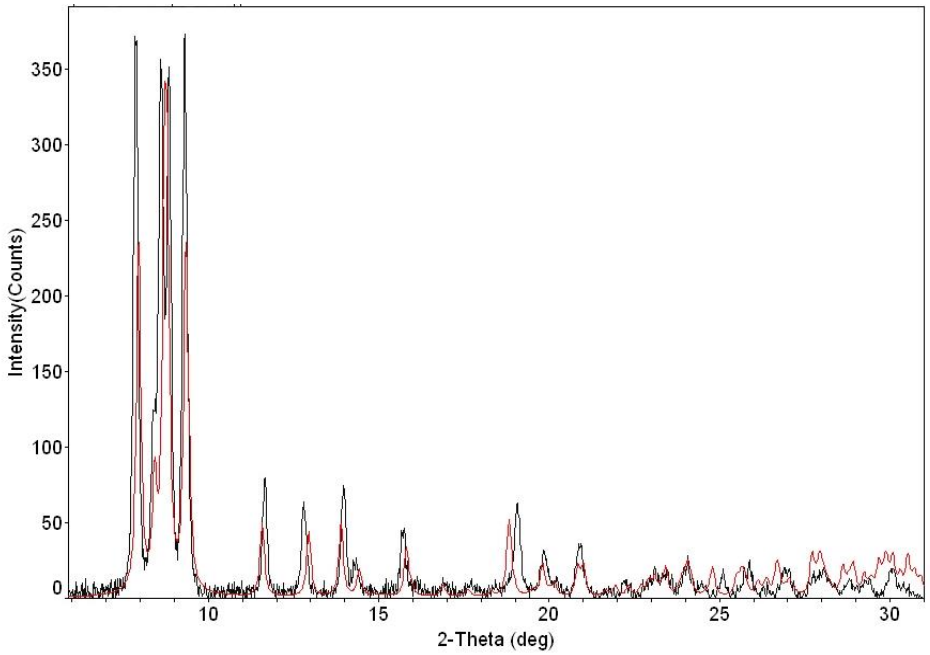

Figure 3.8. PXRD and calculated pattern from single crystal (in red) for **13**

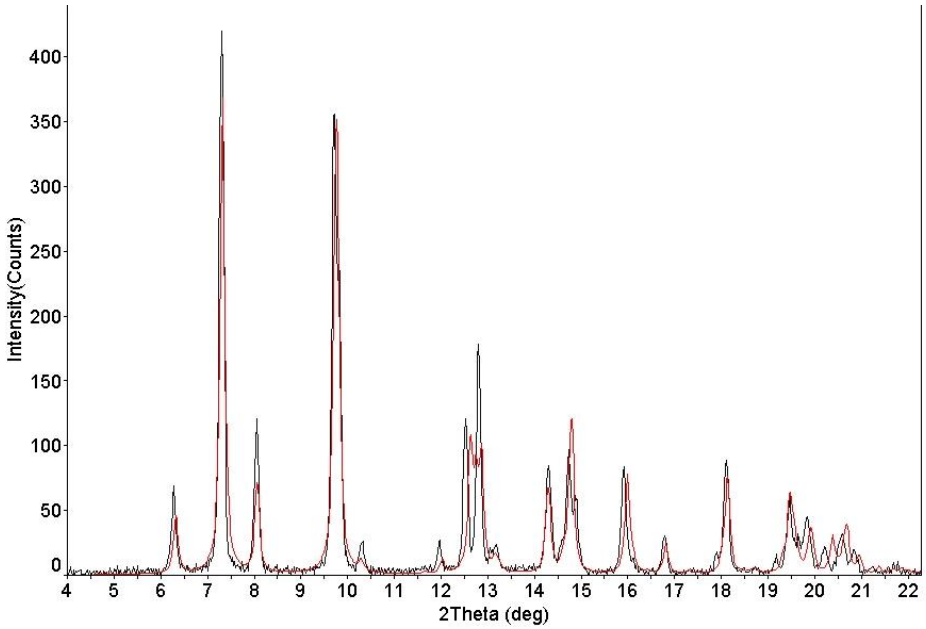

Figure 3.9. PXRD and calculated pattern from single crystal (in red) for **14.**

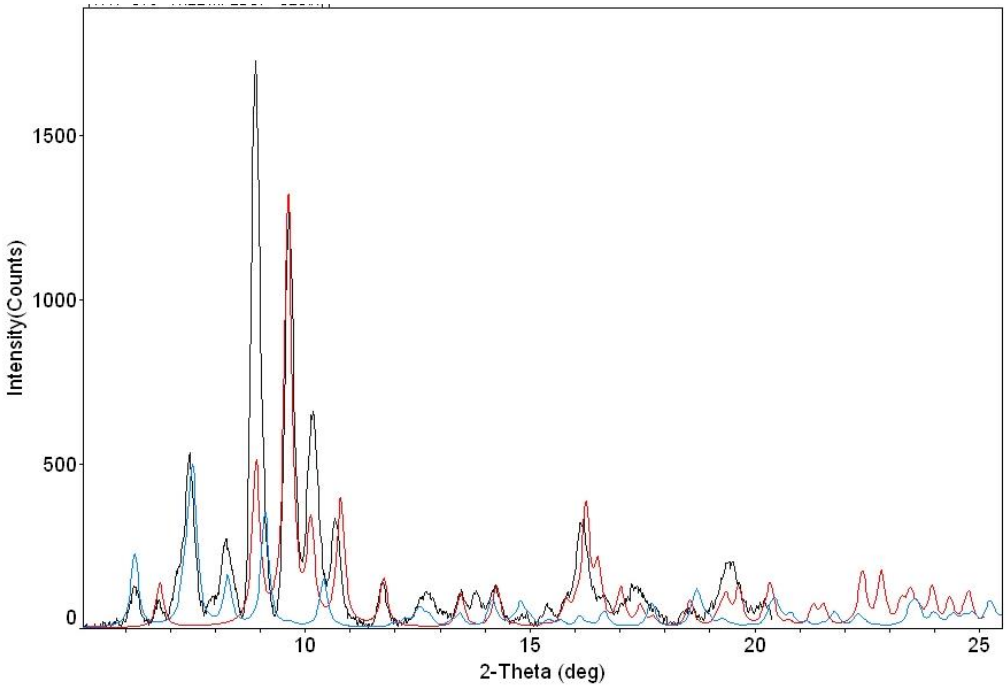

Figure 3.10. PXRD of crystalline products of the reaction (attempt to make **15**) and calculated patterns from single crystal for **15** (in blue) and **16** (in red).

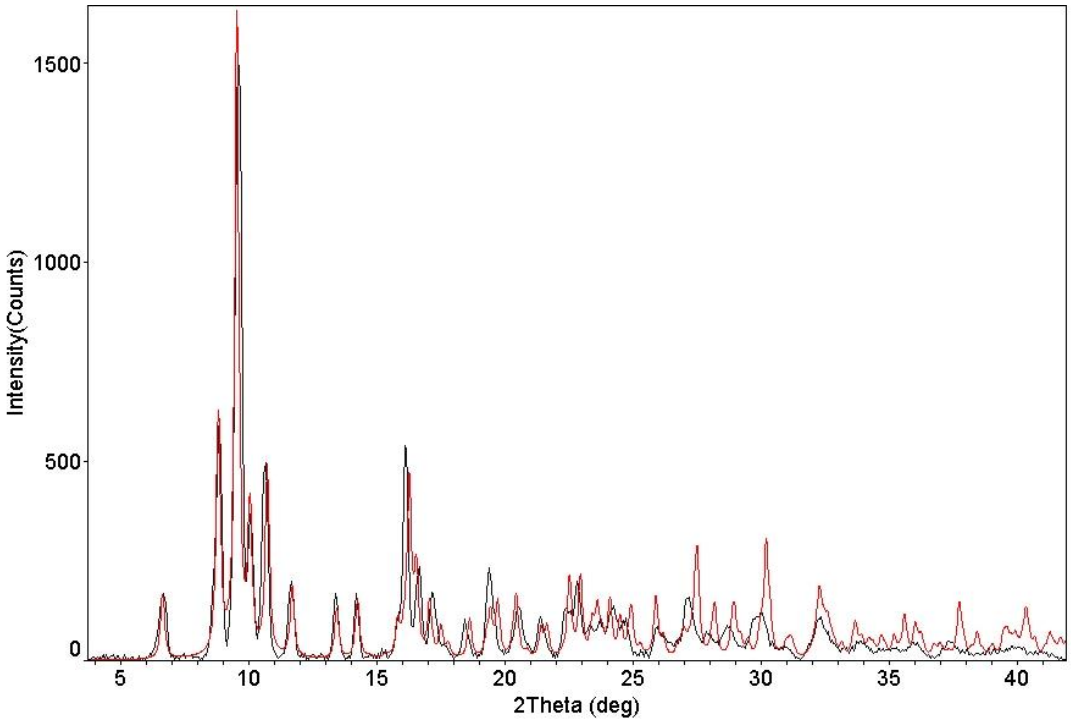

Figure 3.11. PXRD and calculated pattern from single crystal (in red) for **16**.

The PXRD of the product from the intended synthesis of compound **15** indicates that a mixture of **15** and **16** are present. For other three compounds, the comparison of the experimentally determined PXRD profiles with the calculated patterns from the single crystal data indicates high purity of the bulk material.

Selected significant bond lengths and angles given in Table 3.4.

Table 3.4. Selected bond distances (Å) and angles (°) for **13−16** [a]

Compound	13	14	15	16
Th-N(n)	2.607(4), 2.614(4)	2.607-2.677(2)	2.554(3), 2.588(3)	2.572(3)
Th-N(a)	2.393(4), 2.420(4)	2.428(2), 2.439(2)	2.365(3), 2.379(3)	2.399(3), 2.409(3)
Th-ηE	2.982 (1)	2.919-2.943(1)	2.849(1), 2.863(1)	2.859(1)
Th-μE	3.097-3.127(1)	-	3.002(1), 3.005(1)	-
N(a)-Th-N(a)	33.15(<1)	32.80(7)	34.03(9)	33.53(12)
Th-E-Th	83.70-84.19(<1)	-	122.61(2)	-
N(a)-Th-N(n) (acute)	71.26-82.43(13)	70.29-86.74(7)	75.66(9)	78.98(9)
N(a)-Th-N(n) (obtuse)	-	103.41-142.96(7)	109.65(9)	112.50(9)
Th-ηE-C	100.52(15)	112.81-114.48(10)	107.82-107.91(11)	103.77(11)
Th-μE-C	110.86-125.04(15)	-	115.47-115.76(11)	-

a ESD enclosed in parentheses. N(a) refers to N atom in pz or dmpz, N(n) refers to N atom in Hpz or Hdmpz.

The two thorium dimers, although both crystallize in space group Pī, have different numbers of bridging chalcogenolate ligands (four for **13** *versus* two for 15) and terminal chalcogenolates (two for **13** *versus* four for **15**). Although it is not known whether this difference may be due to the presence of F atoms or methyl groups in **15**, the presence of both of these features certainly changes the intramolecular interaction motif from that of **13**.

The similar dimeric actinide compounds which are bridged by chalcogenolate are limited, and there are no examples containing thorium. Compound **13** has four bridging –SePh ligand, and this feature only has two previous examples in the Cambridge Crystallographic Data Center (CCDC), even if we broaden the scope to include all metal. One is $[U(SePh)_2(\mu_2\text{-}SePh)_2(CH_3CN)_2]_2$,[12] which contains eight –SePh ligands (four bridging and four terminal) in total. Each U atom is eight-coordinated, exhibits a square antiprism geometry around the metal; while in **13**, each Th atom is nine-coordinated, and the molecule is centrosymmetric. The bond angles and close contact distances, which indicates intramolecular interactions, are comparable between the two compounds. The distance between the H from μ-SePh and Se from η-SePh is 3.08 Å in **13** while it is 3.05 Å in uranium compound, but **13** also has two short contact between H from Hpz and Se from μ-SePh, namely, 3.04 and 3.06 Å. The Th…Th distance is 4.15 Å while the U…U distance is 3.95 Å, which correspond to the larger M-Se-M angle in **13** compared to the uranium complex (84° versus 82°). The distance between the two Se atoms from η-SePh and μ-SePh are 4.16 and 3.94 Å in **13**, and 4.21 and 4.22

Å in the uranium compound, respectively. The latter distance in **13** is significantly shorter because of the short contact between the H from the nearby Hpz and Se from the η-SePh. The other example is $W_2(CO)_4(\mu_2\text{-SePh})_4(SePh)_2$.[13] In this molecule, the distance between the H from μ-SePh and Se from η-SePh is 3.21Å, indicating no intramolecular interaction between these two groups.

Compound **15** is a Th dimer with two bridging SC_6F_5 ligands. Each Th atom also connects to two terminal -SC_6F_5, one dmpz and two Hdmpz ligands, resulting in an eight-coordinated structure. There are some examples of actinide compounds with terminal SC_6F_5 ligands, but this is the first example of actinide compound containing bridging fluorinated chalcogenolates. Compound **15** can be viewed as having an equatorial plane having the Th atoms, the centroids of dmpz ligands, the all the S atoms from both μ- and η-SC_6F_5. Two Hdmpz ligands extend out of the plane, and the Th-Hdmpz plane is nearly perpendicular to the equatorial plane. This motif leads to a variety of close contacts that are indicative of intramolecular interactions between hydrogen and nitrogen or sulfur acceptor atoms. The comparison between the two dimers, **13** and **15**, is informative. For example, the fluorinated ligand -SC_6F_5 in **15** eliminates the interactions between H atoms to the chalcogenolate, as appears in **13**, but it provides F acceptors for the H donors from the Hdmpz ligands, such as 2.43 Å distance between F from η-SC_6F_5 and H from Hdmpz. The H atoms from Hdmpz also contributes to a short contact (2.97 Å) with S from the μ-SC_6F_5, which also helps to stabilize the bridging ligand in the structure. In addition, the methyl groups in Hdmpz

and dmpz occupy more spaces. As a result, it requires more efficient molecular conformation, and tend to form more intramolecular stacking.

There are also some differences in the two monomers with different pyrazole-derived ligands. Compound **16** is centrosymmetric, with the Th atom bound to two η-SC_6F_5, two Hdmpz and two dmpz ligands, resulting in an eight-coordinated sphere. It can be viewed as a half of the **15**, with the $(\mu_2\text{-}(SC_6F_5))_2$ in **15** replaced by a bidentate dmpz ligand. While compound **14** is not centrosymmetric, the Th atom is bound to three η-SC_6F_5, three Hpz and one pz ligands. It is also eight-coordinate, as it has an additional η-SC_6F_5 instead of a bidentate pz.

Diamagnetic Th (IV) provides an opportunity to probe the solution structures of the compounds, and ^{1}H NMR spectroscopy is particularly useful in these molecules which have both bidentate anionic pz or dmpz and monodentate Hpz or Hdmpz ligands. The integrated intensity of a signal in a ^{1}H NMR spectrum indicates a ratio for the number of hydrogens that are in different chemical environment. The^{1}H NMR spectra are shown in Figure 3.12 and Figure 3.13. Compared to pz and dmpz, Hpz or Hdmpz has one hydrogen atom connected to nitrogen atom, resulting in a higher chemical shift, namely 14.35 ppm in **14**, and 14.98 ppm in **16**. In the ^{1}H NMR spectrum of compound **14**, the ratio between the peaks is approximately 4:10:5, which corresponds to that of the solid state structure where four Hpz and one pz bound to the Th atom. Similarly, in the ^{1}H NMR spectrum of compound **16**, the ratio between the peaks is approximately 1:1:1:12, which also corresponds to the solved structure of the single crystal, where two

Hdmpz and two dmpz connected to the Th atom. These results indicate that the solid-state structures are maintained in solution.

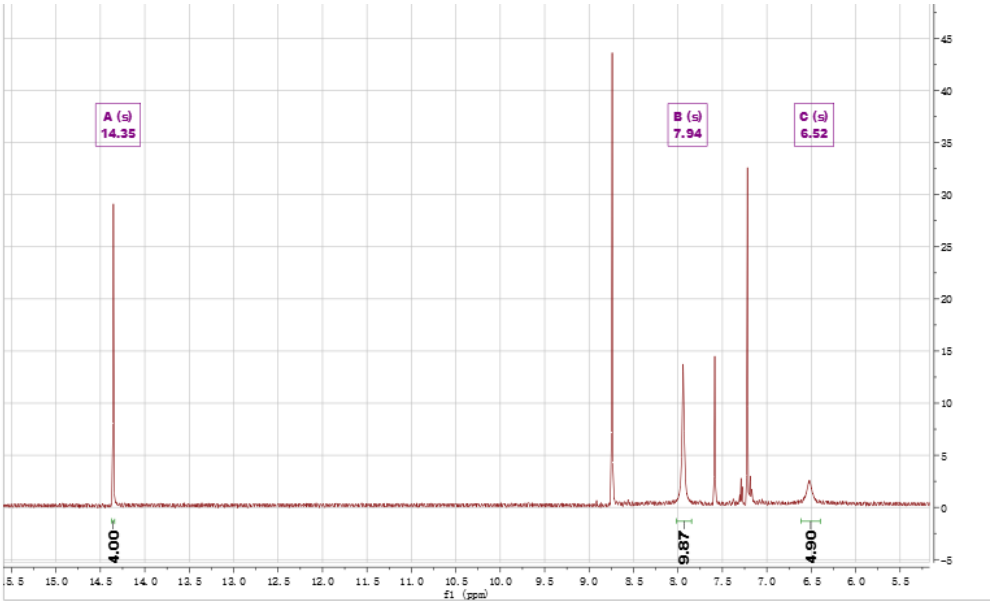

Figure 3.12. ^{1}H NMR spectrum of $(Hpz)_4(pz)Th(SC_6F_5)_3$ (**14**) in pyridine-d_5.

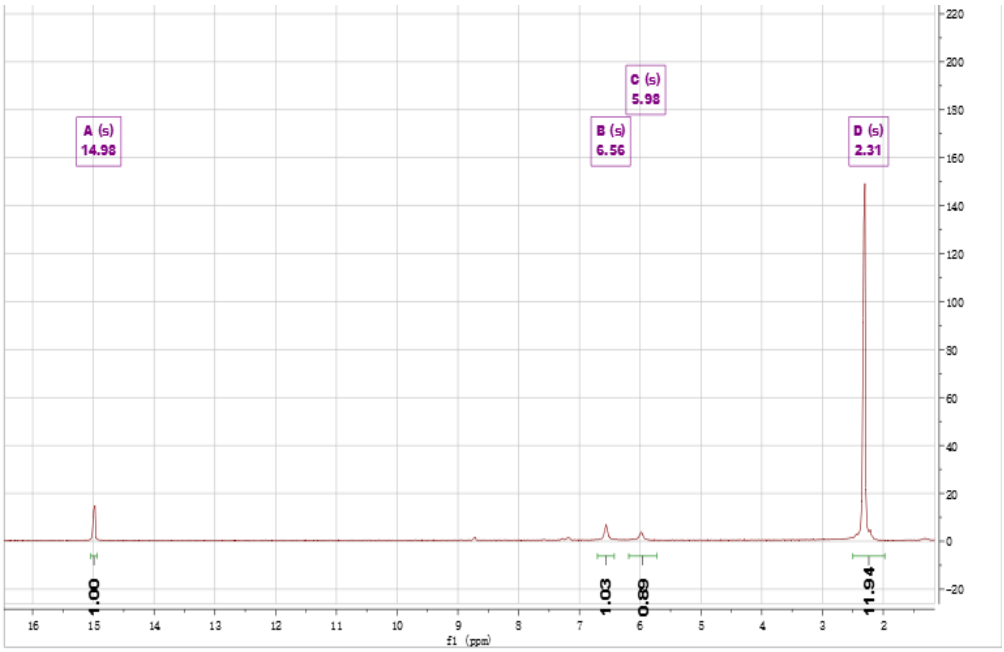

Figure 3.13. ^{1}H NMR spectrum of $(Hdmpz)_2(dmpz)_2Th(SC_6F_5)_2$ (**16**) in pyridine-d_5.

Reaction of thorium metal, $(SeC_6F_5)_2$ ligands and pyrazole in toluene also results in a novel cluster $(Hpz)_8Th_4Se_4(SeC_6F_5)_8$ (**17**). The ORTEP diagram is shown in Figure 3.14. Selected crystallographic details are given in Table 3.5.

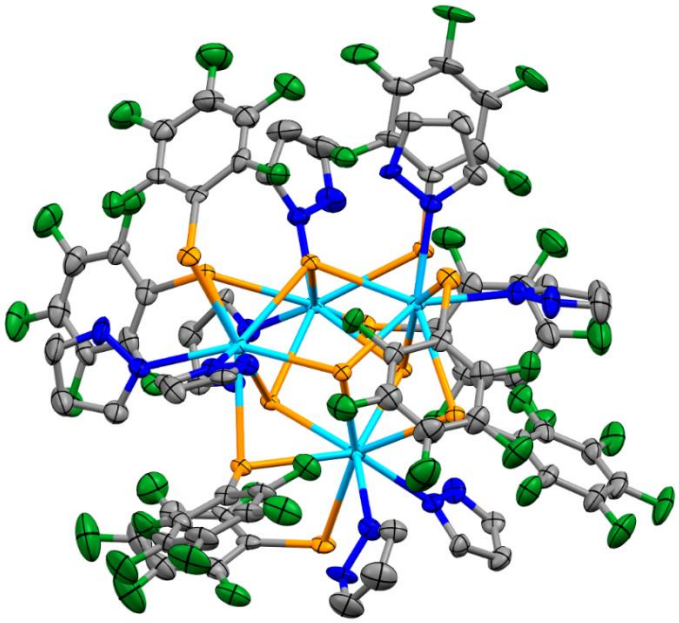

Figure 3.14. ORTEP diagram of $(Hpz)_8Th_4Se_4(SeC_6F_5)_8$ (**17**), with orange Se, green F, light blue Th, dark blue N, grey C, the H atoms removed for clarity and ellipsoids at the 50% probability level.

Table 3.5. Crystallographic data for compound **17**

empirical formula	$C_{72}H_{32}F_{40}N_{16}Se_{12}Th_4$	V (Å^3)	11959.4(19)
fw	3756.74	Z	8
crystal system	monoclinic	D(calcd) (g/cm^3)	1.963
space group	C2/c	T (K)	150(2)
a (Å)	44.381(4)	abs coeff(mm^{-1})	5.038
b (Å)	11.895(1)	R(F)^b [I > 2σ(I)]	0.0649
c (Å)	31.698(3)	$R_w(F^2)^c$ [I > 2σ(I)]	0.1569
α (deg)	90		
β (deg)	134.3804(15)		
γ (deg)	90		

Compound **17** was first synthesized by a "recrystallization" method, namely, repeating the process of concentrating the reaction solution to get powdery product, and heating the solution to redissolve and cooling down. However, attempts to reproduce this compound have not been successful, usually resulting in red powdery product, rather than good crystalline material.

Molecule **17** is a distorted cubane-typed cluster, which is comparable to the previously reported thorium cluster $(py)_8Th_4E_4(EPh)_4(E'C_6F_5)_4$ (E, E' =S, Se).[2b] Four Th atoms and four Se^{2-} anions occupy the alternate vertices of the cube, and the Th_4Se_4 core region is heavily distorted, with the 12 internal angles at the vertices ranging from 72.87° to 105.75°. In this molecule, each Th atom is bound to three μ_3-Se^{2-} anions, two Se atoms of μ_3-$(SeC_6F_5)^-$ anions, one Se atom of terminal $(SeC_6F_5)^-$ anion and two neutral Hpz ligands, resulting in an eight-coordinate geometry.

The average Th-N bond distance is 2.588 Å, which is consistent with the previously reported values in the literature. The Th-Se bond lengths between Th and various Se-containing ligands are different, namely, average 3.127 Å for Th-(μ_2-SePh) and 3.005 Å for Th-(η-SePh), These distances are slightly longer than previously reported value for Th-(SePh), such as 2.938 Å in $[\eta^5$-1,2,4-$(Me_3C)_3C_5H_2]Th(SePh)_3(bipy)$,[14] and 2.918 Å bond in $\{[\eta^5$-1,2,4- $(Me_3C)_3C_5H_2]Th(SePh)\}_2[\mu$-N(p-tolyl)$]_2$.[15] The average Th-$Se^{2-}$ distance in compound **17** is 2.930 Å, ranging from 2.906 Å to 2.950 Å, which is comparable to the values in the cluster $(py)_8Th_4Se_4(SePh)_4(SC_6F_5)_4$ and $(py)_8Th_4Se_4(SePh)_4(SeC_6F_5)_4$,[2b] with ranges of 2.950 – 2.971 Å.

3.5 Conclusions

A series of thorium chalcogenolates with different neutral donor ligands were synthesized and characterized, including six molecular complexes $(bipy)_2Th(SC_6F_5)_4$ (**11**), $(pzn)_4Th_2(SC_6F_5)_8$ (**12**), $(Hpz)_4(pz)_2Th_2(SePh)_6$ (**13**), $(Hpz)_4(pz)Th(SC_6F_5)_3$ (**14**), $(Hpz)_4(pz)Th(SC_6F_5)_3$ (**15**), $(Hdmpz)_2(dmpz)_2Th(SC_6F_5)_2$ (**16**) and one cluster compound $(Hpz)_8Th_4Se_4(SeC_6F_5)_8$ (**17**). All of these were synthesized from direct reaction with metal thorium, chalcogenolate ligands, neutral donor ligands in the nonaquous solution (THF or toluene).

With the same $-SC_6F_5$ ligand, different neutral donor ligands can result in compounds with different coordinating geometries, such as three monomers **11**, **14**, **16** and two dimers **12** and **15**. While with the same pyrazole ligand, different chalcogenolate also lead to compounds with significant coordinating differences, when comparsion is made between **13**, **14** and **17**.

Reference

(1) (a) Siladke, N. A.; Ziller, J. W.; Evans, W. J. Insertion, Isomerization, and Cascade Reactivity of the Tethered Silylalkyl Uranium Metallocene (η^5-$C_5Me_4SiMe_2CH_2$-κC)$_2$U. *J. Am. Chem. Soc.* **2011**, *133*, 3507-3516.(b) Tourneux, J.-C.; Berthet, J.-C.; Cantat, T.; Thuéry, P.; Mézailles, N.; Ephritikhine, M. Exploring the Uranyl Organometallic Chemistry: From Single to Double Uranium−Carbon Bonds. *J. Am. Chem. Soc.* **2011**, *133*, 6162-6165.(c) Zhang, L.; Hou, G.; Zi, G.; Ding, W.; Walter, M. D. Preparation of a uranium metallacyclocumulene and its reactivity towards unsaturated organic molecules. *Dalton Trans.* **2017**, *46*, 3716-3728.(d) Matson, E. M.; Goshert, M. D.; Kiernicki, J. J.; Newell, B. S.; Fanwick, P. E.; Shores, M. P.; Walensky, J. R.; Bart, S. C. Synthesis of terminal uranium (IV) disulfido and diselenido compounds by activation of elemental sulfur and selenium. *Chem. Eur. J.* **2013**, *19*, 16176-16180.(e) Camp, C.; Antunes, M. A.; García, G.; Ciofini, I.; Santos, I. C.; Pécaut, J.; Almeida, M.; Marçalo, J.; Mazzanti, M. Two-electron versus one-electron reduction of chalcogens by uranium(iii): synthesis of a terminal U(v) persulfide complex. *Chem. Sci.* **2014**, *5*, 841-846.(f) Gardner, B. M.; King, D. M.; Tuna, F.; Wooles, A. J.; Chilton, N. F.; Liddle, S. T. Assessing crystal field and magnetic interactions in diuranium-μ-chalcogenide triamidoamine complexes with U^{IV}–E–U^{IV} cores (E = S, Se, Te): implications for determining the presence or absence of actinide–actinide magnetic exchange. *Chem. Sci.* **2017**, *8*, 6207-6217.(g) Arnold, P. L.; Stevens, C. J.; Bell, N. L.; Lord, R. M.; Goldberg, J. M.; Nichol, G. S.; Love, J. B. Multi-electron reduction of sulfur and carbon disulfide using binuclear uranium(iii) borohydride complexes. *Chem. Sci.* **2017**, *8*, 3609-3617.(h) Kiernicki, J. J.; Staun, S. L.; Zeller, M.; Bart, S. C. A Uranium(IV) Triamide Species with Brønsted Basic Ligand Character: Metal–Ligand Cooperativity in the f Block. *Organometallics* **2017**, *36*, 665-672.(i) Vidjayacoumar, B.; Ilango, S.; Ray, M. J.; Chu, T.; Kolpin, K. B.; Andreychuk, N. R.; Cruz, C. A.; Emslie, D. J. H.; Jenkins, H. A.; Britten, J. F. Rigid NON- and NSN-ligand complexes of tetravalent and trivalent uranium: comparison of U–OAr2 and U–SAr2 bonding. *Dalton Trans.* **2012**, *41*, 8175-8189.(j) Tourneux, J.-C.; Berthet, J.-C.; Cantat, T.; Thuéry, P.; Mézailles, N.; Le Floch, P.; Ephritikhine, M. Uranium(IV) Nucleophilic Carbene Complexes. *Organometallics* **2011**, *30*, 2957-2971.(k) Lam, O. P.; Franke, S. M.; Heinemann, F. W.; Meyer, K. Reactivity of U–E–U (E = S, Se) Toward CO_2, CS_2, and COS: New Mixed-Carbonate Complexes of the Types U–CO_2E–U (E = S, Se), U–CS_2E–U (E = O, Se), and U–COSSe–U. *J. Am. Chem. Soc.* **2012**, *134*, 16877-16881.(l) Franke, S. M.; Heinemann, F. W.; Meyer, K. Reactivity of uranium(iv) bridged chalcogenido complexes U^{IV}–E–U^{IV} (E = S, Se) with elemental sulfur and selenium: synthesis of polychalcogenido-bridged uranium

complexes. *Chem. Sci.* **2014**, *5*, 942-950.(m) Matson, E. M.; Breshears, A. T.; Kiernicki, J. J.; Newell, B. S.; Fanwick, P. E.; Shores, M. P.; Walensky, J. R.; Bart, S. C. Trivalent Uranium Phenylchalcogenide Complexes: Exploring the Bonding and Reactivity with CS_2 in the Tp*$_2$UEPh Series (E = O, S, Se, Te). *Inorg. Chem.* **2014**, *53*, 12977-12985.(n) Jones, M. B.; Gaunt, A. J.; Gordon, J. C.; Kaltsoyannis, N.; Neu, M. P.; Scott, B. L. Uncovering f-element bonding differences and electronic structure in a series of 1 : 3 and 1 : 4 complexes with a diselenophosphinate ligand. *Chem. Sci.* **2013**, *4*, 1189-1203.(o) Cleaves, P. A.; Kefalidis, C. E.; Gardner, B. M.; Tuna, F.; McInnes, E. J. L.; Lewis, W.; Maron, L.; Liddle, S. T. Terminal Uranium (V/VI) Nitride Activation of Carbon Dioxide and Carbon Disulfide: Factors Governing Diverse and Well‐Defined Cleavage and Redox Reactions. *Chem. Eur. J.* **2017**, *23*, 2950-2959.(p) Behrle, A. C.; Kerridge, A.; Walensky, J. R. Dithio- and Diselenophosphinate Thorium(IV) and Uranium(IV) Complexes: Molecular and Electronic Structures, Spectroscopy, and Transmetalation Reactivity. *Inorg. Chem.* **2015**, *54*, 11625-11636.(q) Kiernicki, J. J.; Fanwick, P. E.; Bart, S. C. Utility of a redox-active pyridine(diimine) chelate in facilitating two electron oxidative addition chemistry at uranium. *Chem. Commun.* **2014**, *50*, 8189-8192.(r) Maria, L.; Santos, I. C.; Santos, I. Uranium(iii) complexes supported by hydrobis(mercaptoimidazolyl)borates: synthesis and oxidation chemistry. *Dalton Trans.* **2018**, *47*, 10601-10612.

(2) (a) Wu, W.; Rehe, D.; Hrobárik, P.; Kornienko, A. Y.; Emge, T. J.; Brennan, J. G. Molecular Thorium Compounds with Dichalcogenide Ligands: Synthesis, Structure, 77Se NMR Study, and Thermolysis. *Inorg. Chem.* **2018**, *57*, 14821-14833.(b) Stuber, M. A.; Kornienko, A. Y.; Emge, T. J.; Brennan, J. G. Tetrametallic Thorium Compounds with Th_4E_4 (E = S, Se) Cubane Cores. *Inorg. Chem.* **2017**, *56*, 10247-10256.(c) Ren, W.; Song, H.; Zi, G.; Walter, M. D. A bipyridyl thorium metallocene: synthesis, structure and reactivity. *Dalton Trans.* **2012**, *41*, 5965-5973.(d) Settineri, N. S.; Garner, M. E.; Arnold, J. A Thorium Chalcogenolate Series Generated by Atom Insertion into Thorium–Carbon Bonds. *J. Am. Chem. Soc.* **2017**, *139*, 6261-6269.(e) Ren, W.; Zi, G.; Fang, D.-C.; Walter, M. D. Thorium Oxo and Sulfido Metallocenes: Synthesis, Structure, Reactivity, and Computational Studies. *J. Am. Chem. Soc.* **2011**, *133*, 13183-13196.(f) Smiles, D. E.; Wu, G.; Kaltsoyannis, N.; Hayton, T. W. Thorium–ligand multiple bonds via reductive deprotection of a trityl group. *Chem. Sci.* **2015**, *6*, 3891-3899.(g) Zhou, E.; Ren, W.; Hou, G.; Zi, G.; Fang, D.-C.; Walter, M. D. Small Molecule Activation Mediated by a Thorium Terminal Imido Metallocene. *Organometallics* **2015**, *34*, 3637-3647.(h) Rehe, D.; Kornienko, A. Y.; Emge, T. J.; Brennan, J. G. Thorium Compounds with Bonds to Sulfur or Selenium: Synthesis, Structure, and Thermolysis. *Inorg. Chem.* **2016**, *55*, 6961-6967.(i) Smiles, D. E.; Wu, G.; Hrobárik, P.; Hayton, T. W. Use of ^{77}Se and ^{125}Te NMR Spectroscopy to Probe Covalency of the Actinide-Chalcogen

Bonding in $[Th(E_n)\{N(SiMe_3)_2\}_3]^-$ (E = Se, Te; n = 1, 2) and Their Oxo-Uranium(VI) Congeners. *J. Am. Chem. Soc.* **2016**, *138*, 814-825.(j) Yang, P.; Zhou, E.; Fang, B.; Hou, G.; Zi, G.; Walter, M. D. Preparation of $(\eta^5\text{-}C_5Me_5)_2Th(bipy)$ and Its Reactivity toward Small Molecules. *Organometallics* **2016**, *35*, 2129-2139.(k) Ringgold, M.; Rehe, D.; Hrobárik, P.; Kornienko, A. Y.; Emge, T. J.; Brennan, J. G. Thorium Cubanes–Synthesis, Solid-State and Solution Structures, Thermolysis, and Chalcogen Exchange Reactions. *Inorg. Chem.* **2018**, *57*, 7129-7141.

(3) (a) Kaes, C.; Katz, A.; Hosseini, M. W. Bipyridine: the most widely used ligand. A review of molecules comprising at least two 2, 2'-bipyridine units. *Chem. Rev.* **2000**, *100*, 3553-3590.(b) Shaw, A. J.; Corbo, R.; Wilson, D. J.; Dutton, J. L. A 2, 2′-bipyridine coordination complex of $[ICl_2]^+$. *Dalton Trans.* **2015**, *44*, 15083-15087.

(4) (a) Ren, W. S.; Song, H. B.; Zi, G. F.; Walter, M. D. A bipyridyl thorium metallocene: synthesis, structure and reactivity. *Dalton Trans.* **2012**, *41*, 5965-5973.(b) Newell, B. S.; Schwaab, T. C.; Shores, M. P. Synthesis and Characterization of a Novel Tetranuclear 5f Compound: A New Synthon for Exploring U(IV) Chemistry. *Inorg. Chem.* **2011**, *50*, 12108-12115.(c) Jilek, R. E.; Tomson, N. C.; Scott, B. L.; Boncella, J. M. [2+2] cycloaddition reactions at terminal imido uranium(IV) complexes to yield isolable cycloadducts. *Inorg. Chim. Acta* **2014**, *422*, 78-85.(d) Jilek, R. E.; Spencer, L. P.; Kuiper, D. L.; Scott, B. L.; Williams, U. J.; Kikkawa, J. M.; Schelter, E. J.; Boncella, J. M. A General and Modular Synthesis of Monoimidouranium(IV) Dihalides. *Inorg. Chem.* **2011**, *50*, 4235-4237.(e) Zhang, L.; Zhang, C. C.; Hou, G. H.; Zi, G. F.; Walter, M. D. Small-Molecule Activation Mediated by a Uranium Bipyridyl Metallocene. *Organometallics* **2017**, *36*, 1179-1187.(f) Brown, J. L.; Mokhtarzadeh, C. C.; Lever, J. M.; Wu, G.; Hayton, T. W. Facile Reduction of a Uranyl(VI) beta-ketoiminate Complex to U(IV) Upon Oxo Silylation. *Inorg. Chem.* **2011**, *50*, 5105-5112.(g) Brown, J. L.; Batista, E. R.; Boncella, J. M.; Gaunt, A. J.; Reilly, S. D.; Scott, B. L.; Tomson, N. C. A Linear trans-Bis(imido) Neptunium(V) Actinyl Analog: $Np^V(NDipp)_2(^tBu_2bipy)_2Cl$ (Dipp=2,6-$^iPr_2C_6H_3$). *J. Am. Chem. Soc.* **2015**, *137*, 9583-9586.(h) Jilek, R. E.; Spencer, L. P.; Lewis, R. A.; Scott, B. L.; Hayton, T. W.; Boncella, J. M. A Direct Route to Bis(imido)uranium(V) Halides via Metathesis of Uranium Tetrachloride. *J. Am. Chem. Soc.* **2012**, *134*, 9876-9878.(i) Jilek, R. E.; Tomson, N. C.; Shook, R. L.; Scott, B. L.; Boncella, J. M. Preparation and Reactivity of the Versatile Uranium(IV) Imido Complexes $U(NAr)Cl_2(R_2bipy)_2$ (R = Me, ^{t}Bu) and $U(NAr)Cl_2(tppo)_3$. *Inorg. Chem.* **2014**, *53*, 9818-9826.(j) Mora, E.; Maria, L.; Biswas, B.; Camp, C.; Santos, I. C.; Pecaut, J.; Cruz, A.; Carretas, J. M.; Marcalo, J.; Mazzanti, M. Diamine Bis(phenolate) as Supporting Ligands in Organoactinide(IV) Chemistry. Synthesis, Structural Characterization, and

Reactivity of Stable Dialkyl Derivatives. *Organometallics* **2013**, *32*, 1409-1422.(k) Haiges, R.; Vasiliu, M.; Dixon, D. A.; Christe, K. O. The Uranium(VI) Oxoazides $[UO_2(N_3)_2 \cdot CH_3CN]$, $[(bipy)_2(UO_2)_2(N_3)_4]$, $[(bipy)UO_2(N_3)_3]^-$, $[UO_2(N_3)_4]^{2-}$, and $[(UO_2)_2(N_3)_8]^{4-}$. *Chem. Eur. J.* **2017**, *23*, 652-664.(l) Diaconescu, P. L.; Cummins, C. C. Radical anionic versus neutral 2,2'-bipyridyl coordination in uranium complexes supported by amide and ketimide ligands. *Dalton Trans.* **2015**, *44*, 2676-2683.

(5) Real, J. A.; De Munno, G.; Munoz, M. C.; Julve, M. Crystal structure and magnetic properties of bis (isothiocyanato) bis (pyrazine) iron polymer, a 2D sheetlike polymer. *Inorg. Chem.* **1991**, *30*, 2701-2704.

(6) (a) Otieno, T.; Rettig, S.; Thompson, R.; Trotter, J. Synthesis, structure, and vibrational spectrum of poly-μ-pyrazine (pyrazine)(trifluoromethanesulfonato-O) copper (I). *Can. J. Chem.* **1989**, *67*, 1964-1969.(b) Kwak, H.; Lee, S. H.; Kim, S. H.; Lee, Y. M.; Park, B. K.; Lee, E. Y.; Lee, Y. J.; Kim, C.; Kim, S.-J.; Kim, Y. Substituent effects of pyrazine on construction of crystal structures of Zn(II)-benzoate complexes and their catalytic activities (dinuclear, trinuclear, and pentanuclear to 1-D and 2-D). *Polyhedron* **2008**, *27*, 3484-3492.

(7) Trofimenko, S. Coordination chemistry of pyrazole-derived ligands. *Chem. Rev.* **1972**, *72*, 497-509.

(8) (a) Tatebe, C. J.; Johnson, S. A.; Zeller, M.; Bart, S. C. Generation of $Tp^*_2U(N3)$ from a family of new uranium(III) alkyl complexes. *J. Organomet. Chem.* **2018**, *857*, 152-158.(b) Rinehart, J. D.; Bartlett, B. M.; Kozimor, S. A.; Long, J. R. Ferromagnetic exchange coupling in the linear, chloride-bridged cluster $(cyclam)Co^{II}[(\mu\text{-}Cl)U^{IV}(Me_2Pz)_4]_2$. *Inorg. Chim. Acta* **2008**, *361*, 3534-3538.(c) Eigenbrot, C. W.; Raymond, K. N. Organouranium complexes of pyrazole and pyrazolate. Synthesis and x-ray structures of $U(C_5Me_5)_2Cl_2(C_3H_4N_2)$, $U(C_5Me_5)_2Cl(C_3H_3N_2)$, and $U(C_5Me_5)(C_3H_3N_2)_2$. *Inorg. Chem.* **1982**, *21*, 2653-2660.(d) Rinehart, J. D.; Harris, T. D.; Kozimor, S. A.; Bartlett, B. M.; Long, J. R. Magnetic Exchange Coupling in Actinide-Containing Molecules. *Inorg. Chem.* **2009**, *48*, 3382-3395.(e) Johnson, S. A.; Tatebe, C. J.; Gonzalez, S.; Zeller, M.; Bart, S. C. Synthesis and characterization of hydrotris(3-phenylpyrazolyl)borate ligands on low-valent uranium. *Polyhedron* **2017**, *125*, 107-112.(f) Maria, L.; Domingos, Â.; Galvão, A.; Ascenso, J.; Santos, I. The Role of Neutral Coligands on the Stabilization of Mono-Tp^{iPr2} U(III) Complexes. *Inorg. Chem.* **2004**, *43*, 6426-6434.(g) Maria, L.; Paula Campello, M.; Domingos, Â.; Santos, I.; Andersen, R. Synthesis and structure of uranium(III) complexes with dihydrobis(pyrazolyl)borates. *J.Chem. Soc., Dalton Trans.* **1999**, 2015-2020.(h) Evans, W. J.; Miller, K. A.; Kozimor, S. A.; Ziller, J. W.; DiPasquale, A. G.; Rheingold, A. L. Actinide hydride complexes as

multielectron reductants: Analogous reduction chemistry from $[(C_5Me_5)_2UH]_2$, $[(C_5Me_5)_2UH_2]_2$, and $[(C_5Me_5)_2ThH_2]_2$. *Organometallics* **2007**, *26*, 3568-3576.(i) Enriquez, A. E.; Scott, B. L.; Neu, M. P. Uranium(III)/(IV) Nitrile Adducts Including $UI_4(N{:}CPh)_4$, a Synthetically Useful Uranium(IV) Complex. *Inorg. Chem.* **2005**, *44*, 7403-7413.(j) Clark, C. L.; Lockhart, J. J.; Fanwick, P. E.; Bart, S. C. Synthesis of low-valent uranium fluorides by C–F bond activation. *Chem. Commun.* **2015**, *51*, 14084-14087.(k) Matson, E. M.; Kiernicki, J. J.; Fanwick, P. E.; Bart, S. C. Expanding the Family of Uranium (III) Alkyls: Synthesis and Characterization of Mixed‐Ligand Derivatives. *Eur. J. Inorg. Chem.* **2016**, *2016*, 2527-2533.(l) Tatebe, C. J.; Zeller, M.; Bart, S. C. [2π+2π] Cycloaddition of Isocyanates to Uranium(IV) Imido Complexes for the Synthesis of U(IV) κ^2-Ureato Compounds. *Inorg. Chem.* **2017**, *56*, 1956-1965.(m) Domingos, A.; Marques, N.; Pires de Matos, A.; Santos, I.; Silva, M. Hydrotris(pyrazolyl)borate chemistry of uranium(III) and uranium(IV). Synthesis of .sigma.-hydrocarbyl derivatives of uranium(IV) and reactivity of $UCl_2R[HB(3,5\text{-}Me_2pz)_3]$ (R = CH_2SiMe_3, $CH(SiMe_3)_2$) and $UCl_2[HB(3,5\text{-}Me_2pz)_3]$ toward ketones and aldehydes. *Organometallics* **1994**, *13*, 654-662.

(9) (a) Domingos, Â.; Marçalo, J.; de Matos, A. P. Bis[hydrotris(pyrazolyl)borate] thorium(IV) complexes: Synthesis and characterization of alkyl, thiolate, alkoxide and aryloxide derivatives and the x-ray crystal structure of $Th(HBPz_3)_2(OPh)_2$. *Polyhedron* **1992**, *11*, 909-915.(b) Amoroso, A. J.; Jeffery, J. C.; Jones, P. L.; McCleverty, J. A.; Ward, M. D. Complexes of a hexadentate podand ligand with actinides; The syntheses and crystal structures of $[Th(Tp^{Py})(NO_3)_3] \cdot (dmf) \cdot (Et_2O)_{0.5}$ and trans-$[UO_2(Tp^{Py})(OEt)]$ Tp^{Py} = tris[3-(2 ′ -pyridyl)pyrazol-1-yl]hydroborate. *Polyhedron* **1996**, *15*, 2023-2027.(c) Domingos, Â.; MarÇalo, J.; Santos, I.; de Matos, A. P. Bis[hydrotris(pyrazolyl)borato[dichloroactinide(IV) complexes: X-ray crystal structures of $ThCl_2(HBPz_3)_2$ and $UCl_2(HBPz_3)_2$. *Polyhedron* **1990**, *9*, 1645-1652.

(10) Janiak, C. A critical account on [small pi]-[small pi] stacking in metal complexes with aromatic nitrogen-containing ligands. *J. Chem. Soc. Dalton Trans.* **2000**, 3885-3896.

(11) (a) Evans, W. J.; Miller, K. A.; Kozimor, S. A.; Ziller, J. W.; DiPasquale, A. G.; Rheingold, A. L. Actinide Hydride Complexes as Multielectron Reductants: Analogous Reduction Chemistry from $[(C_5Me_5)_2UH]_2$, $[(C_5Me_5)_2UH_2]_2$, and $[(C_5Me_5)_2ThH_2]_2$. *Organometallics* **2007**, *26*, 3568-3576.(b) Behrle, A. C.; Barnes, C. L.; Kaltsoyannis, N.; Walensky, J. R. Systematic Investigation of Thorium(IV)– and Uranium(IV)–Ligand Bonding in Dithiophosphonate, Thioselenophosphinate, and Diselenophosphonate Complexes. *Inorg. Chem.* **2013**, *52*, 10623-10631.

(12) Gaunt, A. J.; Scott, B. L.; Neu, M. P. U(IV) Chalcogenolates Synthesized via Oxidation of Uranium Metal by Dichalcogenides. *Inorg. Chem.* **2006**, *45*, 7401-7407.

(13) Pasynskii, A. A.; Blokhin, A. I.; Torubaev, Y. V.; Dobrokhotova, Z. V. Synthesis and molecular structures of tris(thio- and selenophenyl)stannyl complexes of cyclopentadienylcarbonylnitrosylmanganese and their reaction products with tungsten carbony. *Russ. J. Coord. Chem.* **2011**, *37*, 879-886.

(14) Ren, W. S.; Zi, G. F.; Walter, M. D. Synthesis, Structure, and Reactivity of a Thorium Metallocene Containing a 2,2 '-Bipyridyl Ligand. *Organometallics* **2012**, *31*, 672-679.

(15) Zhou, E. W.; Ren, W. S.; Hou, G. H.; Zi, G. F.; Fang, D. C.; Walter, M. D. Small Molecule Activation Mediated by a Thorium Terminal Imido Metallocene. *Organometallics* **2015**, *34*, 3637-3647.

Chapter 4. Actinide Oxychalcogenides and Halides

4.1 Introduction

Understanding the reactivity and behavior of actinide (An) elements including thorium and uranium is significant for fundamental research and various applications, such as radioactive waste treatment and environmental remediation.

The research of actinide oxo compounds have received increasing attention in recent years. Many studies have focused on uranium oxo clusters and the most explored system is that of actinyl peroxides, which have yielded various unique topologies, including fullerene-type U_{60},[1] and the largest cluster $U_{120}Ox_{90}$, where U and Ox represent uranyl and oxalate, respectively.[2] There also exists some examples of actinide clusters with oxide or hydroxide bridges.[3] While in molecular uranium complexes, the linear uranyl cation $[UO_2]^{2+}$ is the most common form of uranium and it contains strongly covalently bound, rigorously axial oxo groups that exhibit almost no chemistry.[4] All these actinide oxo compounds are commonly prepared in aqueous solution.

It is important to design and synthesize actinide oxychalcogenolate compounds in nonaqueous solution as it can help us probe the nature of An-E (E = S, Se, Te) bonds, and have a better understanding of how the chalcogenolate ligands can influence the molecular geometry of the complex and coordination behavior of the central metal. There are examples of lanthanide oxychalcogenido clusters prepared by reacting

"$Ln(SePh)_3$" with SeO_2 in THF (Ln= Ce, Pr, Nd, Sm),[5] NaN_3 and Na_2O in pyridine (Ln= Er, Ho, Sm)[6] or "$Ln(TePh)_3$" (Ln= Ce, Nd) with Te and TeO_2 in pyridine,[7] but no previous examples of actinide counterparts.

Metal halides are commonly used as starting materials in inorganic and organometallic synthesis. In thorium and uranium chemistry, chlorides and iodides have been widely studied[8] while the fluorides are limited by the difficulty of working with F^- and potential ligand redistribution reactions that lead to the precipitation of insoluble AnF_4.[9]

This chapter will first describe the synthesis and characterizations of two molecular thorium and uranium oxychalcogenides, $(py)_6Th_2O(Se_2)I_4$ (**18**), $(py)_6U_2O(Se_2)I_4$ (**19**) and one thorium oxychalcogenido cluster $(py)_{10}Th_6O_3(Se_2)_8(SC_6F_5)_2$ (**20**). Then the synthesis and characterizations of two actinide halides will also be discussed. Coming from the reactions of metal Th or U, $(SC_6F_5)_2$ and I_2 in py, $(py)_4ThI_3F$ contains fluoride from the original $(SC_6F_5)_2$; while the uranium derivative, $(py)_3UI_3(SC_6F_5)$ follows stoichiometry of the starting materials.

4.2 Actinide Oxychalcogenides

Molecular thorium and uranium oxychalcogenides $(py)_6An_2O(Se_2)I_4$ (An = Th (**18**), U (**19**)) can be prepared by adding 0.75 equivalent of elemental Se and 0.25 equivalent of SeO_2 into a pyridine solution of "$AnI_n(SePh)_{4-n}$" (n = 1 to 4). (Scheme 4.1) Catalytic amount of mercury is added in Th reaction to reduce the reaction completion time.

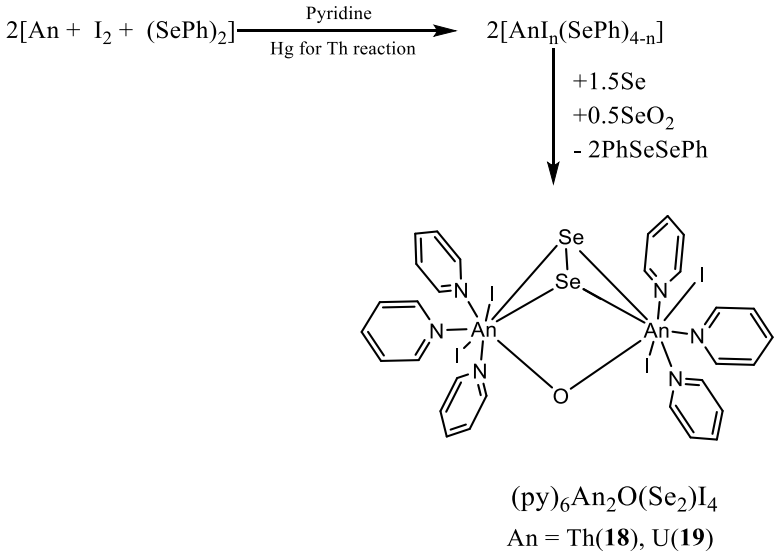

Scheme 4.1. Synthesis of dimeric thorium and uranium complexes with diselenido and oxo bridges.

Compounds **18** and **19** were characterized by conventional methods and low-temperature single-crystal X-ray diffraction. Figures 4.1 and 4.2 show ORTEP diagrams of the molecular structures of **18** and **19**, respectively.

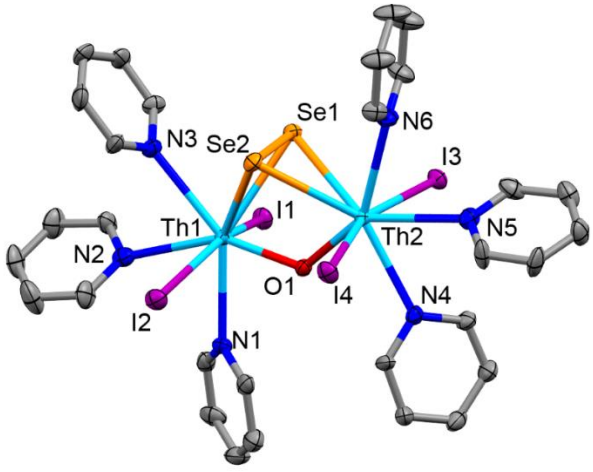

Figure 4.1. ORTEP diagram of $(py)_6Th_2O(Se_2)I_4$ **(18)**, with orange Se, purple I, light blue Th, dark blue N, red O, grey C, the H atoms removed for clarity and ellipsoids at the 50% probability level.

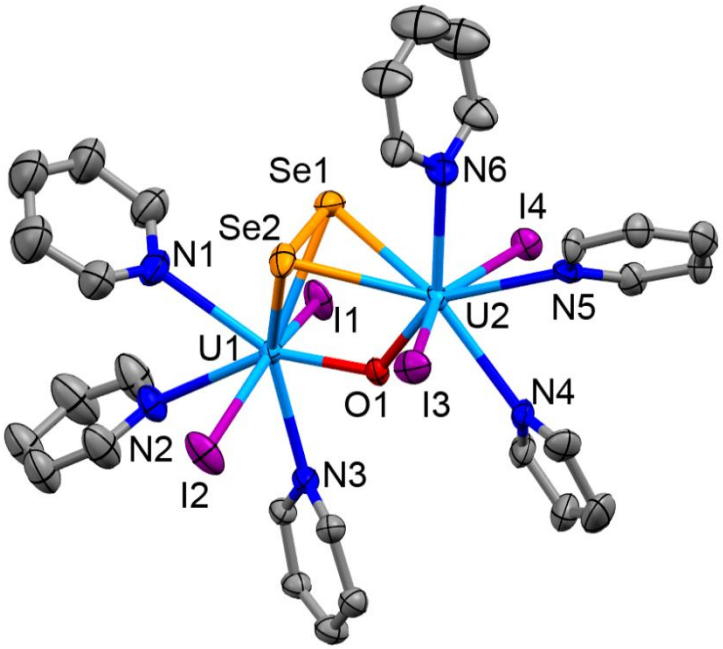

Figure 4.2. ORTEP diagram of $(py)_6U_2O(Se_2)I_4$ **(19)**, with orange Se, purple I, light blue U, dark blue N, red O, grey C, the H atoms removed for clarity and ellipsoids at the 50% probability level.

Selected crystallographic details are given in Table 4.1, with significant bond lengths and angles given in Table 4.2. The two compounds **18** and **19** are isostructural, both containing a central $An_2(\mu_2\text{-}Se_2)(\mu_2\text{-}O)$ core region, with the primary coordination sphere of each metal atom saturated by two additional iodides and three neutral pyridine ligands, resulting in eight-coordinate geometry. **18** crystallizes in space group $P2_1/n$ while **19** crystallizes in space group $P2_1/c$, and this difference can be attributed to the different amounts of solvate pyridine molecules (3 in **18** versus 4 in **19**) co-crystallizes in the lattices. These are the first examples of dimeric actinide complexes with both dichalcogenido and oxo bridges.

Table 4.1. Summary of crystallographic details for $(py)_6Th_2O(Se_2)I_4$ **(18)**, and $(py)_6U_2O(Se_2)I_4$ **(19)**

	18	**19**
empirical formula	$C_{45}H_{45}I_4N_9OSe_2Th_2$	$C_{50}H_{50}I_4N_{10}OSe_2U_2$
fw	1857.50	1948.58
crystal system	monoclinic	monoclinic
space group	$P2_1/n$	$P2_1/c$
a (Å)	11.3794(11)	17.721(4)
b (Å)	34.203(3)	18.788(5)
c (Å)	14.1888(13)	19.000(5)
α (deg)	90	90
β (deg)	92.2119(14)	104.69(2)
γ (deg)	90	90
V ($Å^3$)	5518.3(9)	6119(3)
Z	4	4
D(calcd) (g/cm^3)	2.236	2.115
T (K)	120(2)	120(2)
abs coeff(mm^{-1})	8.981	8.535
$R(F)^b$ [$I > 2\sigma(I)$]	0.0547	0.0828
$R_w(F^2)^c$ [$I > 2\sigma(I)$]	0.0950	0.1936

Table 4.2. Select bond distances (Å) and bond angles (°) for $(py)_6Th_2O(Se_2)I_4$ **(18)**, and $(py)_6U_2O(Se_2)I_4$ **(19)** [a]

18		**19**	
Th(1)-N(1)	2.648(7)	U(1)-N(1)	2.610(20)
Th(1)-N(3)	2.709(7)	U(1)-N(3)	2.615(17)
Th(1)-N(2)	2.793(7)	U(1)-N(2)	2.744(17)
Th(1)-O	2.140(6)	U(1)-O	2.079(12)
Th(1)-I	3.168-3.195(1)	U(1)-I	3.083-3.100(1)
Th(1)-μ_2Se	2.979-2.988(1)	U(1)-μ_2Se	2.971-2.928(2)
Th(2)-N(6)	2.706(7)	U(2)-N(6)	2.630(18)
Th(2)-N(4)	2.715(7)	U(2)-N(4)	2.636(17)
Th(2)-N(5)	2.764(8)	U(2)-N(5)	2.719(16)
Th(2)-O	2.135(5)	U(2)-O	2.073(12)
Th(2)-I	3.132-3.164(1)	U(2)-I	3.095-3.096(1)
Th(2)-μ_2Se	2.999-3.014(1)	U(2)-μ_2Se	2.927-2.929(2)
Se-Se	2.348(1)	Se-Se	2.337(3)
Th-μ_2Se-Th	77.90-77.99(2)	U-μ_2Se-U	77.46-77.59(6)
Th-O-Th	123.6(3)	U-O-U	123.8(7)

a The ESD values are enclosed in parentheses. Refer to figures for Th and N atom labels.

Bond geometries for **18** and **19** follow the similar tendency and are consistent with prior literature. The slight longer bond distances in **18** are due to the larger size of Th atom compared to U atom. The An-μ_2Se-An and An-μ_2O-An angles are almost the same in the two structures, indicating a most chemically stable geometry of the $An_2(\mu_2\text{-}Se_2)(\mu_2\text{-}O)$ core region.

Compound **18** is comparable with the dimeric thorium compounds $(py)_6Th_2I_4(Se_2)_2$ (**7**) with bridging diselenides, as described in Chapter 2. It can be viewed as a μ_2-oxo bridge replacing one μ_2-diselenido bridge in the molecule of **7**. There are a lot of similarities between the two compounds, including the same space group $P2_1/n$ of the single crystals and the consistency of bond distance ranges.

There are also some differences between the two molecules. Firstly, unlike the centrosymmetric molecule **7**, the molecule **18** has a lower symmetry. The metal-ligand bond distances are slightly different between the two Th atoms in **18**. Secondly, the py ligands in **18** have approximately two locations for each Th with respect to the Th…Th vector, namely, the axial ligand N ((N(1) and N(3) for Th(1), N(6) and N(4) for Th(2)) and the nearly equatorial ligand N' (N(2)for Th(1), N(4) for Th(2)). Although it has the same trend as **7** that the Th-N' bond distance is generally longer than Th-N, the difference is more significant in **18**, namely average 0.084 Å, compared to average 0.018 Å in **7**, indicating a much weaker interactions between Th and equatorial py ligand.

This significant difference also appears in molecule **19**, as the difference between

U-N’ and U-N is average 0.109 Å. It suggests that the replacement of oxo bridge for diselenido bridge has some influence on the Th-N’ orbital attractive interactions.

Similar synthetic attempt by adding Se and SeO_2 into a solution of “$ThBr_n(SC_6F_5)_m(SePh)_{4-(n+m)}$” (n = 1 to 4) results in a novel thorium cluster $(py)_{10}Th_6O_3(Se_2)_8(SC_6F_5)_2$ (**20**) with a $Th_6(\mu_3\text{-}O)_2(\mu_4\text{-}O)(\mu_2\text{-}Se_2)_8$ core. It was characterized by conventional methods and low-temperature single-crystal X-ray diffraction. Figures 4.3 shows ORTEP diagrams of **20** and its core region.

(a)

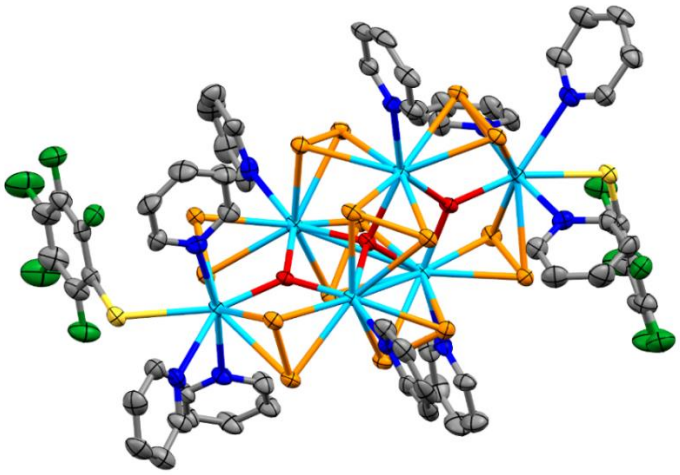

(b)

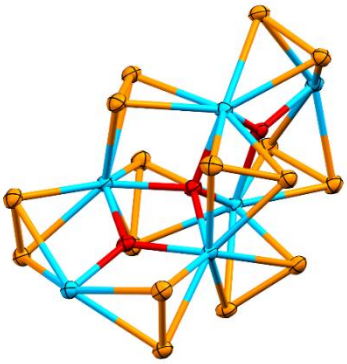

Figure 4.3. (a) ORTEP diagram of $(py)_{10}Th_6O_3(Se_2)_8(SC_6F_5)_2$ (**20**) and (b) its core region, with orange Se, yellow S, green F, light blue Th, dark blue N, red O, grey C, the H atoms removed for clarity and ellipsoids at the 50% probability level.

Selected crystallographic details are given in Table 4.3.

Table 4.3. Crystallographic data for $(py)_{10}Th_6O_3(Se_2)_8(SC_6F_5)_2$ (**20**)

empirical formula	$C_{89.5}H_{84.5}F_{10}N_{15.5}O_{6.5}S_2Se_{16}Th_6$
fw	4390.94
crystal system	monoclinic
space group	C2/c
a (Å)	26.031(3)
b (Å)	17.232(2)
c (Å)	26.604(3)
α (deg)	90
β (deg)	100.5099(17)
γ (deg)	90
V ($Å^3$)	11773(2)
Z	4
D(calcd) (g/cm^3)	2.486
T (K)	120(2)
abs coeff(mm^{-1})	12.646
$R(F)^b$ [$I > 2\sigma(I)$]	0.0404
$R_w(F^2)^c$ [$I > 2\sigma(I)$]	0.0959

Compound **20** was first synthesized by addition of elemental Se and hydrolysis of adventitious trace of water from a "$ThBr_n(SC_6F_5)_m(SePh)_{4-(n+m)}$" solution. Several attempts have been made to prepare this complex in a controlled way, including adding measured quantities of water or oxygen gas. It was eventually reproduced by adding Se and SeO_2 with a 3:1 ratio. In order to test the purity of the product, PXRD was used for characterization and the result is shown in Figure 4.4. Comparison of the experimentally determined PXRD profile with the calculated pattern from the single crystal data indicates high purity of the bulk material.

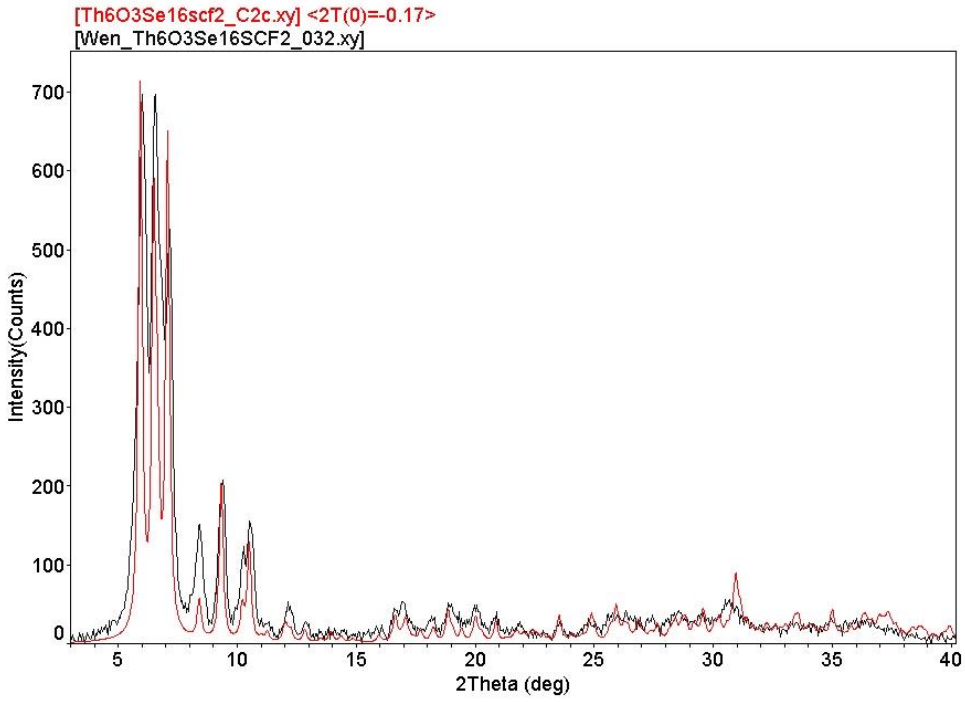

Figure 4.4. PXRD and calculated pattern from single crystal (in red) for

$(py)_{10}Th_6O_3(Se_2)_8(SC_6F_5)_2$ (**20**)

In the molecule of **20**, six Th atoms are connected by diselenido and oxo bridges. Four of them are in the central region, each Th atom is bound to three (μ_2-Se_2), one (μ_3-O), one (μ_4-O) and one py ligands. The remaining two Th atoms are located at the left and right sides, respectively, and each Th atom is connected to two (μ_2-Se_2), one (μ_3-O), one -SC_6F_5 and three py ligands. This results in a nine-coordinated sphere around every Th atoms in the structure.

Compound **20** can be roughly viewed as combination of eight dimeric core of $(py)_6Th_2O(Se_2)I_4$ (**18**), with every two "dimers" sharing a oxo bridge with each other. One terminal -SC_6F_5 ligand is bond to Th atom on each side, and it helps to stabilize the structures and increase the solubility of the compound in organic solvent. Unlike

18, molecule **20** is centrosymmetric, and the asymmetric structural unit of compound **20** is shown in Figure 4.5.

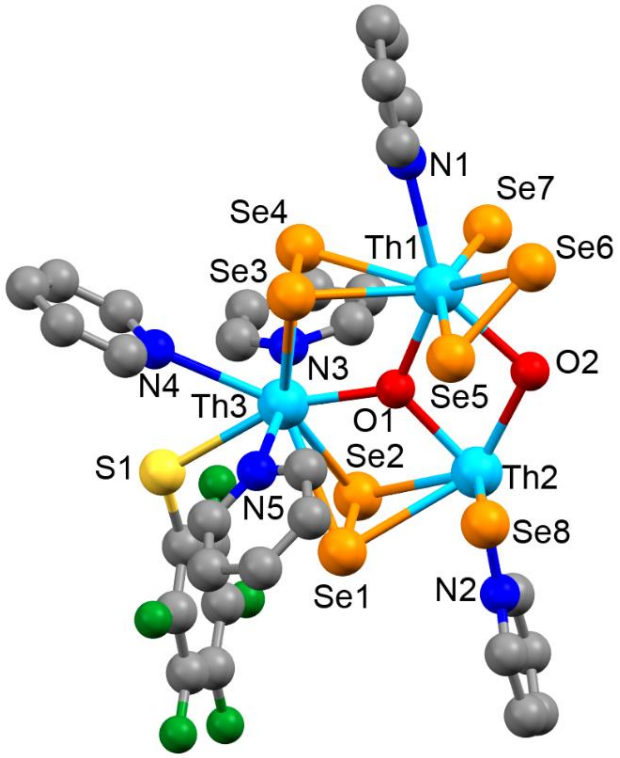

Figure 4.5. Asymmetric structural unit of compound **20**.

Bond geometries for **20** are summarized in Table 4.4.

Table 4.4. Selected bond distances (Å) and bond angles (°) for **20** [a]

Th-N(1),N(2)	2.712(5), 2.728(7)	Th-(μ_2-Se)	2.988-3.127(1)
Th-N(3),N(5)	2.664(5), 2.659(5)	Th(3)-(μ_3-O(1))	2.233(4)
Th-N(4)	2.757(6)	Th(1),Th(2)-(μ_3-O(1))	2.313, 2.317(4)
Th-S	2.939(1)	Th-(μ_4-O(2))	2.430-2.437(3)
S-C	1.751(7)	Se-Se	2.337-2.370(1)
Th-O1-Th	115.8-122.4(1)	Th-O2-Th	107.4-110.3(1)
Th-Se-Th	81.2-83.2(1)	Th-S-C	113.0(2)

a The ESD values are enclosed in parentheses. Refer to figures for Th, N, and O atom labels.

In compound **20**, there are three py ligands bound to Th(3). Similar to compound **7** and **18**, the distance between Th atom and N(4) from equatorial py ligand is much longer (average 0.095 Å) than the distance between Th atom and N(1) or N(3) from axial py ligand. Two other py ligands bound to central Th(1) and Th(2) atoms, respectively, and their Th-N bond lengths (2.71-2.72 Å) are in the middle of these two distances, and are more consistent with the values in compound **7** and **18**.

The average Th-(μ_4-O) bond lengths are 0.12 Å longer than Th-(μ_3-O) distances, and all Th-O distances are consistent within ranges previous literature values, comparing Th-(μ_4-O) (2.43 Å) in **20** with the Th-(μ_4-O) bonds in $Th_4(\mu_4\text{-}O)(\mu\text{-}Cl)_2I_6[\kappa^2(O,O')\text{-}\mu\text{-}O(CH_2)_2OCH_3]_6$ (2.39-2.41 Å)[10] and in $[Th_4Cl_8(O)$(tetraethylene glycolate)$_3]$ (2.34-2.49 Å)[11] . The Th-(μ_3-O) distance in **20** (2.31 Å) is also comparable with the Th-(μ_3-O) bonds in $[Th_6(\mu_3\text{-}O)_4(\mu_3\text{-}OH)_4(H_2O)_6(Gly)_6(HGly)_6]^{6+}$ (2.26-2.33 Å) Å[12] and in $Th_6O_4(OH)_4$(4-hydroxybenzoate)$_{12}(H_2O)_6$ (2.28-2.37 Å)[13].

The Se-Se bond lengths in diselenido bridges are in the narrow range 2.34-2.37 Å , which are comparable to the 2.397(1) Å terminally bound diselenido ligand in [K(18-crown-6)][Th(η^2-E_2)$(NR_2)_3$],[14] and fall within the range of expected values for diselenide moieties bound to lanthanides[15] and transition metals[16].

Compound **20** is the first actinide cluster containing both diselenido and oxo bridges. Even if we broad the searching range to the compounds containing only $An_6(\mu_3\text{-}O)_2(\mu_4\text{-}O)$ motif, there are only few examples, and all of them are based on uranium[17].

4.3 Actinide Halides

Two thorium and uranium halides $(py)_4ThI_3F$ (**21**) and $(py)_3UI_3(SC_6F_5)$ (**22**) can be synthesized from the reaction of actinide metal (Th or U), I_2 and $(SC_6F_5)_2$ in pyridine solution. Trace amount of mercury needs to be added into thorium reaction as a catalyst to reduce the reaction completion time.

Compounds **21** and **22** were characterized by low-temperature single-crystal X-ray diffraction. Figures 4.6 and 4.7 show ORTEP diagrams of the molecular structures of **21** and **22**, respectively.

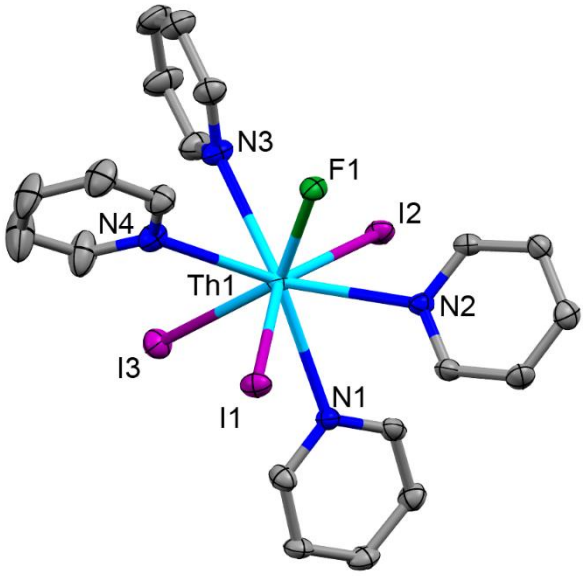

Figure 4.6. ORTEP diagram of $(py)_4ThI_3F$ (**21**), with green F, purple I, light blue Th, dark blue N, grey C, the H atoms removed for clarity and ellipsoids at the 50% probability level.

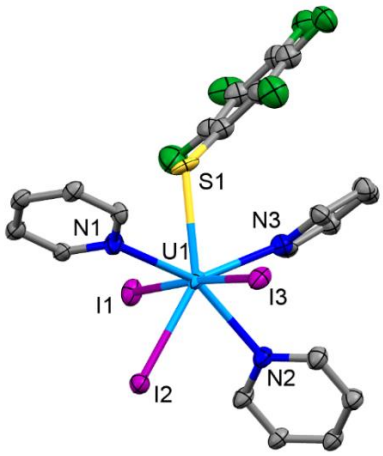

Figure 4.7. ORTEP diagram of $(py)_3UI_3(SC_6F_5)$ (**22**), with green F, purple I, yellow S, light blue U, dark blue N, grey C, the H atoms removed for clarity and ellipsoids at the 50% probability level.

Selected crystallographic details are given in Table 4.5, with significant bond lengths and angles given in Table 4.6.

Table 4.5. Summary of Crystallographic Details for **21** and **22**

	21	**22**
empirical formula	$C_{25}H_{25}FI_3N_5Th$	$C_{31}H_{25}F_5I_3N_5SU$
fw	1027.24	1213.35
crystal system	triclinic	monoclinic
space group	P-1	$P2_1/c$
a (Å)	9.7514(7)	17.470(6)
b (Å)	14.1544(10)	9.043(3)
c (Å)	22.5897(16)	21.207(7)
α (deg)	97.1234(14)	90
β (deg)	101.4896(14)	113.395(12)
γ (deg)	91.0940(14)	90
V ($Å^3$)	3028.8(4)	3074.1(17)
Z	2	4
D(calcd) (g/cm^3)	2.253	2.622
T (K)	120(2)	120(2)
abs coeff(mm^{-1})	8.009	8.425
$R(F)^b$ [$I > 2\sigma(I)$]	0.0435	0.1016
$R_w(F^2)^c$ [$I > 2\sigma(I)$]	0.1020	0.2207

Table 4.6. Selected bond distances (Å) and bond angles (°) for **21** and **22** [a]

21		**22**	
Th-N	2.697-2.745(6)	U-N	2.541-2.592(17)
Th-I	3.150-3.162(1)	U-I	2.972-3.028(4)
Th-F	2.118(3)	U-S	2.778(12)
N(1)-Th-N(2)	70.77(15)	N(2)-U-N(3)	65.86(8)
N(3)-Th-N(4)	67.25(17)	I(1)-U-I(2)	87.66(9)
I(1)-Th-I(2)	148.97(13)	I(1)-U-I(3)	175.18(11)
N(3)-Th-F	71.23(15)	N(3)-U-S	74.52(7)

a The ESD values are enclosed in parentheses. Refer to figures for Th or U, N, and I atom labels.

Reacting with $(SC_6F_5)_2$ and I_2 in pyridine solution, different actinide metal (Th or U) can form different compounds with different coordination geometries. In thorium compound **21**, the Th atom is bound to four py, three I^- and one F^- abstracted from the original $(SC_6F_5)_2$, resulting in an eight-coordinate structure. While in uranium derivative **22**, the U atom is bound to three py, three I- and one (SC_6F_5), forming a seven-coordinate structure. The smaller coordination number can be attributed to smaller ionic radius of U. These two compounds also crystallize in different space groups, namely, P-1 for **21** and $P2_1/c$ for **22**.

The structural difference can also be probed by ^{19}F NMR in solution. Compound **21** shows a single peak at -129 ppm, while **22** shows three peaks with 2:1:2 integration ratio, which are attributed to its SC_6F_5 ligand.

4.4 Conclusions

Two actinide molecular oxychalcogenides $(py)_6Th_2O(Se_2)I_4$ (**18**), $(py)_6U_2O(Se_2)I_4$ (**19**) and one thorium oxychalcogenido cluster $(py)_{10}Th_6O_3(Se_2)_8(SC_6F_5)_2$ (**20**) have been synthesized and characterized. These are the first examples of actinide compounds containing both oxo and dichalcogenido bridges. Elemental Se and SeO_2 are the sources for the μ-oxo and μ-Se_2 bridges.

Two actinide halides $(py)_4ThI_3F$ (**21**) and $(py)_3UI_3(SC_6F_5)$ (**22**) have been synthesized from similar reactions of actinide metal, iodine and $(SC_6F_5)_2$ ligands. The identity of metal has influenced the final structure, as **21** only contains fluoride abstracted from the original $(SC_6F_5)_2$ component, whereas the uranium derivative **22**, follows the stoichiometry of the starting materials.

References

(1) Sigmon, G. E.; Unruh, D. K.; Ling, J.; Weaver, B.; Ward, M.; Pressprich, L.; Simonetti, A.; Burns, P. C. Symmetry versus Minimal Pentagonal Adjacencies in Uranium‐Based Polyoxometalate Fullerene Topologies. *Angew. Chem. Int. Ed.* **2009**, *48*, 2737-2740.

(2) Ling, J.; Qiu, J.; Burns, P. C. Uranyl Peroxide Oxalate Cage and Core–Shell Clusters Containing 50 and 120 Uranyl Ions. *Inorg. Chem.* **2012**, *51*, 2403-2408.

(3) Qiu, J.; Burns, P. C. Clusters of actinides with oxide, peroxide, or hydroxide bridges. *Chem. Rev.* **2012**, *113*, 1097-1120.

(4) Arnold, P. L.; Jones, G. M.; Odoh, S. O.; Schreckenbach, G.; Magnani, N.; Love, J. B. Strongly coupled binuclear uranium–oxo complexes from uranyl oxo rearrangement and reductive silylation. *Nat. Chem.* **2012**, *4*, 221.

(5) Banerjee, S.; Huebner, L.; Romanelli, M. D.; Kumar, G. A.; Riman, R. E.; Emge, T. J.; Brennan, J. G. Oxoselenido clusters of the lanthanides: Rational introduction of oxo ligands and near-IR emission from Nd (III). *J. Am. Chem. Soc.* **2005**, *127*, 15900-15906.

(6) Moore, B. F.; Emge, T. J.; Brennan, J. G. Lanthanide Clusters with Azide Capping Ligands. *Inorg. Chem.* **2013**, *52*, 6021-6027.

(7) Norton, K.; Banerjee, S.; Das, S.; Huebner, L.; Emge, T. J.; Brennan, J. G. Lanthanide oxochalcogenido clusters. *Dalton Trans.* **2010**, *39*, 6794-6800.

(8) (a) Bagnall, K. W. The coordination chemistry of the actinide halides. *Coord. Chem. Rev.* **1967**, *2*, 145-162.(b) Baker, R. J. The coordination and organometallic chemistry of UI_3 and $U\{N(SiMe_3)_2\}_3$: Synthetic reagents par excellence. *Coord. Chem. Rev.* **2012**, *256*, 2843-2871.

(9) Gotthelf, G.; Stuber, M. A.; Kornienko, A. Y.; Emge, T. J.; Brennan, J. G. Organosoluble tetravalent actinide di- and trifluorides. *Chem. Commun.* **2018**, *54*, 12018-12020.

(10) Travia, N. E.; Scott, B. L.; Kiplinger, J. L. A rare tetranuclear thorium (IV) μ 4‐oxo cluster and dinuclear thorium (IV) complex assembled by carbon–oxygen bond activation of 1, 2‐dimethoxyethane (DME). *Chem. Eur. J* **2014**, *20*, 16846-16852.

(11) Rogers, R. D.; Bond, A. H.; Witt, M. M. Macrocycle complexation chemistry 34. Polyethylene glycol and glycolate complexes of Th^{4+}. Preparation and structural characterization of $[ThCl_3$(pentaethylene glycol)$]Cl{\cdot}CH_3CN$ and the

$(Th^{4+})_4$ cluster, $[Th_4Cl_8(O)(tetraethylene\ glycolate)_3]\cdot 3CH_3CN$. *Inorg. Chim. Acta* **1991**, *182*, 9-17.

(12) Hennig, C.; Takao, S.; Takao, K.; Weiss, S.; Kraus, W.; Emmerling, F.; Scheinost, A. C. Structure and stability range of a hexanuclear Th(iv)–glycine complex. *Dalton Trans.* **2012**, *41*, 12818-12823.

(13) Vanagas, N. A.; Wacker, J. N.; Rom, C. L.; Glass, E. N.; Colliard, I.; Qiao, Y.; Bertke, J. A.; Van Keuren, E.; Schelter, E. J.; Nyman, M.; Knope, K. E. Solution and Solid State Structural Chemistry of Th(IV) and U(IV) 4-Hydroxybenzoates. *Inorg. Chem.* **2018**, *57*, 7259-7269.

(14) Smiles, D. E.; Wu, G.; Hrobarik, P.; Hayton, T. W. Use of ^{77}Se and ^{125}Te NMR Spectroscopy to Probe Covalency of the Actinide-Chalcogen Bonding in $[Th(E_n)\{N(SiMe_3)_2\}_3]^-$ (E = Se, Te; n=1, 2) and Their Oxo-Uranium(VI) Congeners. *J. Am. Chem. Soc.* **2016**, *138*, 814-825.

(15) (a) Huebner, L.; Kornienko, A.; Emge, T. J.; Brennan, J. G. Lanthanide clusters with internal Ln: Fragmentation and the formation of dimers with bridging Se^{2-} and Se_2^{2-} ligands. *Inorg. Chem.* **2005**, *44*, 5118-5122.(b) Kornienko, A. Y.; Emge, T. J.; Brennan, J. G. Chalcogen-rich lanthanide clusters: Cluster reactivity and the influence of ancillary ligands on structure. *J. Am. Chem. Soc.* **2001**, *123*, 11933-11939.

(16) (a) Yao, S. L.; Xiong, Y.; Zhang, X. H.; Schlangen, M.; Schwarz, H.; Milsmann, C.; Driess, M. Facile Dissociation of $[(LNi^{II})_2E_2]$ Dichalcogenides: Evidence for $[LNi^{II}E_2]$ Superselenides and Supertellurides in Solution. *Angew. Chem. Int. Ed.* **2009**, *48*, 4551-4554.(b) Wu, D. H.; Xu, B. H.; Li, Y. Z.; Yan, H. Diruthenium half-sandwich complexes containing one μ-E_2 (E = S, Se) unit and two chelating 1,2-dicarba-closo-dodecaborane-1,2-dithiolate ligands: Reactivity studies with methyl acetylene carboxylates. *Organometallics* **2007**, *26*, 6300-6306.(c) Fedin, V. P.; Sokolov, M. N.; Gerasko, O. A.; Virovets, A. V.; Podberezskaya, N. V.; Fedorov, V. Y. Triangular $M_3Se_7^{4+}$ and $M_3Se_4^{4+}$Complexes (M = Mo, W). An X-Ray Study of $Mo_3Se_7(Et_2NCS_2)_4$ and $W_3Se_7(Et_2NCS_2)_4$ *Inorg. Chim. Acta* **1991**, *187*, 81-90.(d) Ryu, S.; Whang, D.; Kim, H. J.; Kim, K.; Yoshida, M.; Hashimoto, K.; Tatsumi, K. Novel disulfido- and diselenido-bridged zirconium and hafnium porphyrin dimers with unusual coordination geometries: $[M(TPP)]_2(\mu\text{-}\eta^2\text{-}Q_2)_2$ (M=Zr, Hf; Q=S, Se). *Inorg. Chem.* **1997**, *36*, 4607-4609.

(17) (a) Chatelain, L.; White, S.; Scopelliti, R.; Mazzanti, M. Isolation of a Star-Shaped Uranium (V/VI) Cluster from the Anaerobic Photochemical Reduction of Uranyl (VI). *Angew. Chem. Int. Ed.* **2016**, *55*, 14325-14329.(b) Falaise, C.; Volkringer, C.; Vigier, J.-F.; Beaurain, A.; Roussel, P.; Rabu, P.; Loiseau, T.

Isolation of the Large {Actinide}$_{38}$ Poly-oxo Cluster with Uranium. *J. Am. Chem. Soc.* **2013**, *135*, 15678-15681.(c) Biswas, B.; Mougel, V.; Pécaut, J.; Mazzanti, M. Base-Driven Assembly of Large Uranium Oxo/Hydroxo Clusters. *Angew. Chem. Int. Ed.* **2011**, *50*, 5745-5748.(d) Martin, N. P.; Volkringer, C.; Henry, N.; Trivelli, X.; Stoclet, G.; Ikeda-Ohno, A.; Loiseau, T. Formation of a new type of uranium(iv) poly-oxo cluster {U$_{38}$} based on a controlled release of water via esterification reaction. *Chem. Sci.* **2018**, *9*, 5021-5032.

Experimental Section

Caution: Depleted uranium (primary isotope ^{238}U) is a weak α-emitter (4.197 MeV) with a half-life of 4.47×10^9 years and thorium (primary isotope ^{232}Th) is a weak α-emitter (4.012 MeV) with a half-life of 1.41×10^{10} years; manipulations should be carried out in monitored fume hoods or in inert atmosphere gloveboxes in a radiation laboratory equipped with α- and β-counting equipment.

General Methods

All syntheses were carried out under ultrapure nitrogen (Welco Praxair) using conventional glovebox or standard Schlenk techniques. Pyridine, DME, THF and hexane (Aldrich) was purified with a dual-column Solv-Tek solvent purification system and collected immediately prior to use. Toluene (Aldrich) was dried over molecular sieves and stored in glovebox. $(SC_6F_5)_2$ [1] and $(SeC_6F_5)_2$ [2] were synthesized according to the literature procedures, respectively. PhSeSePh (Aldrich) was purchased and recrystallized from hexanes. PhSSPh (Acros), 2,2'-bipyridine, pyrazole, 3,5-dimethylpyrazole, pyrazine, sulfur, selenium, iodine, selenium dioxide, PhSeBr, PhSeCl (Aldrich), thorium chips, uranium turnings (International Bioanalytical Industries Inc.), lanthanides and mercury (Strem Chemicals) were purchased and used as received. Melting points were recorded in sealed glass capillaries and are uncorrected. IR spectra were recorded on a Thermo Nicolet Avatar 360 FTIR spectrometer from 4000 to 400 cm^{-1} as Nujol mulls using CsI plates. Gas chromatography-mass

spectrometry (GC-MS) data were collected on a Varian Saturn 2100T instrument fitted with a capillary column (30mm length, 0.25 mm ID, 0.25 mm film thickness). All NMR data were collected on a Varian VNMRS 500 spectrometer at 25 °C with the compounds dissolved in deuterated solvents. ^{1}H and ^{19}F NMR spectra were obtained at 499 and 476 MHz, respectively; ^{77}Se NMR spectra were acquired with a longer relaxation delay (7.0 s) in hydrogen or fluorine decoupled mode at 95 MHz using $(SePh)_2$ as an external standard. Elemental analyses were performed by Quantitative Technologies, Inc. (Whitehouse, NJ).

Single Crystal X-ray Structure Determination.

All the data were collected on a Bruker Smart APEX CCD diffractometer with graphite monochromatized Mo Kα radiation (λ = 0.71073 Å) at 100 or 120 K.[3] Crystals were immersed in Paratone oil and examined at low temperatures. The data were corrected for Lorenz effects and polarization, and absorption, the latter by a face-based numerical method.[3] The structures were solved by direct methods.[4] All non-hydrogen atoms were refined[4] based upon F_{obs}^2. All hydrogen atom coordinates were calculated with idealized geometries. All structures were drawn using the Mercury 3.10 program.[5]

Synthesis of $(DME)_2Nd(SeC_6F_5)_3$ (1)

Nd (0.072 g, 0.50 mmol), $(SeC_6F_5)_2$ (0.344 g, 0.70 mmol) and catalytic Hg (0.010

g, 0.05 mmol) were combined in DME (15 mL) and stirred for 6 h, to give a light blue solution with a trace amount of mercury at the bottom of the flask. The solution was filtered, concentrated and layered with hexanes to give light blue needles (241 mg, 49%) that melt at 228 °C and turn black at 308 °C. Anal. Calcd for $C_{26}H_{20}F_{15}O_4Se_3Nd$: C 29.4; H 1.90. Found: C 28.9; H 1.91. IR: 2959(s), 2924(m), 2849(s), 2141(w), 1676(w), 1603(m), 1459(s), 1359 (s), 1228(m), 965(w), 833(w), 815(w), 723(w), 554(w) cm^{-1}. UV-vis: 432, 463, 473, 518, 531, 587, 686, 751, 807, 884, 1179, 1374, 1396 nm.

Synthesis of $(DME)_2Er(SeC_6F_5)_3$ (2)

Er (0.084 g, 0.50 mmol), $(SeC_6F_5)_2$ (0.344 g, 0.70 mmol) and catalytic Hg (0.010 g, 0.05 mmol) were combined in DME (15 mL) and stirred for 8 h, to give a pale pink solution with a trace amount of mercury at the bottom of the flask. The solution was filtered, concentrated and layered with hexanes to give light pink needles (293 mg, 58%) that melt at 265 °C and turn black at 288 °C. Anal. Calcd for $C_{26}H_{20}F_{15}O_4Se_3Er$: C 28.8; H 1.86. Found: C 29.3; H 2.30. IR: 2957(s), 2923(w), 2849(s), 1609(w), 1507(s), 1458(s), 1376(s), 1260(w), 1190(w),1078(w), 1027(w), 964(s), 864(m), 815(m), 722(s), 576(w) cm^{-1}. UV-vis: 488, 522, 545, 654, 796, 898, 982, 1178, 1373, 1397, 1428, 1496, 1536 nm.

Synthesis of $(DME)_2Tm(SeC_6F_5)_3$ (3)

Tm (0.085 g, 0.50 mmol), $(SeC_6F_5)_2$ (0.344g, 0.70 mmol) and catalytic Hg (0.010g, 0.05mmol) were combined in DME (15 mL) and stirred for 8h, to give a straw yellow solution with a trace amount of mercury at the bottom of the flask. The solution was

filtered, concentrated and layered with hexanes to give light yellow needle crystals (279 mg, 55%) that melt at 315 ºC and turn black at 330 ºC. Anal. Calcd for $C_{26}H_{20}F_{15}O_4Se_3Tm$: C 28.7; H 1.85. Found: C 28.2; H 1.82. IR: 2961(s), 2924(w), 2849(s), 2724(w), 1611(m), 1504(s), 1462(s), 1377(s), 1269(w), 1245(m), 1192(m), 1123(m), 1079(s), 1030(w), 966(s), 867(s), 813(s), 722(m), 575(w) cm^{-1}. UV-vis: 493, 693, 797, 1138, 1153, 1187, 1215, 1392 nm. Unit cell at 100K from single crystal X-ray diffraction data: $P2_1/n$, a = 7.826(3) Å, b = 17.060(5) Å, c = 23.12(1) Å, β = 95.00(2) º, V = 3075.0(2) $Å^3$.

Synthesis of $(py)_6Th_2I_4(S_2)_2 \cdot 2py$ (4).

Th (0.232 g, 1.00 mmol), PhSSPh (0.218 g, 1.00 mmol), and I_2 (0.254 g, 1.00 mmol) were combined in pyridine (20 mL) with a catalytic amount of Hg (0.010 g, 0.05 mmol). The mixture was stirred for 12 h until all Th metal was completely consumed to give a yellow solution with trace black powder**.** Sulfur (0.064 g, 2.00 mmol) and toluene (10 mL) were added and the mixture was stirred for 1 h to give a yellow solution that was filtered to remove pale-yellow powder, concentrated to 20 mL and layered with hexanes (15 mL) to form colorless crystals (0.36 g, 46%) that melt at 181ºC and decompose (turn black) at 291ºC. IR: 2924 (w), 2852(w), 1598 (m), 1463 (m), 1365 (m), 1219 (m), 1151 (w), 1065 (m), 1037 (m), 1002 (m), 738 (s), 695 (s), 623 (s), 542 (m), 466 (w), 417 (m) cm^{-1}. Anal. Calcd for $C_{40}H_{40}I_4N_8S_4Th_2$: C, 27.7; H, 2.33; N, 6.47 (without lattice pyridine $C_{30}H_{30}N_6I_4Th_2S_4$: C, 22.9; H, 1.92; N, 5.34.) Found: C, 23.0; H, 2.06; N, 5.24. ^{1}H NMR (toluene-d_8): 8.48 (d, *J* = 4.8 Hz, 2H, py), 7.00 (m, 1H, py), 6.67 (t,

J = 6.0 Hz, 2H, py).

Synthesis of $(py)_6Th_2Br_2(SC_6F_5)_2(S_2)_2$ (5)

Th (0.232 g, 1.00 mmol), PhSSPh (0.109 g, 0.50 mmol), $F_5C_6SSC_6F_5$ (0.199 g, 0.50 mmol) and PhSeBr (0.236 g, 1.00 mmol) were combined in pyridine (10 mL) with a catalytic amount of Hg (0.010 g, 0.05 mmol), and the mixture was stirred for 12 h until the thorium metal was completely consumed to give a yellow solution. Sulfur (0.064 g, 2.00 mmol) and toluene (10 mL) were added and the mixture was stirred for an additional 30 min. The bright yellow solution was filtered to remove light grey powder, concentrated to 15 mL and layered with hexanes (15 mL) to give colorless crystals (0.29 g, 36%) that melt at 213°C and decompose at 273°C. IR: 2924 (s), 2854 (s), 1630(w), 1601 (m), 1462 (s), 1365 (s), 1261 (m), 1222 (m), 1153 (w), 1079 (w), 1037 (w), 967 (s), 859 (s), 801(s), 741 (s), 694 (s), 624 (m), 578(w), 482(w), 419(w) cm^{-1}. Anal. Calcd for $C_{42}H_{30}N_6Th_2F_{10}Br_2S_6$: C, 31.0; H, 1.86; N, 5.17. Found: C, 31.0; H, 1.91; N, 5.17. ^1H NMR (toluene-d_8): 8.54 (broad, 2H, py), 6.94 (m, 1H, py), 6.64 (m, 2H, py). ^{19}F NMR (toluene-d_8): -138 (m, 2F), -159(t, 1F), -162 (m, 2F).

Synthesis of $(py)_6Th_2Cl_2(SC_6F_5)_2(S_2)_2$ (6).

Th (0.232 g, 1.00 mmol), PhSSPh (0.109 g, 0.50 mmol), $F_5C_6SSC_6F_5$ (0.199 g, 0.50 mmol) and PhSeCl (0.192 g, 1.00 mmol) were combined in pyridine (10 mL) with a catalytic amount of Hg (0.010 g, 0.05 mmol), and the mixture was stirred for 12 hrs until the thorium metal was completely consumed to give a pale yellow solution. Sulfur (0.064 g, 2.00 mmol) and toluene (10 mL) were added and the mixture was stirred for

an additional 45 min. The yellow solution was filtered to remove light grey powder, concentrated to 15 mL and layered with hexanes (15 mL) to give colorless crystals, one of which was identified by single crystal diffraction as $(py)_6Th_2Cl_2(SC_6F_5)_2(S_2)_2 \cdot 1.5$ py (**6**). PXRD of the powdered product revealed that this reaction co-crystallizes as a number of products, including **6** and monomeric $(py)_4ThCl_4$ (**10**)

Synthesis of $(py)_6Th_2I_4(Se_2)_2 \cdot 2py$ (7).

Th (0.232 g, 1.00 mmol), PhSeSePh (0.312 g, 1.00 mmol), and I_2 (0.254 g, 1.00 mmol) were combined in pyridine (20 mL) with a catalytic amount of Hg (0.010 g, 0.05 mmol). The mixture was stirred for 12 h until the thorium metal was consumed to give a yellow solution and trace black powder**.** Elemental selenium (0.158 g, 2.00 mmol) was added and the mixture was stirred for an additional 30 min. The yellow solution was filtered, concentrated to 10 mL and layered with hexanes (15 mL) to form yellow crystals (0.53 g, 61%) that melt at 252ºC and decompose (turn black) at 384ºC. IR: 2924 (s), 2853(s), 1598 (w), 1463 (m), 1365 (s), 1261 (w), 1220 (w), 1067 (w), 1037 (w), 801 (m), 722 (w), 700 (w), 489(w) cm^{-1}. UV-vis: This compound shows an absorption plateau at ca. 400nm, but a well-defined maximum was not observed. Anal. Calcd for $C_{40}H_{40}N_8Th_2I_4Se_4$: C, 25.0; H, 2.10; N, 5.84. (Lattice pyridine removed $C_{30}H_{30}N_6Th_2I_4Se_4$: C, 20.5; H, 1.72; N, 4.77) Found: C, 25.1; H, 2.29; N, 5.64. ^{1}H NMR (benzene-d_6): 8.98 (broad, 2H, py), 6.88 (m, 1H, py), 6.62 (m, 2H, py). ^{77}Se NMR (pyridine-d_5): 241 (s).

Synthesis of $(py)_6Th_2I_2(SC_6F_5)_2(Se_2)_2 \cdot py$ (8).

Th (0.232 g, 1.00 mmol), PhSeSePh (0.312 g, 1.00 mmol), $F_5C_6SSC_6F_5$ (0.199 g, 0.50 mmol) and I_2 (0.127 g, 0.50 mmol) were combined in pyridine (20 mL) with a catalytic amount of Hg (0.010 g, 0.05 mmol), and the mixture was stirred for 12 h until the metal was completely consumed to give a yellow solution. Elemental selenium (0.158 g, 2.0 mmol) was added and the mixture was stirred for 1 h. The pale orange solution was filtered, concentrated to 15 mL and layered with hexanes (15 mL) to give orange crystals (0.30 g, 31%) that became deep orange and melt at 181ºC and decompose at 290 ºC. IR: 2924 (s), 2854(s), 1601 (w), 1460 (s), 1376 (s), 1261 (w), 1221(w), 1152 (w), 1038 (w), 969 (m), 859(w), 833(w), 802(w), 722 (m), 698 (w), 623(w) cm^{-1}. UV-vis: This compound shows an absorption plateau at ca. 400 nm. Anal. Calcd for $C_{47}H_{35}N_7Th_2F_{10}I_2S_2Se_4$: C, 28.4; H, 1.78; N, 4.94. (Lattice pyridine removed $C_{42}H_{30}N_6Th_2F_{10}I_2S_2Se_4$: C, 26.5; H, 1.59; N, 4,41) Found: C, 28.2; H, 1.97; N, 4.47. ^{1}H NMR (toluene-d_8): 8.71(broad, 2H, py), 6.91 (m, 1H, py), 6.63 (m, 2H, py). ^{19}F NMR (toluene-d_8): -138 (d, 2F), -159(t, 1F), -162 (m, 2F). ^{77}Se NMR (pyridine-d_5): 336 (s).

Synthesis of $(py)_6Th_2Br_2(SC_6F_5)_2(Se_2)_2 \cdot 2py$ (9).

Th (0.232 g, 1.00 mmol), PhSeSePh (0.156 g, 0.50 mmol), $F_5C_6SSC_6F_5$ (0.199 g, 0.50 mmol) and PhSeBr (0.236 g, 1.00 mmol) were combined in pyridine (20 mL) with a catalytic amount of Hg (0.010 g, 0.05 mmol), and the mixture was stirred for 12 h until the thorium metal was consumed to give a yellow solution. Elemental selenium (0.158 g, 2.00 mmol) was added and the mixture was stirred for an additional 10 min.

The pale orange solution was filtered, concentrated to 15 mL and layered with hexanes (10 mL) to give orange crystals (0.40 g, 44%) that melt at 145°C and decompose at 416 °C. IR: 2923 (s), 2854 (s), 1601 (m), 1503 (w), 1463 (s), 1376 (s), 1262 (w), 1221 (m), 1151 (w), 1079 (w), 1069 (w), 1038 (m), 1003 (m), 969 (m), 860 (s), 752 (m), 698 (s), 623 (s) cm^{-1}. Anal. Calcd for $C_{52}H_{40}F_{10}Br_2N_8S_2Se_4Th_2$·: C, 31.7; H, 2.05; N, 5.69. (Lattice pyridine removed $C_{42}H_{30}F_{10}Br_2N_6S_2Se_4Th_2$: C, 27.83; H, 1.67; N, 4,64) Found: C, 31.6; H, 2.11; N, 5.63. ^{1}H NMR (toluene-d_8): 8.72 (broad, 2H, py), 6.89 (broad, 1H, py), 6.58 (broad, 2H, py). ^{19}F NMR (toluene-d_8): -138(m, 2F), -159 (t, 1F), -162 (m, 2F). ^{77}Se NMR (pyridine-d_5): 309 (s).

Attempt to prepare $(py)_6Th_2Cl_2(SC_6F_5)_2(Se_2)_2$.

Th (0.232 g, 1.00 mmol), PhSeSePh (0.156 g, 0.50 mmol), $F_5C_6SSC_6F_5$ (0.199 g, 0.50 mmol) and PhSeCl (0.192 g, 1.00 mmol) were combined in pyridine (15 mL) with a catalytic amount of Hg (0.010 g, 0.05 mmol), and the mixture was stirred for 12 h until the metal was completely consumed to give an orange solution. Elemental selenium (0.158 g, 2.00 mmol) was added and the mixture and then stirred for 10 min. The pale orange solution was filtered, concentrated to 15 mL and layered with hexanes (15 mL) to give crystals that were ground and identified by PXRD as a mixture of the tetrachloride **7** and $(py)_8Th_4Se_4(SePh)_4(SC_6F_5)_4$.[6]

Synthesis of $(bipy)_2Th(SC_6F_5)_4$· 2THF (11)

Th (0.116 g, 0.50 mmol), $(SC_6F_5)_2$ (0.398 g, 1.00 mmol) and 2,2'-bipyridine (0.156 g, 1.00 mmol) were combined with Hg (0.010 g, 0.05 mmol) in THF (10 mL) and stirred

for 24 h at 25°C. The solution was filtered to remove trace grey precipitate, concentrated to 3 mL, and cooled to -30°C to yield colorless crystals (0.31 g, 42%) that melt at 179°C and decompose at 318°C. Anal. Calcd for $C_{52}H_{32}F_{20}O_2N_4S_4Th$: C, 42.1; H, 2.17; N, 3.77 (lattice desolvated $C_{44}H_{16}F_{20}N_4S_4Th$: C, 39.4, H,1.20, N, 4.18). Found: C, 43.2; H, 2.68; N, 4.28. IR: 2924 (m), 2584 (w), 1599 (m), 1500 (w), 1458 (s), 1376 (s), 1162 (w), 1076 (m), 1012 (m), 969 (s), 862 (s), 766 (m), 734 (m), 646 (m), 628 (w) cm^{-1}. ^1H NMR (pyridine-d_5): 8.76 (d, 2H, J=5.0Hz, bipy), 8.71 (dt, 2H, J = 8.0, 1.2 Hz, bipy), 7.77 (td, 2H, J = 8.0, 1.5 Hz, bipy), 7.25 (ddd, 2H, J = 7.5, 4.8, 1.3 Hz, bipy), 3.67 (m, 3H, THF), 1.61 (m, 3H, THF). ^{19}F NMR (pyridine-d_5): -132 (m, 2F), -161 (s, 1F), -165 (m, 2F).

Synthesis of $(pzn)_4Th_2(SC_6F_5)_8 \cdot$ 3tol (12).

Th (0.116 g, 0.50 mmol), $(SC_6F_5)_2$ (0.398 g, 1.0 mmol) and pyrazine (0.120 g, 1.5 mmol) were combined in toluene (20 mL) with a catalytic amount of Hg (0.010 g). The mixture was stirred for 3 days until Th was consumed. The orange-yellow solution was filtered away from the Hg, reduced in volume under vacuum to ca. 3 mL and kept at 2°C for a week to give colorless crystals.

Synthesis of $(Hpz)_4(pz)_2Th_2(SePh)_6$ (13).

Th (0.116 g, 0.50 mmol), $(SePh)_2$ (0.234 g, 0.75 mmol) and pyrazole (0.102 g, 1.5 mmol) were combined in toluene (15 mL) with a catalytic amount of Hg (0.010 g), and the mixture was stirred at 90°C in oil bath until Th was consumed. The light yellow solution was filtered away from the Hg, reduced in volume under vacuum to ca. 5 mL,

and kept at 2°C to give colorless crystals (0.12 g, 27 %) that melt at 82 °C. IR: 2964 (s), 2853 (s), 2726 (m), 2671 (w), 1574 (w), 1463 (s), 1377 (s), 1300 (w), 1154 (w), 1041 (w), 1021 (w), 936 (w), 767 (m), 722(s), 689(w), 465 (w), cm^{-1}. Anal. Calcd for $C_{54}H_{48}N_{12}Se_6Th_2$: C, 35.9; H, 2.68; N, 9.32. Found: C, 37.6; H, 3.31; N, 9.09.

Synthesis of $(Hpz)_4(pz)Th(SC_6F_5)_3 \cdot tol$ (14).

Th (0.116 g, 0.50 mmol), $(SC_6F_5)_2$ (0.299 g, 0.75 mmol) and pyrazole (0.102 g, 3.0 mmol) were combined in toluene (15 mL) with a catalytic amount of Hg (0.010 g). The mixture was stirred for 12 h until Th was consumed. The colorless solution was filtered away from the Hg, reduced in volume under vacuum to ca. 5 mL, and kept at 2°C to give colorless crystals (0.72 g, 73%) that melt at 99 °C. IR: 2959 (m), 2923 (m), 2852 (m), 1505 (m), 1463 (s), 1377 (s), 1285 (w), 1261 (w), 1118 (w), 1082 (w), 1045 (m), 966 (m), 937 (w), 858 (m), 782 (w), 723 (w), 669 (w), 603 (w), 564 (w) cm^{-1}. Anal. Calcd for $C_{40}H_{27}F_{15}N_{10}S_3Th$: C, 38.1; H, 2.16; N, 11.1. Found: C, 35.9; H, 2.42; N, 11.0. ^{1}H NMR(pyridine-d_5): 14.35 (broad, 4H), 7.94 (broad, 10H), 6.52 (broad, 5H)

Synthesis of $(Hdmpz)_4(dmpz)_2Th_2(SC_6F_5)_6 \cdot 6tol$ (15).

Th (0.116 g, 0.50 mmol), $(SC_6F_5)_2$ (0.398 g, 1.0 mmol) and 3,5-dimethylpyrazole (0.144 g, 1.5 mmol) were combined in toluene (15 mL) with a catalytic amount of Hg (0.010 g). The mixture was stirred for 2 days until Th was consumed. The colorless solution was filtered away from the Hg, reduced in volume under vacuum to ca. 2 mL, some colorless crystals (0.26 g, 37%) appeared immediately, a couple of which were identified by single crystal diffraction as $(Hdmpz)_4(dmpz)_2Th_2(SC_6F_5)_6$ (**3**). PXRD of

the powdery product revealed that this reaction co-crystallizes as a mixture of **15** and $(Hdmpz)_2(dmpz)_2Th(SC_6F_5)_2$ **(16)**.

Synthesis of $(Hdmpz)_2(dmpz)_2Th(SC_6F_5)_2$ (16).

Th (0.116 g, 0.50 mmol), $(SC_6F_5)_2$ (0.398 g, 1.0 mmol) and 3,5-dimethylpyrazole (0.144 g, 1.5 mmol) were combined in toluene (15 mL) with a catalytic amount of Hg (0.010 g). The mixture was stirred for 2 days until Th was consumed. The colorless solution was filtered away from the Hg, reduced in volume under vacuum to ca. 5 mL, some colorless crystals (0.19g, 38%) appeared after 2 days that that melt at 179 ^oC and decomposed at 238^oC. IR: 2927(m), 2724(w), 1514 (m), 1456 (s), 1377 (s), 1305(w), 1260 (m), 1153 (w), 1094 (m), 1022 (m), 982 (w), 955(s), 890(w), 861 (w), 808 (s), 723 (s), 653(m), 598(w), 518(w) cm^{-1}. Anal. Calcd for $C_{32}H_{30}F_{10}N_8S_2Th$: C, 37.9; H, 2.99; N, 11.1. Found: C, 37.7; H, 3.17; N, 11.1. ^1H NMR(pyridine-d_5): 14.98 (broad, 1H), 6.56 (broad, 1H), 5.98 (broad, 1H), 2.31(broad, 12H).

Synthesis of $(Hpz)_8Th_4Se_4(SeC_6F_5)_8 \cdot 3tol$ (17)

Th (0.116 g, 0.50 mmol), $(SeC_6F_5)_2$ (0.368 g, 0.75 mmol), pyrazole (0.102g, 1.5 mmol) and catalytic amount of Hg (0.01 g, 0.05 mmol) were combined in toluene (15 mL) and stirred for 2 days, to give a light yellow solution with some black powder. The solution was filtered to ca. 15ml, and concentrated to ca. 3mL, then put into refrigerator at 2^oC for a week, forming powdery product. The product was able to redissolve in 60^oC water bath, and some colorless crystals, which were suitable for single-crystal X-ray diffraction, appeared when the solution cooled down to room temperature.

Synthesis of $(py)_6Th_2O(Se_2)I_4 \cdot 3py$ (18)

Th (0.232 g, 1.00 mmol), PhSeSePh (0.312 g, 1.00 mmol), and I_2 (0.254 g, 1.00 mmol) were combined in pyridine (20 mL) with a catalytic amount of Hg (0.010 g, 0.05 mmol). The mixture was stirred for 12 h until the thorium metal was consumed to give a yellow solution and trace black powder**.** Elemental selenium (0.079 g, 1.0 mmol) and SeO_2 (0.028 g, 0.25 mmol) was added and the mixture was stirred for 3 h. The orange solution was filtered, concentrated to 12 mL and layered with hexanes (10 mL). The solution was kept at -30°C in two weeks to give light yellow crystals that melt at 168°C and decompose at 196 °C. IR: 2962 (s), 2844 (s), 2724(w), 1599 (w), 1459 (s), 1377 (s), 1262 (m), 1219 (w), 1097 (w), 1037 (w), 801 (s), 722 (m), 700 (m), 623 (w), 547 (w), 463 (w) cm^{-1}.

Synthesis of $(py)_6U_2O(Se_2)I_4$ (19)

U (0.220 g, 0.92 mmol), PhSeSePh (0.288 g, 0.92 mmol), and I_2 (0.235 g, 0.92 mmol) were combined in pyridine (20 mL). The mixture was stirred for 5 days until the uranium metal was consumed. Elemental selenium (0.073 g, 0.92 mmol) and SeO_2 (0.026 g, 0.23 mmol) was added and the mixture was stirred for 4 h. The dark red solution was filtered, concentrated to 15 mL and layered with hexanes (10 mL). The solution was kept at -30°C in two weeks to give black crystals.

Synthesis of $(py)_{10}Th_6O_3(Se_2)_8(SC_6F_5)_2$ (20)

Th (0.116 g, 0.50 mmol), PhSeSePh (0.078 g, 0.25 mmol), $F_5C_6SSC_6F_5$ (0.099 g, 0.25 mmol) and PhSeBr (0.118 g, 0.50 mmol) were combined in pyridine (15 mL) with

a catalytic amount of Hg (0.010 g, 0.05 mmol), and the mixture was stirred for 12 h until the thorium metal was consumed to give an orange solution. Elemental selenium (0.079 g, 1.00 mmol) and SeO_2 (0.014 g, 0.25 mmol) was added and the mixture was stirred for additional 3h. The dark orange-red solution was filtered, concentrated to 12 mL and layered with hexanes (10 mL) to give orange crystals. IR: 2962 (s), 2925 (s), 2852 (s), 1460 (s), 1377 (s), 1298 (w), 1256 (w), 1216 (w), 1153 (w), 1035(w), 967 (w), 885(w), 853 (w), 722 (s), 693(s), 618(w), 466(m) cm^{-1}.

Synthesis of $(py)_4ThI_3F \cdot py$ (21)

Th (0.232 g, 1.00 mmol), I_2 (0.381 g, 1.50 mmol), and $(SC_6F_5)_2$ (0.199 g, 0.50 mmol) were combined in pyridine (15 mL) with a catalytic amount of Hg (0.010 g, 0.05 mmol), and the mixture was stirred for 4 days. The dark red solution was filtered, concentrated and layered with hexanes to give colorless crystals that melt at 110°C and decomposed at 165°C. IR: 2923 (s), 2854(s), 2725(w), 1599 (m), 1463 (s), 1377 (s), 1220(w), 1152 (w), 1065(w), 1038 (w), 999(m), 968 (w), 833(w), 722 (m), 701 (m), 622(w) cm^{-1}. Anal. Calcd for $C_{25}H_{25}FI_3N_5Th$: C, 29.2; H, 2.45; N, 6.82. Found: C, 29.0; H, 2.83; N, 6.16. ^{1}H NMR (pyridine-d_5): 8.74(d, J = 4.80 Hz, 2H, py), 7.58(m, 1H, py), 7.22(m, 2H, py). ^{19}F NMR (pyridine-d_5): -129(s).

Synthesis of $(py)_3UI_3(SC_6F_5) \cdot py$ (22)

U (0.184 g, 0.77 mmol) and I_2 (0.294 g, 1.15 mmol) were combined in pyridine (15 mL) and stirred at 2°C for 12 h, and continued to stir at room temperature for 24h. $(SC_6F_5)_2$ (0.154 g, 0.38mmol) was added into the dark purple solution and stirred for

12h. The dark red solution was filtered and layered with hexanes, and kept at -30°C for a week, to give red crystals.

Synthesis of $(py)_8U_3O_2I_8$

U (0.172 g, 0.72 mmol) and I_2 (0.275 g, 0.72 mmol) were combined in pyridine (15 mL) and stirred at 2°C for 12 h, and continued to stir at room temperature for 24h. Trace amount (1 drop) of H_2O was added by syringe into the dark purple solution and stirred for 12h. The dark red solution was filtered and layered with hexanes, and kept at 2°C for a week, to give orange crystals that were identified by single crystal X-ray diffraction as $(py)_8U_3O_2I_8$.

Reaction of U/$(SeC_6F_5)_2$/I_2/Py

U (0.127 g, 0.54 mmol), $(SeC_6F_5)_2$ (0.526 g, 1.1 mmol) and catalytic amount of I_2 (0.01 g, 0.04 mmol) were combined in pyridine (15 mL) and stirred at 60°C for 2 days, to give a dark brown solution. The solution was filtered and concentrated, and put into refrigerator at 2°C for a week, forming powdery product.

Reaction of U/$(SC_6F_5)_2$/I_2/Py

U (0.126 g, 0.53 mmol), $(SC_6F_5)_2$ (0.422 g, 1.1 mmol) and catalytic amount of I_2 (0.01 g, 0.04 mmol) were combined in pyridine (15 mL) and stirred at 60°C for 2 days, to give a dark reddish brown solution. The solution was filtered, concentrated, and layered with hexanes, forming green precipitate in a week.

Reaction of U/$(SC_6F_5)_2$/py-SO_3/I_2/Py

U (0.122 g, 0.51 mmol), $(SC_6F_5)_2$ (0.408 g, 1.0 mmol) and catalytic amount of I_2

(0.01 g, 0.04 mmol) were combined in pyridine (15 mL) and stirred at 60°C for 2 days, to give a dark reddish brown solution. The solution was filtered to 10 mL, py-SO_3 (0.020 g, 0.13mmol) was added, and continue to stir for 3 days. The resulting green solution was filtered, concentrated, and put into refrigerator at 2°C for a week, forming green precipitate.

Reaction of U/$(TePh)_2$/I_2/Py

U (0.106 g, 0.45 mmol), $(TePh)_2$ (0.364 g, 0.89 mmol) and catalytic amount of I_2 (0.01 g, 0.04 mmol) were combined in pyridine (15 mL). The flask was wrapped with aluminum foil. After stirring for 3 days, there was still some metal left. Elemental Te (0.057g, 0.45 mmol) was added, and the mixture was stirred for 2 more days. Then the solution was filtered, concentrated, and layered with hexanes, forming black precipitate in 3 days.

Reaction of Th/$(SePh)_2$/Se/Hg/THF

Th (0.116 g, 0.50 mmol), $(SePh)_2$ (0.312 g, 1.0 mmol) and catalytic amount of Hg (0.01 g, 0.05 mmol) were combined in THF (15 mL), and stirred for 12 h to give an orange-red solution. Elemental Se (0.060g, 0.75 mmol) was added, and the mixture was stirred for another 12 h. The resulting yellow solution was filtered, concentrated, and layered with hexanes, forming yellow precipitate in a week.

Reaction of U/$(SC_6F_5)_2$/AgF/Py

U (0.087 g, 0.36 mmol), $(SC_6F_5)_2$ (0.290 g, 0.72 mmol) and catalytic amount of I_2 (0.01 g, 0.04 mmol) were combined in pyridine (15 mL) and stirred for 2 days, to give

a dark reddish brown solution. AgF was (0.185g, 1.46 mmol) was added, and the mixture was stirred for 5 days. The resulting dark red solution was filtered, concentrated, and put into refrigerator at 2^{o}C for a week, forming brown precipitate.

Reaction of Th/$(SC_6F_5)_2$/AgF/Hg/Py

Th (0.116 g, 0.50 mmol), $(SC_6F_5)_2$ (0.398 g, 1.0 mmol) and catalytic amount of Hg (0.01 g, 0.05 mmol) were combined in pyridine (10 mL) and stirred for 24 h, to give a pale yellow solution with a little black powder. AgF (0.128g, 1.0 mmol) was added, and the mixture was stirred for 7 days. The resulting dark red solution was filtered, concentrated, and put into refrigerator at 2^{o}C for a week, forming red gel.

Reaction of Th/$(SPh)_2$/Hpz/Hg/Tol

Th (0.116 g, 0.50 mmol), $(SPh)_2$ (0.164 g, 0.75 mmol), pyrazole (0.102g, 1.5 mmol) and catalytic amount of Hg (0.01 g, 0.05 mmol) were combined in toluene (10 mL) and stirred for 2 days at 90^{o}C, to give a colorless solution with a little black powder. The solution was filtered, concentrated and put into refrigerator at 2^{o}C for a week, forming tiny colorless crystals, which had poor quality, and were not suitable for single-crystal x-ray diffraction.

Reaction of Th/$(SPh)_2$/Hpz/Hg/THF

Th (0.232 g, 1.0 mmol), $(SPh)_2$ (0.436 g, 2.0 mmol), and catalytic amount of Hg (0.01 g, 0.05 mmol) and $(SePh)_2$ (0.01 g, 0.03 mmol) were combined in pyridine (10 mL) and stirred for 2 days to give a pale yellow solution with gray powder. The solution was filtered and removed in vacuo. Pyrazole (0.204 g, 3.0 mmol) and THF (10 mL)

was added and stirred for 12 h. The resulting light yellow solution was filtered and layered with hexanes, forming yellow powder in a week.

Reaction of Th/$(SePh)_2$/Se/Hpz/Hg/Tol

Attempt A: Th (0.116 g, 0.50 mmol), $(SePh)_2$ (0.234 g, 0.75 mmol), pyrazole (0.102g, 1.5 mmol) and catalytic amount of Hg (0.01 g, 0.05 mmol) were combined in toluene (10 mL) and stirred for 2 days at 90^{o}C, to give a light yellow solution with gray powder. The solution was filtered away from the powder, elemental Se (0.039g, 0.5 mmol) was added, and stirred for another 1 h. The resulting yellow solution was filtered, concentrated and put into refrigerator at 2^{o}C for a week, forming no crystals.

Attempt B: Th (0.116 g, 0.50 mmol), $(SePh)_2$ (0.234 g, 0.75 mmol), pyrazole (0.102g, 1.5 mmol) and catalytic amount of Hg (0.01 g, 0.05 mmol) were combined in toluene (10 mL) and stirred for 2 days at 90^{o}C, to give a light yellow solution with gray powder. The solution was filtered away from the powder, elemental Se (0.039g, 0.5 mmol) was added, and stirred for another 2 h. The resulting orange color solution was filtered to ca. 5ml, and layered with ca. 5ml of hexanes, forming yellow precipitate in a week.

Reaction of Th/$(SePh)_2$/Se/Hpz/Hg/THF

Th (0.116 g, 0.50 mmol), $(SePh)_2$ (0.234 g, 0.75 mmol), and catalytic amount of Hg (0.01 g, 0.05 mmol) were combined in pyridine (10 mL) and stirred for 12 h, to give a pale yellow solution with gray powder. The solution was removed in vacuo, pyrazole (0.102g, 1.5 mmol) and THF (15mL) was added into solution, and stirred for 2 days at

90°C. Elemental Se (0.039g, 0.5 mmol) was added, and stirred for another 2 h. The resulting orange color solution was filtered and layered with hexanes, forming yellow precipitate in a week.

Reaction of Th/$(SePh)_2$/S/Hpz/Hg/Tol

Th (0.116 g, 0.50 mmol), $(SePh)_2$ (0.234 g, 0.75 mmol), pyrazole (0.102g, 1.5 mmol) and catalytic amount of Hg (0.01 g, 0.05 mmol) were combined in toluene (10 mL) and stirred for 3 days at 90°C, to give a light yellow solution with gray powder. The solution was filtered away from the powder, elemental S (0.016g, 0.5 mmol) was added, and stirred for 2 days. The resulting yellow solution was filtered, concentrated and put into refrigerator at 2°C for a week, forming a little yellow precipitate.

Reaction of Th/$(SPh)_2$/S/Hpz/Hg/Tol

Th (0.116 g, 0.50 mmol), $(SPh)_2$ (0.164 g, 0.75 mmol), pyrazole (0.102g, 1.5 mmol) and catalytic amount of Hg (0.01 g, 0.05 mmol) were combined in toluene (10 mL) and stirred for 2 days at 90°C, to give a colorless solution with gray powder. The solution was filtered away from the powder, elemental S (0.016g, 0.5 mmol) was added, and stirred for another 1 h. The resulting colorless solution was filtered, concentrated to ca. 3ml and put into refrigerator at 2°C for a week, forming no crystals.

Reaction of Th/$(SC_6F_5)_2$/4,4'-Bipy/Hg/THF

Attempt A: Th (0.116 g, 0.50 mmol), $(SC_6F_5)_2$ (0.398 g, 1.0 mmol), 4,4'-bipyridine (0.156 g, 1.0mmol) and catalytic amount of Hg (0.01 g, 0.05 mmol) were combined in THF (15 mL), and stirred for 12h, to give a dark yellow solution with some

black precipitate. The solution was filtered, concentrated and put into refrigerator at 2^{o}C for 2 weeks, resulting dark red gel at bottom.

Attempt B: Th (0.116 g, 0.50 mmol), $(SC_6F_5)_2$ (0.398 g, 1.0 mmol), and catalytic amount of Hg (0.01 g, 0.05 mmol) were combined in pyridine (10 mL) and stirred for 12h, to give an orange-red solution with some black precipitate. The solution was filtered, and pyridine was removed in vacuo. 4,4'-Bipyridine (0.156 g, 1.0mmol) and THF (15mL) were added, and the mixture was stirred for 12 h. The solution was filtered and layered with hexanes, resulting in many yellow powder in a week.

Reaction of Th/$(SPh)_2$/$(SC_6F_5)_2$/Hpz/Hg/Tol

Attempt A: Th (0.116 g, 0.50 mmol), $(SPh)_2$ (0.164 g, 0.75 mmol), pyrazole (0.102g, 1.5 mmol) and catalytic amount of Hg (0.01 g, 0.05 mmol) were combined in toluene (10 mL) and stirred for 2 days at 90^{o}C, to give a colorless solution with gray powder. In another flask, Th (0.116 g, 0.50 mmol), $(SC_6F_5)_2$ (0.299 g, 0.75 mmol) and pyrazole (0.102 g, 3.0 mmol) were combined in toluene (15 mL) with a catalytic amount of Hg (0.010 g). The mixture was stirred for 12 h until Th was consumed. The solution in the two flasks was filtered together into a new flask, and elemental S (0.016g, 0.5 mmol) was added. The resulting light yellow solution was filtered, concentrated to ca. 3 mL and put into refrigerator at 2^{o}C for a week, forming tiny needle crystals, which had poor quality, and were not suitable for single-crystal x-ray diffraction.

Attempt B: Th (0.116 g, 0.50 mmol), $(SPh)_2$ (0.109 g, 0.50 mmol), $(SC_6F_5)_2$ (0.199 g, 0.50 mmol), pyrazole (0.068 g, 1.0 mmol) and catalytic amount of Hg (0.01 g, 0.05

mmol) were combined in toluene (10 mL) and stirred for 4 days, to give a colorless solution with black powder. Elemental S (0.032g, 1.0 mmol) was added into solution, and stirred for 2 h. The resulting light yellow solution was filtered, concentrated to ca. 5 mL and layered with ca. 5 mL of hexanes, forming white powder.

Reaction of Th/$(SePh)_2$/pzn/Hg/Tol

Th (0.116 g, 0.50 mmol), $(SePh)_2$ (0.312 g, 1.0 mmol) and catalytic amount of Hg (0.01 g, 0.05 mmol) were combined in pyridine (20mL). The solution was filtered, and remove the solvent in vacuo. Pyrazine (0.120 g, 1.5mmol) and toluene (15mL) was added and stirred for 12 h. The resulting light yellow solution was filtered, concentrated to ca. 3ml and put into refrigerator at 2^{o}C for a week, forming no crystals.

Reaction of Th/$(SC_6F_5)_2$/Hpz/SeO_2/Hg/Tol

Th (0.116 g, 0.50 mmol), $(SC_6F_5)_2$ (0.398 g, 1.0 mmol) and pyrazole (0.102 g, 3.0 mmol) were combined in toluene (15 mL) with a catalytic amount of Hg (0.010 g). The mixture was stirred for 12 h until Th was consumed. The colorless solution was filtered, and SeO_2 (0.056 g, 0.50 mmol) was added, and stirred in 60^{o}C oil bath for 12 h. The resulting bright yellow solution was filtered, concentrated to ca. 3ml and put into refrigerator at 2^{o}C for a week, forming no crystals.

Reaction of Th/$(SePh)_2$/$(SC_6F_5)_2$/Hpz/Hg/Tol

Th (0.232 g, 1.0 mmol), $(SePh)_2$ (0.156 g, 0.50 mmol), $(SC_6F_5)_2$ (0.398 g, 1.0 mmol), pyrazole (0.136 g, 2.0 mmol) and catalytic amount of Hg (0.01 g, 0.05 mmol) were combined in toluene (10 mL) and stirred for 3 days, to give a light yellow solution

with gray powder. Elemental Se (0.079 g, 1.0 mmol) was added into solution, and stirred for 2 days. The resulting pale yellow solution was filtered, concentrated to ca. 5 mL and layered with ca. 5 mL of hexanes, forming many powder.

Reaction of Th/$(SePh)_2$/$(SeC_6F_5)_2$/I_2/Se/Hg/py

Th (0.232 g, 1.0 mmol), $(SePh)_2$ (0.312 g, 1.0 mmol), I_2 (0.127g, 0.5 mmol), $(SeC_6F_5)_2$ (0.246 g, 0.50 mmol) and catalytic amount of Hg (0.01 g, 0.05 mmol) were combined in pyridine (20 mL), and the mixture was stirred for 12 h until the metal was completely consumed to give a red solution with some red powder. Elemental selenium (0.079 g, 1.0 mmol) was added and the mixture was stirred for 1 h. The dark red solution was filtered to ca. 15mL and layered with hexanes (15 mL) to give orange crystals, which were identified by single-crystal X-ray diffraction as $(py)_6Th_2I_4Se_4$ (**7**).

Reaction of Th/$(SPh)_2$/$(SC_6F_5)_2$/I_2/S/Hg/Py

Th (0.232 g, 1.0 mmol), $(SPh)_2$ (0.218 g, 1.0 mmol), I_2 (0.127g, 0.5 mmol), $(SC_6F_5)_2$ (0.199 g, 0.50 mmol) and catalytic amount of Hg (0.01 g, 0.05 mmol) were combined in pyridine (20 mL), and the mixture was stirred for 12 h until the metal was completely consumed to give a red solution with some red powder. Elemental sulfur (0.032 g, 1.0 mmol) was added and the mixture was stirred for 1 h. The orange red solution was filtered to ca. 15mL and layered with hexanes (18 mL), forming no crystals in a week.

Reaction of Th/$(SPh)_2$/$(SeC_6F_5)_2$/I_2/S/Hg/Py

Th (0.232 g, 1.0 mmol), $(SPh)_2$ (0.218 g, 1.0 mmol), I_2 (0.127g, 0.5 mmol),

$(SeC_6F_5)_2$ (0.246 g, 0.50 mmol) and catalytic amount of Hg (0.01 g, 0.05 mmol) were combined in pyridine (20 mL), and the mixture was stirred for 12 h until the metal was completely consumed to give a red solution with some red powder. Elemental sulfur (0.032 g, 1.0 mmol) was added and the mixture was stirred for 1 h. The resulting pale brown solution was filtered to ca. 15mL and layered with hexanes (18 mL) to give orange crystals, which were identified by single-crystal X-ray diffraction as $(py)_{12}Th_6I_6S_9$.

Reaction of Th/$(SePh)_2$/$(SPh)_2$/I_2/Se/Hg/Py

Th (0.116 g, 0.5 mmol), $(SePh)_2$ (0.156 g, 0.5 mmol), I_2 (0.063g, 0.25 mmol), $(SPh)_2$ (0.055 g, 0.25 mmol) and catalytic amount of Hg (0.01 g, 0.05 mmol) were combined in pyridine (20 mL), and the mixture was stirred for 12 h until the metal was completely consumed to give a pale yellow solution with some black powder. Elemental selenium (0.040 g, 0.5 mmol) was added and the mixture was stirred for 1 h. The resulting pale orange solution was filtered to ca. 15mL and layered with hexanes (15 mL) to give powdery product at the bottom of the flask.

Reaction of U/$(SePh)_2$/$(SC_6F_5)_2$/I_2/Se/Py

U (0.212 g, 0.90 mmol), $(SePh)_2$ (0.278 g, 0.90 mmol), I_2 (0.113g, 0.45 mmol), and SC_6F_5 (0.178 g, 0.45 mmol) were combined in pyridine (20 mL), and the mixture was stirred for 3 days until the metal was completely consumed to give a dark red solution. Elemental selenium (0.070 g, 0.90 mmol) was added and the mixture was stirred for 1 h. The dark red solution was filtered to ca. 15mL and layered with hexanes (10 mL) to

give many small crystals, which had poor quality, and were not suitable for single-crystal x-ray diffraction.

Reaction of U/$(SeC_6F_5)_2$/I_2/Py

U (0.179 g, 0.75 mmol) and I_2 (0.287 g, 1.13 mmol) were combined in pyridine (15 mL) and stirred at 2°C for 12 h, and continued to stir at room temperature for 24h. $(SeC_6F_5)_2$ (0.185 g, 0.38mmol) was added into the dark purple solution and stirred for 12h. The dark red solution was filtered and layered with hexanes, and kept at -30°C for a week, to give very tiny crystals that were not suitable for single-crystal x-ray diffraction.

Reaction of U/$(SePh)_2$/I_2/Py

U (0.174 g, 0.73 mmol), and I_2 (0.278 g, 1.10 mmol) were combined in pyridine (15 mL) and stirred at 2°C for 12 h, and continued to stir at room temperature for 24 h. $(SePh)_2$ (0.114 g, 0.36 mmol) was added into the solution, and stirred for another 12 h. The resulting dark red solution was filtered to ca. 17mL and layered with hexanes (12 mL) to give many black powders.

Reaction of U/$(SePh)_2$/I_2/Se/Py

Attempt A: U (0.178 g, 0.74 mmol), and I_2 (0.285 g, 1.13 mmol) were combined in pyridine (15 mL) and stirred at 2°C for 12 h, and continued to stir at room temperature for 24 h. $(SePh)_2$ (0.117 g, 0.37 mmol) was added into the solution, and stirred for another 12 h. Elemental selenium (0.058 g, 0.74 mmol) was added and the mixture was stirred for 1 h. The resulting dark red solution was filtered to ca. 15mL and layered with

hexanes (10 mL) to give some black particles in a week, which had poor quality, and were not suitable for single-crystal x-ray diffraction.

Attempt B: U (0.125 g, 0.53 mmol), $(SePh)_2$ (0.164 g, 0.53 mmol) and I_2 (0.133g, 0.53 mmol), were combined in pyridine (10 mL), and the mixture was stirred in 60 ^oC oil bath for 2 days until the metal was completely consumed to give a dark red solution. Elemental Se (0.041 g, 0.53 mmol) and toluene (5 mL) was added and the mixture was stirred for 1 h. The dark red solution was filtered to ca. 15mL, layered with hexanes (10 mL) and kept at 2^oC for a week to give many black powders.

Reaction of Th/$(SePh)_2$/$(SC_6F_5)_2$/$HgBr_2$/Hg/Py

Th (0.232 g, 1.0 mmol), $(SePh)_2$ (0.312 g, 1.0 mmol), $HgBr_2$ (0.180 g, 0.5 mmol), $(SC_6F_5)_2$ (0.199 g, 0.50 mmol) and catalytic amount of Hg (0.01 g, 0.05 mmol) were combined in pyridine (20 mL), and the mixture was stirred for 12 h until the metal was completely consumed to give a pale brown solution with some black powder and a large drop of mercury. Elemental selenium (0.079 g, 1.0 mmol) was added and the mixture was stirred for 1 h. The pale brown solution was filtered to ca. 15mL and layered with hexanes (20 mL), forming many tiny crystals that were identified by single-crystal x-ray diffraction as $(py)_4ThBr_4$.

Reaction of Th/$(SePh)_2$/$HgBr_2$/Hg/Py

Th (0.232 g, 1.0 mmol), $(SePh)_2$ (0.312 g, 1.0 mmol), $HgBr_2$ (0.360 g, 1.0 mmol), and catalytic amount of Hg (0.01 g, 0.05 mmol) were combined in pyridine (15 mL), and the mixture was stirred for 12 h until the metal was completely consumed to give a

yellow solution with some grey powder and a large drop of mercury. Elemental selenium (0.079 g, 1.0 mmol) was added and the mixture was stirred for 1 h, resulting in a pale green suspension, which was difficult to filter.

Reaction of U/I_2/H_2O/THF

U (0.126 g, 0.53 mmol) and I_2 (0.202 g, 0.80 mmol) were combined in pyridine (15 mL) and stirred at 2°C for 12 h, and continued to stir at room temperature for 24 h. Trace amount (1 drop) of H_2O was added by syringe into the dark purple solution and continue stirring for 12h. The solution turned to green in the first 30 min. The dark green solution was filtered, concentrated, and kept at 2°C for a week, to give some green powder.

Reaction of U/$(SC_6F_5)_2$/I_2/AgF/Py

U (0.192 g, 0.81 mmol) and I_2 (0.287 g, 1.21 mmol) were combined in pyridine (15 mL) and stirred at 2°C for 12 h, and continued to stir at room temperature for 24 h. $(SC_6F_5)_2$ (0.160 g, 0.40 mmol) and AgF (0.205 g, 1.62 mmol) were added into the dark purple solution and stirred for 12h. The dark red-black solution was filtered and layered with hexanes, to give colorless crystals that which has a similar unit cell as a previously published silver-derived byproduct.

Reaction of U/$(SC_6F_5)_2$/I_2/THF

U (0.205 g, 0.86 mmol) and I_2 (0.328 g, 1.3 mmol) were combined in THF (15 mL) and stirred at 2°C for 12 h, and continued to stir at room temperature for 24h. $(SC_6F_5)_2$ (0.171 g, 0.43 mmol) was added into the dark blue solution and stirred for 12h. The

dark red solution was filtered and layered with hexanes, and kept at -30ºC for a week, to give black needles which were identified by single-crystal x-ray diffraction as $(THF)_4UI_3$.

Reaction of U/I_2/Se/Py

U (0.205 g, 0.86 mmol), and I_2 (0.285 g, 1.29 mmol) were combined in pyridine (15 mL) and stirred at 2ºC for 12 h, and continued to stir at room temperature for 24 h. Elemental Se (0.034 g, 0.43 mmol) was added into the solution, and stirred for another 2 h. The resulting dark red solution was filtered to ca. 18mL and layered with hexanes (20 mL) to give many black powders in a week.

Reaction of U/I_2/S/Py

U (0.117 g, 0.50 mmol), and I_2 (0.187 g, 0.75 mmol) were combined in pyridine (15 mL) and stirred at 2ºC for 12 h, and continued to stir at room temperature for 24 h. Elemental S (0.008 g, 0.25 mmol) was added into the solution, and stirred for 2 days. The resulting dark red solution was filtered and layered with hexanes, to give many black powders in a week.

Reaction of Th/$(SePh)_2$/I_2/Se/Hg/THF

Th (0.232 g, 1.0 mmol), $(SePh)_2$ (0.312 g, 1.0 mmol), I_2 (0.254g, 1.0 mmol) and catalytic amount of Hg (0.01 g, 0.05 mmol) were combined in pyridine (15 mL), and stirred for 12 h to give an orange-red solution. The solution was filtered and removed in vacuo. THF (15mL) was first added and stirred for 3h. Then, elemental Se (0.060g, 0.75 mmol) was added, and the mixture was stirred for another 1.5 h, resulting a yellow

suspension, which was difficult to filter.

Reaction of Th/$(SePh)_2$/I_2/Se/Hg/DME

Th (0.116 g, 0.50 mmol), $(SePh)_2$ (0.116 g, 0.50 mmol), I_2 (0.127g, 0.50 mmol) and catalytic amount of Hg (0.01 g, 0.05 mmol) were combined in pyridine (15 mL), and stirred for 12 h to give an orange-red solution. The solution was filtered and removed in vacuo. DME (15mL) was first added and stirred for 2 days. Then, elemental Se (0.040g, 0.50 mmol) was added, and the mixture was stirred for another 0.5 h. The resulting yellow color solution was filtered and layered with hexanes, leading to some white precipitate.

Reaction of Th/$(SePh)_2$/AgBr/Se/Hg/Py

Th (0.116 g, 0.50 mmol), $(SePh)_2$ (0.312 g, 1.0 mmol), and catalytic amount of Hg (0.01 g, 0.05 mmol) were combined in pyridine (10 mL) and stirred for 12 h, to give a pale yellow solution with gray powder. AgBr (0.187g, 1.0 mml) was added into the solution, and stirred for 1 h. The bright solution was filtered from the yellow precipitate, elemental Se (0.040g, 0.50mmol) was added, and the solution was continued to stir for 30 min. The resulting orange color solution was filtered and layered with hexanes, forming orange powder in a week.

Reaction of Th/$(SePh)_2$/HgF_2/Se/Hg/Py

Th (0.116 g, 0.50 mmol), $(SePh)_2$ (0.156 g, 0.50 mmol), HgF_2 (0.119g, 0.50 mmol) and catalytic amount of Hg (0.01 g, 0.05 mmol) were combined in pyridine (15 mL), and stirred for 12 h to give a light yellow solution with large mercury drop at the bottom.

Elemental Se (0.040g, 0.50 mmol) was added, and stirred for another 30 min. The resulting orange color solution was filtered and layered with hexanes, and kept at 2°C for a week, to give red needles, which were identified by single-crystal x-ray diffraction as $HgSe_8$.

Reaction of Th/$(SePh)_2$/HgF_2/S/Hg/Py

Th (0.116 g, 0.50 mmol), $(SePh)_2$ (0.156 g, 0.50 mmol), HgF_2 (0.119g, 0.50 mmol) and catalytic amount of Hg (0.01 g, 0.05 mmol) were combined in pyridine (15 mL), and stirred for 12 h to give a light yellow solution with large mercury drop at the bottom. Elemental S (0.016g, 0.50 mmol) was added, and stirred for 1 h. The resulting bright yellow solution was filtered and layered with hexanes, and kept at 2°C. No crystal was formed in two weeks.

Reaction of Th/$(SePh)_2$/$(SC_6F_5)_2$/HgF_2/Se/Hg/Py

Th (0.116 g, 0.50 mmol), $(SePh)_2$ (0.156 g, 0.50 mmol), HgF_2 (0.060g, 0.25 mmol) $(SC_6F_5)_2$ (0.100 g, 0.25mmol) and catalytic amount of Hg (0.01 g, 0.05 mmol) were combined in pyridine (15 mL), and stirred for 12 h to give a light yellow solution with large mercury drop at the bottom. Elemental Se (0.040g, 0.50 mmol) was added, and stirred for 2 h. The resulting orange color solution was filtered and layered with hexanes, and kept at 2°C for a week, to give black powders at bottom of the flask.

Reaction of U/$(SC_6F_5)_2$/Hpz/I_2/Tol

U (0.095 g, 0.40 mmol), $(SC_6F_5)_2$ (0.238 g, 0.60 mmol), pyrazole (0.136 g, 2.0 mmol) and catalytic amount of Hg (0.01 g, 0.05 mmol) were combined in toluene (10

mL) and stirred in 80 °C oil bath for 3 days, to give a dark green solution with black powder. The solution was filtered, concentrated and kept at 2°C. No crystal was formed in three weeks.

Reaction of U/$(SPh)_2$/I_2/S/Py

U (0.111 g, 0.47 mmol), $(SPh)_2$ (0.102 g, 0.47 mmol) and I_2 (0.118g, 0.47 mmol), were combined in pyridine (15 mL), and the mixture was stirred in 60 °C oil bath for 2 days until the metal was completely consumed to give a dark red solution. Elemental sulfur (0.030 g, 0.94 mmol) was added and the mixture was stirred for 1 h. The dark red solution was filtered to ca. 10mL, layered with hexanes (10 mL) and kept at 2°C for two weeks. Some tiny crystals appeared, but they had poor quality and were not suitable for single-crystal x-ray diffraction.

Reaction of Th/$(SePh)_2$/PhSeBr/Se/Hg/Py

Th (0.232 g, 1.0 mmol), $(SePh)_2$ (0.312 g, 1.0 mmol), PhSeBr (0.236 g, 1.0 mmol) and catalytic amount of Hg (0.01 g, 0.05 mmol) were combined in pyridine (15 mL), and stirred for 6 h to give a yellow-orange solution. Elemental Se (0.120 g, 1.5 mmol) was added and continue stirring. Some yellow precipitate formed quickly, and the solution was stirred for 30 min. The resulting yellow solution was filtered, concentrated, and layered with hexanes, forming yellow precipitate in a week.

Reaction of Th/PhSeBr/Se/Hg/Py

Th (0.232 g, 1.0 mmol), PhSeBr (0.472 g, 2.0 mmol) and catalytic amount of Hg (0.01 g, 0.05 mmol) were combined in pyridine (15 mL), and stirred for 12 h to give a

yellow-orange solution. Elemental Se (0.079 g, 1.0 mmol) was added and the solution was stirred for 10 min. The resulting yellow solution was filtered to 15 mL and layered with 10 mL of hexanes, forming yellow precipitate in two days.

Reaction of U/$(SePh)_2$/PhSeBr/Se/I_2/Py

U (0.128 g, 0.54 mmol), $(SePh)_2$ (0.168 g, 0.54 mmol), PhSeBr (0.127 g, 0.54 mmol) and catalytic amount of I_2 (0.01 g, 0.04 mmol) were combined in pyridine (15 mL), and stirred for 2 days until the metal was completely consumed to give a dark red solution. Elemental Se (0.042 g, 0.54 mmol) was added and the solution was stirred for 1 h. The resulting dark red solution was filtered, concentrated, and kept at -30^oC to give orange powders in two weeks.

Reaction of Th/$(SePh)_2$/Hdmpz/Hg/Tol

Th (0.116 g, 0.50 mmol), $(SePh)_2$ (0.312 g, 1.0 mmol), 3,5-dimethylpyrazole (0.192 g, 2.0 mmol) and catalytic amount of Hg (0.01 g, 0.05 mmol) were combined in toluene (15 mL) and stirred for 12 h until Th was consumed. The resulting yellow solution was filtered away from the Hg, concentrated to ca. 3 mL, and kept at 2^oC to give colorless crystals which were identified by single-crystal x-ray diffraction as 3,5-dimethylpyrazole, the ligand itself.

Reaction of Th/$(SPh)_2$/Hdmpz/Hg/Tol

Th (0.232 g, 1.0 mmol), $(SPh)_2$ (0.436 g, 2.0 mmol), 3,5-dimethylpyrazole (0.192 g, 2.0 mmol) and catalytic amount of Hg (0.01 g, 0.05 mmol) were combined in toluene (15 mL) and stirred for 3 days until Th was consumed. The resulting light yellow

solution was filtered away from the Hg, concentrated to ca. 5 mL, and kept at 2°C. No crystal was formed in two weeks.

Reaction of Th/$(SPh)_2$/$(SC_6F_5)_2$/Ag_2O/Hg/Py

Th (0.116 g, 0.50 mmol), $(SPh)_2$ (0.109 g, 0.50 mmol), $(SC_6F_5)_2$ (0.199 g, 1.0 mmol) and catalytic amount of Hg (0.01 g, 0.05 mmol) were combined in pyridine (10 mL), and stirred for 12 h to give a orange solution. Ag_2O (0.058 g, 0.25 mmol) was added, and stirred for 12h with flask wrapped with Al foil. The resulting orange solution was filtered and layered with hexanes, and kept at 2°C. No crystal was formed in two weeks.

Reaction of Th/$(SePh)_2$/SeO_2/Hg/Py

Th (0.116 g, 0.50 mmol), $(SePh)_2$ (0.312 g, 1.0 mmol) and catalytic amount of Hg (0.01 g, 0.05 mmol) were combined in pyridine (15 mL), and stirred for 12 h to give a light yellow solution. SeO_2 (0.055 g, 0.50 mmol) was added, and stirred in 60 °C oil bath for 3 h. The resulting pale yellow solution was filtered, layered with hexanes, and kept at 2°C. No crystal was formed in two weeks.

Reaction of Th/$(SePh)_2$/Se/SeO_2/Hg/Py

Th (0.116 g, 0.50 mmol), $(SePh)_2$ (0.312 g, 1.0 mmol) and catalytic amount of Hg (0.01 g, 0.05 mmol) were combined in pyridine (15 mL), and stirred for 12 h to give a light yellow solution. Elemental Se (0.040g, 0.50 mmol and SeO_2 (0.014 g, 0.13 mmol) was added, and stirred for 3 h. The resulting bright yellow solution was filtered, layered with hexanes, and kept at 2°C for two weeks to give powdery product.

Reaction of Th/$(SePh)_2$/I_2/Se/SeO_2/Hg/Py

Th (0.116 g, 0.50 mmol), $(SePh)_2$ (0.468 g, 1.5 mmol), I_2 (0.064 g, 0.5mmol) and catalytic amount of Hg (0.01 g, 0.05 mmol) were combined in pyridine (15 mL), and stirred for 12 h to give an orange solution. Elemental Se (0.040g, 0.50 mmol) and SeO_2 (0.028g, 0.25 mmol) was added, and stirred for 4 h. The resulting orange-red solution was filtered, layered with hexanes, and kept at 2°C. No crystal was formed in two weeks, only oily product.

Reaction of U/$(SePh)_2$/I_2/Se/SeO_2/Py

U (0.130 g, 0.55 mmol), $(SePh)_2$ (0.170 g, 0.55 mmol), I_2 (0.139 g, 0.55 mmol) were combined in pyridine (15 mL), and stirred for 2 days to give a dark red solution. Elemental Se (0.043 g, 0.55 mmol) and SeO_2 (0.015g, 0.14 mmol) was added, and stirred for 5 h. The resulting dark red solution was filtered, layered with hexanes, and kept at 2°C for two weeks to give some yellow-red crystals, which had poor quality and were not suitable for single-crystal x-ray diffraction.

Reaction of Th/$(SePh)_2$/$(SC_6F_5)_2$/Se/SeO_2/Hg/Py

Th (0.116 g, 0.50 mmol), $(SePh)_2$ (0.156 g, 0.50 mmol), $(SC_6F_5)_2$ (0.100 g, 0.25mmol) and catalytic amount of Hg (0.01 g, 0.05 mmol) were combined in pyridine (15 mL), and stirred for 12 h to give a light yellow solution. Elemental Se (0.040g, 0.50 mmol) and SeO_2 (0.028g, 0.25 mmol) was added, and stirred for 4 h. The resulting orange-red solution was filtered away from black powder and layered with hexanes, and kept at 2°C. No crystal was formed in two weeks.

References

(1) McKillop, A.; Koyuncu, D.; Krief, A.; Dumont, W.; Renier, P.; Trabelsi, M. Efficicient, high yield, oxidation of thiols and selenols to disulphides and diselenides. *Tetrahedron Lett.* **1990**, *31*, 5007-5010.

(2) Klapötke, T. M.; Krumm, B.; Polborn, K. Synthesis, Chemistry, and Characterization of Perfluoroaromatic Selenium Derivatives. *Eur. J. Inorg. Chem.* **1999**, *1999*, 1359-1366.

(3) Bruker.; Bruker-AXS Inc.: Madison, Wisconsin, USA.

(4) (a) Sheldrick, G. M. A short history of SHELX. *Acta Crystallogr.* **2008**, *64(1)*, 112-120.(b) Sheldrick, G. M. Crystal structure determination with SHELX. *Acta Crystallogr.* **2015**, *C71*, 3-8.(c) Sheldrick, G. M. *SHELXS v.2013/1 and SHELXL v.2013/4 ; Programs for Crystal Structure Analysis*; University of Göttingen Göttingen, Germany, **2013**.

(5) Macrae, C. F.; Edgington, P. R.; McCabe, P.; Pidcock, E.; Shields, G. P.; Taylor, R.; Towler, M.; van De Streek, J. Mercury: visualization and analysis of crystal structures. *J. Appl. Crystallogr.* **2006**, *39*, 453-457.

(6) Stuber, M. A.; Kornienko, A. Y.; Emge, T. J.; Brennan, J. G. Tetrametallic Thorium Compounds with Th_4E_4 (E = S, Se) Cubane Cores. *Inorg. Chem.* **2017**, *56*, 10247-10256.